

UNIVERSITY OF SOUTHERN CALIFORNIA

**Computational tumor ecology:  
a model of tumor evolution, heterogeneity, and  
chemotherapeutic response**

by

Jeffrey West

---

A dissertation presented to the  
FACULTY OF THE GRADUATE SCHOOL  
UNIVERSITY OF SOUTHERN CALIFORNIA  
In Partial Fulfillment of the  
Requirements for the Degree of  
DOCTOR OF PHILOSOPHY  
(Mechanical Engineering)

December 2017

# **Dedication**

Soli Deo gloria

## *Acknowledgements*

Nobel laureate Hermann Muller was right in saying, “If you prefer an ‘academic life’ as a retreat from reality, do not go into biology. This field is for a man or woman who wishes to get even closer to life.” With this in mind, I first thank my advisor Paul Newton, who beckoned me to join the crusade against cancer using math. It has been immensely rewarding to work with you. I thank my committee members Aiichiro Nakano and Niema Pahlevan. I also wish to thank helpful collaborators and mentors such as (but not limited to), Paul Macklin, the Kuhn lab (Peter Kuhn, Jorge Nieva), Stacey Finley, the CAMM group (David Agus, Shannon Mumenthaler, Dan Ruderman). I thank my fellow comrades Jeremy Mason, Zaki Hasnain, and Yongian Ma for their patient feedback, helpful suggestions, and kind friendship.

# Contents

<b>Dedication</b>	i
<b>Acknowledgements</b>	ii
<b>List of Figures</b>	vi
<b>Abstract</b>	viii
<b>1 Introduction</b>	1
1.1 Cancer as an evolutionary and ecological process . . . . .	3
1.2 Chapter Summaries . . . . .	6
1.3 Emergent Features . . . . .	7
<b>2 The prisoner's dilemma as a cancer model</b>	9
2.1 Abstract . . . . .	10
2.2 Introduction . . . . .	11
2.3 The prisoner's dilemma evolutionary game . . . . .	13
2.4 A tumor growth model . . . . .	17
2.4.1 Mutations and heritability . . . . .	19
2.4.2 The fitness landscape . . . . .	20
2.4.3 Heterogeneity drives growth . . . . .	25
2.5 Simulated drug dosing strategies and therapeutic response . . . . .	28
2.6 Mathematical modeling and tumor analytics . . . . .	32
<b>3 An evolutionary model of tumor cell kinetics and the emergence of molecular heterogeneity driving Gompertzian growth</b>	36
3.1 Abstract . . . . .	37
3.2 Introduction . . . . .	38
3.3 Description of the model . . . . .	41
3.3.1 The Moran birth-death process . . . . .	42
3.3.2 The prisoner's dilemma payoff matrix . . . . .	43
3.3.3 The fitness landscape . . . . .	46
3.3.4 Passenger and driver mutations . . . . .	49
3.4 Results . . . . .	50

3.4.1	Gompertzian tumor growth and three growth regimes . . . . .	52
3.4.2	Heterogeneity and growth via statistical mechanics . . . . .	56
3.4.3	Quantitative measures of tumor heterogeneity and growth . . . . .	58
3.4.4	Dynamic phylogenetic trees and evolution of fitness . . . . .	62
3.4.5	A comparison of early vs. late therapy . . . . .	65
3.5	Discussion . . . . .	66
3.6	Appendix . . . . .	69
<b>4</b>	<b>Chemotherapeutic dose scheduling based on tumor growth rates: the case for low dose metronomic high entropy therapies</b>	<b>70</b>
4.1	Abstract . . . . .	71
4.2	Introduction . . . . .	74
4.2.1	Administration of metronomic chemotherapy . . . . .	76
4.2.2	The classic tumor regression laws . . . . .	78
4.2.2.1	Skipper's Laws . . . . .	78
4.2.2.2	Norton-Simon Hypothesis . . . . .	79
4.2.3	The Implications of the Norton-Simon Hypothesis . . . . .	81
4.3	Materials and methods . . . . .	83
4.3.1	Chemotherapeutic agents alter the fitness landscape . . . . .	83
4.3.2	The model . . . . .	84
4.3.3	Dose concentration versus dose density . . . . .	89
4.4	Results . . . . .	91
4.4.1	Quantifying chemotherapeutic strategies via entropy metric . . . . .	91
4.4.2	LDM versus MTD chemotherapies . . . . .	94
4.5	Discussion . . . . .	97
<b>5</b>	<b>Harnessing the evolutionary cost of chemotherapeutic resistance by shaping the fitness landscape of a tumor</b>	<b>100</b>
5.1	Abstract . . . . .	101
5.2	Introduction . . . . .	102
5.2.1	Pre-existing resistance . . . . .	104
5.2.2	Using evolutionary principles to model chemotherapy . . . . .	106
5.3	Materials and Methods . . . . .	110
5.3.1	The Model . . . . .	111
5.3.2	Replicator equation dynamics . . . . .	114
5.3.3	The pairwise prisoner's dilemmas . . . . .	116
5.4	Results . . . . .	117
5.4.1	Treating the strategy: competitive release . . . . .	119
5.4.2	Treating the game: adaptive therapy . . . . .	122
5.5	Discussion . . . . .	125
<b>6</b>	<b>High Performance Computing Techniques</b>	<b>128</b>
6.1	Hybrid MPI + OpenMP Parallelization . . . . .	129
6.2	Error in Hybrid MPI + OpenMP Parallelization . . . . .	130

6.3 Speedup and Efficiency . . . . .	134
6.4 Performance Tunability . . . . .	134
<b>7 Future Work</b>	<b>136</b>
7.1 Chemotherapy scheduling and metastasis . . . . .	137
7.2 Control theory methods to minimize stable tumor burden . . . . .	137
7.3 Heterogeneity drives tumor growth . . . . .	138
7.4 Integrating preclinical and clinical trial data . . . . .	139
<b>Bibliography</b>	<b>140</b>

# List of Figures

2.1	Schematic of the Moran Process . . . . .	18
2.2	Emergence of Gompertzian growth via selection . . . . .	19
2.3	Markov Point Mutation Diagram . . . . .	20
2.4	Tumor fitness drives tumor growth . . . . .	24
2.5	Moran Process fit to Gompertzian Growth Data . . . . .	25
2.6	Sample Dendritic Phylogenetic Tree . . . . .	27
2.7	Effects of varied dose density for early-stage, mid-stage, and late-stage therapies . . . . .	29
2.8	Growth-dependent tumor regression . . . . .	31
3.1	Stochastic Moran birth-death process . . . . .	44
3.2	Fitness as a function of the selection parameter $w \equiv w_H \equiv w_C$ . . . . .	50
3.3	Markov Point Mutation Diagram . . . . .	51
3.4	Gompertzian equation . . . . .	55
3.5	Moran birth-death process with selection . . . . .	61
3.6	Tumor initiation prediction . . . . .	62
3.7	Comparison of stochastic Moran birth-death process, Gompertzian, and Shannon entropy growth curves . . . . .	63
3.8	Emergence of genetic heterogeneity . . . . .	64
3.9	Simulated therapy . . . . .	66
3.10	A flow chart of the Moran process with selection and mutation algorithm .	69
4.1	Chemotherapy is a selective agent that alters the fitness landscape of cells .	85
4.2	Classical Tumor Regression Laws . . . . .	87
4.3	Response of murine tumors to 5-Fluorouracil (5-FU) treatment with model best-fit . . . . .	88
4.4	Diminishing returns of dose escalation compared to linear relationship of dose density . . . . .	91
4.5	Shannon entropy as an index to compare treatment strategies . . . . .	92
4.6	High entropy, LDM-like chemotherapies outperform low entropy MTD-like chemotherapies . . . . .	96
4.7	High entropy strategies lead to an increase in tumor regression . . . . .	97
5.1	Clonal evolution of competitive release . . . . .	106
5.2	Schematic of competitive release in a tumor . . . . .	109

5.3	Dynamics of competitive release under continuous therapy . . . . .	112
5.4	Fitness landscape before and during therapy . . . . .	114
5.5	The effect of growth rate, cost, and fractional resistance under continuous therapy . . . . .	118
5.6	The effect of dose on tumor relapse and progression free survival under continuous therapy . . . . .	120
5.7	Dynamic phase portraits before and during chemotherapy . . . . .	123
5.8	Adaptive therapy strategy to control resistant population . . . . .	125
6.1	Schematic diagram of the Hybrid MPI + OpenMP Parallelization technique.	130
6.2	Strong scalability of Hybrid Parallelization . . . . .	131
6.3	Error in the Hybrid MPI + OpenMP primary tumory growth simulation. .	133

## *Abstract*

Tumor development is an evolutionary process in which a heterogeneous population of cells with different growth capabilities compete for resources in order to gain a proliferative advantage. We describe a cell-molecular based evolutionary mathematical model of tumor development driven by a stochastic Moran birth-death process, in which cancer cells and healthy cells compete for dominance in the population. Each are assigned payoffs according to a prisoner’s dilemma evolutionary game where the healthy cells are the cooperators and the cancer cells are the defectors. The cells in the tumor carry molecular information in the form of a numerical genome which we represent as a four-digit binary string used to differentiate cells into 16 molecular types. The binary string is able to undergo stochastic point mutations that are passed to a daughter cell after each birth event. The value of the binary string determines the cell fitness, with lower fit cells (e.g. 0000) defined as healthy phenotypes, and higher fit cells (e.g. 1111) defined as malignant phenotypes. The model is used to explore key emergent features associated with tumor development, including tumor growth rates (e.g. Gompertzian growth) as it relates to intratumor molecular heterogeneity (e.g. heterogeneity is a driver of tumor growth).

Next, the model is extended to include tumor regression due to chemotherapy, allowing for the design of chemotherapeutic “strategies,” or schedules, tailored to different tumor growth characteristics. Using the Shannon entropy as a novel tool to quantify dosing strategies, we contrast maximum tolerated dose (MTD) strategies as compared with low dose, high density metronomic strategies (LDM) for tumors with different growth rates, concluding that LDM strategies can outperform MTD strategies, especially for fast growing tumors

that thrive on long periods of unhindered growth without chemotherapy. The model shows good agreement with tumor growth data for unperturbed tumor growth and regression under drug therapy.

The final section of this thesis is focused on the pre-existing resistant clones present in a tumor at the start of treatment, which remains a major problem in cancer therapeutics today. Tumor relapse and the development of chemotherapeutic resistance is now thought largely to be a consequence of the mechanism of “competitive release” of pre-existing resistant cells in the tumor which are selected for growth after chemotherapeutic agents attack the sub-population of chemo-sensitive cells which had previously dominated the collection of competing sub-clones in the tumor. We explain the important parameters (cost of resistance and initial fraction of resistance) in anticipating the evolutionary adaptations of the tumor in order to design therapies that exploit or mitigate the harmful effects of potential future adaptions. We introduce an “adaptive therapy” concept of utilizing information in the dynamical phase plane to target the growth of the resistant population indirectly, by introducing periods of drug holidays.

# Chapter 1

## Introduction

In this thesis, a stochastic birth-death mathematical model is developed that describes the complex tumor kinetics arising from a single malignant cell leading to the evolution of the fitness of a tumor and its subsequent growth. The model incorporates cell reproduction and death, mutations, natural selection, and genetic drift. The mathematical framework developed will be used as a platform for testing chemotherapeutic strategies to mitigate the development and growth of the tumor. These models are developed in order to better understand the complex interplay of several biological principals associated with tumor growth that drive the non-equilibrium dynamics of clonal subpopulations in a tumor and how to exploit these dynamics for the optimization of drug schedules that mitigate chemotherapeutic resistance. This thesis is careful to give the historical context of mathematical tumor modeling and a defense of the need for the model to include evolutionary principals when used in the design and optimization of chemotherapeutic drug schedules.

A fundamental observation of cancer is the upregulation of cell division among malignant cells which leads to the increase in the size of a tumor [1]. This observation led to an explosion of mathematical models with the goal of addressing questions of how tumor size increases over time (see [2] for one summary of historical development of mathematical models of tumor growth). The simplest model of cell division (whereby each cell repeatedly passes through the cell cycle and divides in an unconstrained fashion) is the exponential growth model, implying a constant doubling time for tumors [3]. While shown to be a good model during early tumor growth, long term slowed growth was first addressed in a seminal paper by Laird [4]. A tumor increasing in size contains a proliferating region of a roughly constant width, which means a diminishing fraction of proliferating cells. This fraction doubles at a constant rate, but the overall tumor growth rate is modeled as decreasing at a constant growth rate, known as Gompertzian growth [5].

Later, these growth models were extended to give insight into the effects of chemotherapy [3, 6, 7]. These predictive drug models were pioneered in a clinical setting by Skipper et al. [8] who stated that the relationship between dose and tumor cytotoxicity is linear-log (i.e. exponential decay) [6]. Skipper et al. were the first to develop a set of theoretical laws governing the behavior (and imply the design) of chemotherapy schedules in cancer in the late 1970's [9]. This understanding was later refined by Norton and Simon [7] in the context of Gompertzian growth where the targeted proliferating fraction changes (i.e. decreasing) over time.

## 1.1 Cancer as an evolutionary and ecological process

Yet cancer is an evolutionary and ecological process [10–13]. Ecology is the study of the dynamics of competition within a population of interacting individuals, each with various levels of fitness [10]. In ecological interactions, the competing individuals can be classified into many different types of relationships including competition, parasitism, predation, mutualism, commensalism and amensalism [10]. One of these relationships observed in nature, cooperation (or mutualism) had puzzled evolutionary biologists for many years [14]. As Nowak eloquently explains in his evolutionary dynamics book [15], “In fact, for biology the problem is as old as evolution itself. Evolutionary progress, the construction of new features, often requires the cooperation of simpler parts that are already available. . . . Animals cooperate to form social structures, groups and societies. Worker bees risk their lives to defend the beehive. Moreover they forgo their own reproductive potential and instead raise the offspring of another individual, the queen. In some bird species, helpers assist the parents in feeding their young. Humans cooperate on a large scale, giving rise to cities, states and countries. Cooperation allows specialization. Nobody needs to know everything. But cooperation is always vulnerable to exploitation.” Nowak extensively studied the interplay between cooperation and defection as seen repeatedly in nature and published a book describing methods of applying evolutionary game theory to various biological interactions [15].

Tumor progression can be described by the same phenomena of cooperators (i.e. healthy cells) overtaken by the invasive and exploiting malignant cancer cells. In tumor progression, there is evidence of competition, predation, parasitism, and mutualism between co-evolving

clones [10]. In order to model these evolutionary traits in cancer, many theoretical biologists (including work done in this thesis) have followed Nowak’s approach and turned to a coevolutionary game theory framework to study cancer progression (see [14, 16–20]). Evolutionary game theory provides a framework for analyzing contests (competition) between various species in a population as ‘strategies’ and provides mathematical tools to predict the prevalence of each species over time based on the strategies. Game theory was originally developed by John von Neumann and Oscar Morgenstern in order to predict the optimal strategies in competition [21]. The rules of the game govern the payoff of each player, where the strategy chosen by each player is the approach on how they play the game. Game theory can be extended to model the evolution of interactions between multiple players in a population competing according to predefined strategies in a framework called coevolutionary game theory [22]. In this research, we begin with a well-studied game known as the Prisoner’s Dilemma [23] to model cell-scale competition and kinetics of a malignant tumor.

Studying cancer as a disease of clonal evolution has major implications on tumor progression, prevention and therapy [24, 25]. From an ecological perspective, tumourigenesis is the “process by which the homoeostasis that characterizes a healthy tissue is disrupted either via changes in the tissue microenvironment, or by an invading species (some bacteria and viruses are known to be able to lead to tumourigenesis), or by a local invasion (a resident species producing a brand new one as a result of mutations)” [26]. As such, the need for tumor growth models to include concepts of evolutionary forces such as genetic drift with heritable mutations and natural selection operating on a fitness landscape that is influenced

by tumor microenvironment and the interactions between competing cell types is well documented [27, 28]. Selection will influence the rates of proliferation and survival, which cause the population of cells within a tumor to progress toward more invasive, metastatic, or therapeutic resistant cell types [29, 30].

As mentioned previously, cancer is an evolutionary process which is driven by mutational events and genetic diversification typically arising via waves of clonal and sub-clonal expansions [10, 25]. As a result, the chance of success is low for all but the most well-designed and tailored therapeutic strategies combating tumor growth. In fact, some tumors develop an enhanced ability to resist future therapeutic attacks [31]. In order to avoid drug resistance, chemotherapy has the prospect for greatest impact during the initial stages of tumor progression, before the tumor cell population has been selected for growth and survival, the tumor size is small, and genetic diversification is low [32].

Therapies can work to alter the competition between cancerous and healthy cells by altering the fitness landscape, select for genetic stability, optimize therapy timing, and introduce multi-drug therapies [10]. Math modeling has already been used successfully to better understand the evolutionary nature of therapeutic resistance and relapse in cancer (e.g. [33–35]). This thesis will seek to develop a model of drug resistance and refined therapeutic techniques in the context of primary tumor growth with the future goal of extending some of the same principles to the deadly metastatic phase of cancer.

## 1.2 Chapter Summaries

In chapter 2 of this thesis, the mathematical model is introduced and general features such as neutral drift, the fitness landscape [10, 11], and genetic heterogeneity [36] are described. The Prisoner’s dilemma is introduced as a model of cell-cell interactions (the clonal and subclonal expansion of cancer subpopulations that are competing with the surrounding healthy tissue) and evolution (heritable genetic passenger or driver mutations). A discussion of the model within the context of previously developed mathematical hypotheses such as Gompertzian tumor growth (unperturbed growth) and the Norton-Simon cell kill hypothesis (kinetic resistance to chemotherapy) is presented.

In chapter 3, the model is developed in more detail with a special focus on the role of molecular heterogeneity in the growth of the tumor. We present a statistical mechanics model which focuses on a measure of tumor heterogeneity driving tumor growth. We introduce a metric based on Shannon entropy [37] for quantifying molecular heterogeneity in the Prisoner’s dilemma evolutionary model. Finally, we highlight the need for early detection of cancer in the high growth fraction (highly susceptible to chemotherapeutic drugs) and low diversity growth regimes.

In chapter 4, the model is used to design and test various chemotherapeutic dosing ‘strategies’ including current paradigms used in clinical practice such maximum tolerated dose (MTD) and low dose metronomic chemotherapies (LDM) [38, 39]. All strategies are simulated using the stochastic model, and the Shannon entropy is used as a novel tool to quantify the effectiveness of each strategy in reducing the tumor size. Key results show that LDM chemotherapy strategies can outperform MTD strategies [40]. The advantage

is magnified for fast growing tumors that thrive on long periods of unhindered growth between doses. The effectiveness of LDM-like chemotherapy strategies is negligible after a single cycle but grows after each subsequent cycle of repeated chemotherapy.

In chapter 5, the model is extended to include resistant cell types and the evolutionary phenomenon of competitive release is discussed [41]. Important parameters such as initial fraction of resistance must be noted prior to therapy and traditional metrics like progression-free survival (PFS) are often misleading when describing the effectiveness of a therapy which ultimately fails due to resistance upon recurrence [42]. Finally, a proof of concept of adaptive therapy using the phase portrait to inform bang-bang control is introduced.

In chapter 6, computational methods used to solve stochastic Moran process models for large cell numbers are explained, and chapter 7 outlines future work beyond the scope of this thesis and exciting directions for future research.

### 1.3 Emergent Features

The famous mathematician and historian of science Jacob Bronowski once defined science as “the organization of our knowledge in such a way that it commands more of the hidden potential in nature.” A model is nothing more than a clever organization of knowledge that is used for testing scientific hypotheses. The concept of emergence, or emergent features, describes the properties that result from developing a model formed of its many distinct parts interacting as whole, complex system [43]. While the emergent features are not explicitly modeled or observed within the subsystems or constituent parts of the overall

system, they are viewed as novel properties, functions or behaviors that result by the complex interactions between subsystems. It is useful to study emergent features in modeling biological systems to understand the influence of individual, subsystem parameters on the system-level behavior. Emergent features can also be used as a form of model validation; a model that realizes some biological phenomena on a macro-scale can help uncover the basic mechanisms driving that phenomena [44].

In this thesis, several emergent features resulting from the evolutionary underpinning of tumor kinetics are highlighted. For example, the evolutionary game of the Prisoner’s dilemma reveals the benefits of early detection and early therapy (see chapter 2). The emergence of molecular heterogeneity results in Gompertzian-like growth (see chapter 2). The novel development of Shannon entropy as a tool to quantify drug dosing strategies leads to an emergence of superior performing, high-entropy strategies for fast growing tumors (see chapter 4). The development of models that describe the cost of resistant mutations leads to the counter-intuitive result that drug therapy holidays outperform continuous drug therapy schedules (see chapter 5). The last section will be devoted to a discussion of future goals of continuing work. We believe mathematical models of the type developed in this thesis will play an increasingly important role in identifying and implementing novel chemotherapeutic strategies and will join the arsenal of tools that clinicians will turn to as they continue to develop strategies to fight cancer.

## Chapter 2

# The prisoner's dilemma as a cancer model

Jeffrey West, Zaki Hasnain, Jeremy Mason, Paul K. Newton

The Prisoner's Dilemma as a Cancer Model [45]

Convergent Science Physical Oncology 2:3, 035002 (2016)

## 2.1 Abstract

Tumor development is an evolutionary process in which a heterogeneous population of cells with different growth capabilities compete for resources in order to gain a proliferative advantage. What are the minimal ingredients needed to recreate some of the emergent features of such a developing complex ecosystem? What is a tumor doing before we can detect it? We outline a mathematical model, driven by a stochastic Moran process, in which cancer cells and healthy cells compete for dominance in the population. Each are assigned payoffs according to a prisoner's dilemma evolutionary game where the healthy cells are the cooperators and the cancer cells are the defectors. With point mutational dynamics, heredity, and a fitness landscape controlling birth and death rates, natural selection acts on the cell population and simulated 'cancer-like' features emerge, such as Gompertzian tumor growth driven by heterogeneity, the log-kill law which (linearly) relates therapeutic dose density to the (log) probability of cancer cell survival, and the Norton–Simon hypothesis which (linearly) relates tumor regression rates to tumor growth rates. We highlight the utility, clarity, and power that such models provide, despite (and because of ) their simplicity and built-in assumptions.

## 2.2 Introduction

Cancer is an evolutionary process taking place within a genetically and functionally heterogeneous population of cells that traffic from one anatomical site to another via hematogenous and lymphatic routes [11, 46–49]. The population of cells associated with the primary and metastatic tumors evolve, adapt, proliferate, and disseminate in an environment in which a fitness landscape controls survival and replication [10]. Tumorigenesis occurs as the result of inherited and acquired genetic, epigenetic and other abnormalities accumulated over a long period of time in otherwise normal cells [50, 51]. Before we can typically detect the presence of a tumor, the cells are already competing for resources in a Darwinian struggle for existence in tissues that progressively age and evolve. It is well established that the regenerative capacity of individual cells within a tumor, and their ability to traffic multi-directionally from the primary tumor to metastatic tumors all represent significant challenges associated with the efficacy of different cancer treatments and our resulting ability to control systemic spread of many soft-tissue cancers [52, 53]. Details of the metastatic and evolutionary process are poorly understood, particularly in the subclinical stages when tumors are actively developing but not yet clinically visible [54]. It could be argued that in order to truly understand cancer progression at the level in which quantitative predictions become feasible, it is necessary to understand how genetically and epigenetically heterogeneous populations of cells compete and evolve within the tumor environment well before the tumor is clinically detectable. Additionally, a better understanding of how these populations develop resistance to specific therapies [55, 56] might help in developing optimal strategies to attack the tumor, slow disease progression, or maintain it at a stable level.

Evolutionary game theory is perhaps the best quantitative framework for modeling evolution and natural selection. It is a dynamic version of classical game theory in which a game between two (or more) competitors is played repeatedly, giving each participant the ability to adjust their strategy based on the outcome of the previous string of games. While this may seem like a minor variant of classical (static) game theory, as developed by the mathematicians von Neumann and Morgenstern in the 1940's [57], it is not. Developed mostly by the mathematical biologists John Maynard Smith and George Price in the 1970s [22, 58] and Martin Nowak and Karl Sigmund [59, 60] more recently, this dynamic generalization of classical game theory has proven to be one of the main quantitative tools available to evolutionary biologists (if coupled with a fitness landscape) whose goal is to understand natural selection in evolving populations. In this biological context, a strategy is not necessarily a deliberate course of action, but an inheritable trait [61]. Instead of identifying Nash equilibria, as in the static setting [62, 63], one looks for evolutionary stable strategies (ESS) and fixation probabilities [59, 64] of a subpopulation. This subpopulation might be traced to a specific cell with enhanced replicative capacity (high fitness), for example, that has undergone a sequence of mutations and is in the process of clonally expanding [24]. A relevant question in that case is what is the probability of fixation of that subpopulation? More explicitly, how does one subpopulation invade another in a developing colony of cells?

One game in particular, the Prisoner's Dilemma game, has played a central role in cancer modeling (as well as other contexts such as political science and economics) [14, 16–18, 60, 64–78]. It was originally developed by Flood, Dresher and Tucker in the 1950s as an example of a game which shows how rational players might not cooperate, even if it seems to be in their best interest to do so. The evolutionary version of the Prisoner's

Dilemma game has thus become a paradigm for the evolution of cooperation among a group of selfish individuals and thus plays a key role in understanding and modeling the evolution of altruistic behavior [14, 65]. Perhaps the best introductory discussion of these ideas is found in Dawkins' celebrated book, *The Selfish Gene* [79]. The framework of evolutionary game theory allows the modeler to track the relative frequencies of competing subpopulations with different traits within a bigger population by defining mutual payoffs among pairs within the group. From this, one can then define a fitness landscape over which the subpopulations evolve. The fitness of different phenotypes is frequency dependent and is associated with reproductive prowess, while the ‘players’ in the evolutionary game compete selfishly for the largest share of descendants [64, 78]. Our goal in this article is provide a brief introduction to how the Prisoner’s Dilemma game can be used to model the interaction of competing subpopulations of cells, say healthy, and cancerous, in a developing tumor and beyond.

### **2.3 The prisoner’s dilemma evolutionary game**

An evolutionary game between two players is defined by a  $2 \times 2$  payoff matrix which assigns a reward to each player (monetary reward, vacation time, reduced time in jail, etc.) on a given interaction. Let us call the two players A and B. In the case of a prisoner’s dilemma game between cell types in an evolving population of cells, let there be two subpopulations of cell types which we will call ‘healthy’, and ‘cancerous’. We can think of the healthy cells as the subpopulation that is cooperating, and the cancer cells as formerly cooperating cells that have defected via a sequence of somatic driver

mutations. Imagine a sequence of ‘games’ played between two cells (A and B) selected at random from the population, but chosen in proportion to their prevalence in the population pool. Think of a cancer-free organ or tissue as one in which a population of healthy cells are all cooperating, and the normal organ functions are able to proceed, with birth and death rates that statistically balance, so an equilibrium healthy population is maintained (on average). Now imagine a mutated cell introduced into the population with enhanced proliferative capability as encoded by its genome as represented as a binary sequence of 0’s and 1’s carrying forward its genetic information (which is passed on to daughter cells). A schematic diagram associated with this process is shown in Figure 1. We can think of this cancer cell as a formerly cooperating cell that has defected and begins to compete against the surrounding population of healthy cells for resources and reproductive prowess. From that point forward, one can imagine tumor development to be a competition between two distinct competing subpopulations of cells, healthy (cooperators) and cancerous (defectors). We are interested in the growth rates of a ‘tumor’ made up of a collection of cancer cells within the entire population, or equivalently, we are interested in tracking the proportion of cancer cells,  $i(t)$ , vs. the proportion of healthy cells,  $N - i(t)$ , in a population of  $N$  cells comprising the simulated tissue region.

To quantify how the interactions proceed, and how birth/death rates are ultimately assigned, we introduce the  $2 \times 2$  prisoner’s dilemma payoff matrix:

$$A = \begin{pmatrix} a & b \\ c & d \end{pmatrix} = \begin{pmatrix} 3 & 0 \\ 5 & 1 \end{pmatrix}. \quad (2.1)$$

What defines a prisoner's dilemma matrix are the inequalities  $c > a > d > b$ . The chosen values in (2.1) are relatively standard, but not unique<sup>1</sup>. The essence of the prisoner's dilemma game is the two players compete against each other, and each has to decide what best strategy to adopt in order to maximize their payoff. This  $2 \times 2$  matrix assigns the payoff (e.g. reward) to each player on each interaction. My options, as a strategy or, equivalently, as a cell type, are listed along the rows, with row 1 associated with my possible choice to cooperate, or equivalently my cell type being healthy, and row 2 associated with my possible choice to defect, or equivalently my cell type being cancerous. Your options are listed down the columns, with column 1 associated with your choice to cooperate (or you being a healthy cell), and column 2 associated with your choice to defect (or you being a cancer cell). The analysis of a rational player in a prisoner's dilemma game runs as follows. I do not know what strategy you will choose, but suppose you choose to cooperate (column 1). In that case, I am better off defecting (row 2) since I receive a payoff of 5 instead of 3 (if I also cooperate). Suppose instead you choose to defect (column 2). In that case, I am also better off defecting (row 2) since I receive a payoff of 1 instead of 0 (if I were to have cooperated). Therefore, *no matter what you choose, I am better off (from a pure payoff point of view) if I defect*. What makes this game such a useful paradigm for strategic interactions ranging from economics, political science, biology, and even psychology [58, 65, 78] is the following additional observation. *You will analyze the game in exactly the same way I did (just switch the roles of me and you in the previous rational analysis), so you will also decide to defect no matter what I do.* The upshot if we both defect is that we will each receive a payoff of 1, instead of each receiving a

---

<sup>1</sup>A general investigation of how the values in the PD payoff matrix affects evolutionary dynamics of the subpopulations is addressed in [80].

payoff of 3 if we had both chosen to cooperate. The defect-defect combination is a Nash equilibrium [62, 63], and yet it is sub-optimal for both players and for the system as a whole. Rational thought rules out the cooperate-cooperate combination which would be better for each player (3 points each) and for both players combined (6 points). In fact, the Nash equilibrium strategy of defect-defect is the worst possible system wide choice, yielding a total payoff of 2 points, compared to the cooperate-defect or defect-cooperate combination, which yields a total payoff of 5 points, or the best system-wide strategy of cooperate-cooperate yielding a total payoff of 6 points.

The game becomes even more interesting if it is played repeatedly [78], stochastically [77], and with spatial structure [81] with each player allowed to decide what strategy to use on each interaction so as to accumulate a higher payoff than the competition over a sequence of  $N$  games. In order to analyze this kind of an evolving set-up, a fitness function must be introduced based on the payoff matrix  $A$ . Let us now switch our terminology so that the relevance to tumor cell kinetics becomes clear. When modeling cell competition, one has to be careful about the meaning of the term ‘choosing a strategy’. Cells do not choose a strategy, but they do behave in different ways depending on whether they are normal healthy cells cooperating as a cohesive group, with birth and death rates that statistically balance, or whether they are cancer cells with an overactive cell division mechanism (as triggered by the presence of oncogenes) and an underactive ‘break’ mechanism (as triggered by the absence of tumor suppressor genes) [49]. In our context, it is not the strategies that evolve, as cells cannot change type based on strategy (only based on mutations), but the prevalence of each cell type in the population is evolving, with the winner identified as the sub-type that first saturates in the population.

## 2.4 A tumor growth model

Consider a population of  $N$  cells driven by a stochastic birth-death process as depicted in Figure 2.1, with red cells depicting cancer cells (higher fitness) and blue cells depicting healthy cells (lower fitness, but cooperative). We model the cell population as a stochastic Moran process [82] of  $N$  cells, ' $i$ ' of which are cancerous, ' $N - i$ ' of which are healthy. If each cell had equal fitness, the birth-death rates would all be equal and a statistical balance would ensue. At each step, a cell is chosen (randomly but based on the prevalence in the population pool) and eliminated (death), while another is chosen to divide (birth). If all cells had equal fitness, the birth/death rates of the cancer cells would be  $i/N$ , while those of the healthy cells would be  $(N - i)/N$ . With no mechanism for introducing a cancer cells in the population, the birth/death rates of the healthy cells would be equal, and no tumor would form.

Now, introduce one cancer cell into the population of healthy cells, as shown in Figure 2.1a. At each step, there would be a certain probability of this cell dividing ( $P_{i,i+1}$ ), being eliminated ( $P_{i,i-1}$ ), or simply not being chosen for either division or death ( $P_{i,i}$ ). Based on this random process, it might be possible for the cancer cells to saturate the population, as shown by one simulation in Figure 2.2 depicting  $N = 1000$  cells, with initially  $i = 1$  cancer cell, and  $N - i = 999$  healthy cells. However, the growth curve would not show any distinct shape (Figure 2.2 (black)), and might well become extinct after any number of cell divisions, as opposed to reaching saturation. But we emphasize that without mutational dynamics, heritability, and natural selection operating on the cell population, the shape of the growth curve would look random, and we know this is not how tumors tend to grow [4, 83]. By

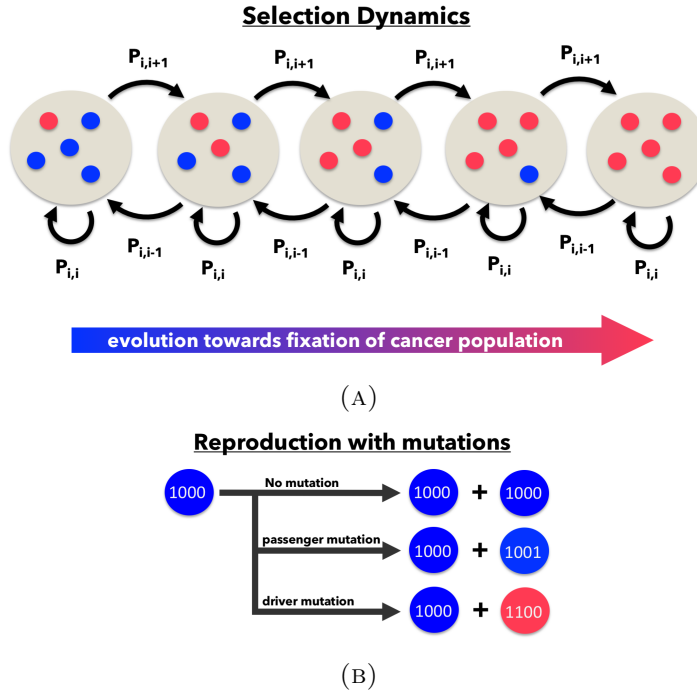
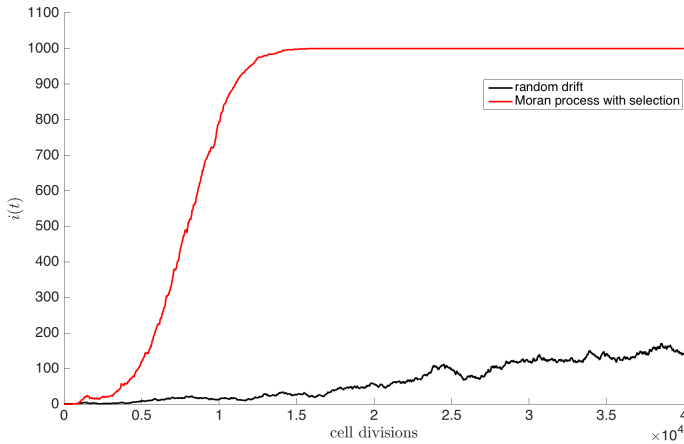


FIGURE 2.1: **Schematic of the Moran Process** — (a) The number of cancer cells,  $i$ , is defined on the state space  $i = 0, 1, \dots, N$  where  $N$  is the total number of cells. The cancer population can change at most by one each time step, so a transition exists only between state  $i$  and  $i - 1$ ,  $i$ , and  $i + 1$ . (b) During each time step, a single cell is chosen for reproduction, where an exact replica is produced. With probability  $m$  ( $0 \leq m \leq 1$ ), a mutation may occur.

contrast, Figure 2.2 (red) shows a Gompertzian growth curve starting with exponential growth of the cancer cell subpopulation, followed by linear growth, ending with saturation. The growth rate is not constant throughout the full history of tumor development, but after an initial period of exponential growth, the rate decelerates until the region saturates with cancer cells. The basic ingredients necessary to sustain Gompertzian growth seem to be: an underlying stochastic engine of developing cells, mutational dynamics, heritability, and a fitness landscape that governs birth and death rates giving rise to some sort of natural selection.



**FIGURE 2.2: Emergence of Gompertzian growth via selection** — Random drift (black) plotted for a single simulation of  $10^3$  cells for  $4 \cdot 10^4$  generations shows no particular shape. A single simulation of the Moran process (red) with selection ( $w = 0.5$ ) and mutations ( $m = 0.1$ ) gives rise to the characteristic S-shaped curve associated with Gompertzian growth.

#### 2.4.1 Mutations and heritability

Each of the  $N$  cells in our simulated population carries with it a discrete packet of information that represents some form of molecular differences among the cells. In our model, we code this information in the form of a 4-digit binary string from 0000 up to 1111, giving rise to a population made up of 16 distinct cell types. At each discrete step in the birth-death process, one of the digits in the binary string is able to undergo a point mutation [50, 84], where a digit spontaneously flips from 0 to 1, or 1 to 0, with probability  $p_m$ . The mutation process is shown in Figure 2.1, while a mutation diagram is shown in Figure 2.3 in the form of a directed graph. This figure shows the possible mutational transitions that can occur in each cell, from step to step in a simulation. A typical simulation begins with a population of  $N$  healthy cells, all with identical binary strings 0000. The edges on the directed graph represent possible mutations that could occur on a given step. The first 11

binary string values (0-10) represent healthy cells in our model that are at different stages in their evolutionary progression towards becoming a cancer cell (the exact details of this genotype to phenotype map do not matter much). Mutations strictly within this subpopulation are called passenger mutations as the cells all have the same fitness characteristics. The first driver mutation occurs when a binary string reaches value 11-15. The first cell that transitions from the healthy state to the cancerous state is the renegade cell in the population that then has the potential to clonally expand and take over the population.

How does this process occur?

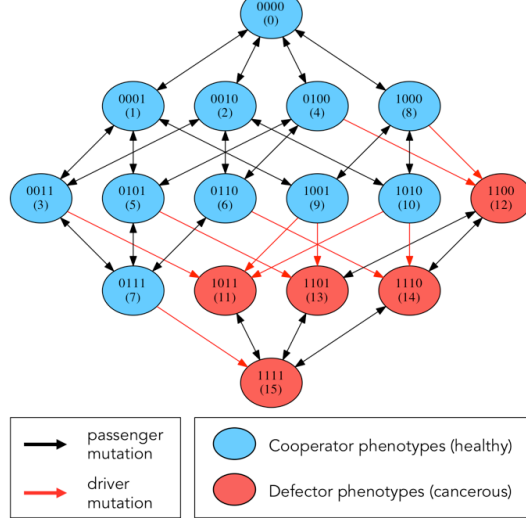


**FIGURE 2.3: Markov Point Mutation Diagram** — Diagram shows 16 genetic cell types based on 4-digit binary string and the effect of a point mutation on each cell type. Blue indicates healthy cell type (0000 — 1010), red indicates cancerous cell type (1011 — 1111). Black arrows indicate passenger mutations (healthy to healthy or cancer to cancer), red arrows indicate driver mutations (healthy to cancer).

#### 2.4.2 The fitness landscape

At the heart of how the Prisoner's Dilemma evolutionary game dictates birth and death rates which in turn control tumor growth, is the definition of cell fitness. Let us start by

laying out the various probabilities of pairs of cells interacting and clearly defining payoffs when there are  $i$  cancer cells, and  $N - i$  healthy cells in the population. The probability that a healthy cell interacts with another healthy cell is given by  $(N - i - 1)/(N - 1)$ , whereas the probability that a healthy cell interacts with a cancer cell is  $i/(N - 1)$ . The probability that a cancer cell interacts with a healthy cell is  $(N - i)/(N - 1)$ , whereas the probability that a cancer cell interacts with another cancer cell is  $(i - 1)/(N - 1)$ .

In a fixed population of  $N$  cells, with  $i$  cancer cells, the number of healthy cells is given by  $N - i$ . The average payoff of a single cell  $(\pi^H, \pi^C)$ , is dependent on the payoff matrix value weighted by the relative frequency of types in the current population:

$$\pi_i^H = \frac{a(N - i - 1) + bi}{N - 1} \quad (2.2)$$

$$\pi_i^C = \frac{c(N - i) + d(i - 1)}{N - 1} \quad (2.3)$$

Here,  $a = 3$ ,  $b = 0$ ,  $c = 5$ ,  $d = 1$  are the entries in the Prisoner's Dilemma payoff matrix (2.1). For the Prisoner's dilemma game, the average payoff of a single cancer cell is always greater than the average payoff for a healthy cell (Figure 2.4c). With the invasion of the first cancer cell, the higher payoff gives a higher probability of survival when in competition with a single healthy cell.

Selection acts on the entire population of cells as it depends not on the payoff, but on the effective fitness of the subtype population. The effective fitness of each cell type ( $f^H$ ,

$f^C$ ) is given by the relative contribution of the payoff of that cell type, weighted by the selection pressure:

$$f_i^H = 1 - w + w\pi_i^H \quad (2.4)$$

and the fitness of the cancer cells as:

$$f_i^C = 1 - w + w\pi_i^C \quad (2.5)$$

The probability of birthing a new cancer cell depends on the relative frequency (random drift) weighted by the effective fitness, and the death rate is proportional to the relative frequency. The transition probabilities can be written:

$$P_{i,i+1} = \frac{if_i^C}{if_i^C + (N-i)f_i^H} \frac{N-i}{N} \quad (2.6)$$

$$P_{i,i-1} = \frac{(N-i)f_i^H}{if_i^C + (N-i)f_i^H} \frac{i}{N} \quad (2.7)$$

$$P_{i,i} = 1 - P_{i,i+1} - P_{i,i-1}; \quad P_{0,0} = 1; \quad P_{N,N} = 1. \quad (2.8)$$

In the event of the first driver mutation, the first cancer cell is birthed. At the beginning of the simulation, the effective fitness of the healthy population is much greater than the

fitness of the cancer population (Figure 2.4b). This is because although the single cancer has a higher *payoff* than any of the healthy cells, the number of healthy cells far outnumber the single cancer cells. That single cancer cell initiates a regime of explosive high growth and the fitness of the cancer population steadily increases. Cancer cells are continually competing with healthy cells and receiving a higher payoff in this regime (compare the payoff entries of a cancer cell receiving  $c = 5$  vs a healthy cell receiving  $b = 0$ ). At later times, growth slows because cancer cells are competing in a population consisting mostly of other cancer cells. The payoff for a cancer cell is dramatically lower when interacting with a cancer cell (observe the payoff entry of both cancer cells receiving  $d = 1$  when interacting). As the cancer population grows, the payoff attainable decreases and growth slows. In addition, the average fitness of the total population steadily declines because each interaction derives less total payoff, from  $c + b = 5$  to  $d + d = 1$ . It is precisely the payoff structure of the Prisoner's Dilemma matrix that produces this declining average population fitness as the cancer cells saturate the population. Although they receive higher payoffs than healthy cells on pairwise interactions, these cancer-healthy interactions mostly take place early on in the evolution of the tumor. As the cancer cells take over the population, most of the interactions take place between pairs of cancer cells (i.e. they eventually start competing with each other) causing the population fitness to decline.

This complex process of competition among cell types and survival of subpopulations, where defection is selected over cooperation, produces a Gompertzian growth curve shown in Figure 2.5, and compared with a compilation based on a wide range of data first shown in [4, 83]. It is now well established that tumor cell populations (and other competing populations, such as bacteria and viral populations) generally follow this growth pattern,

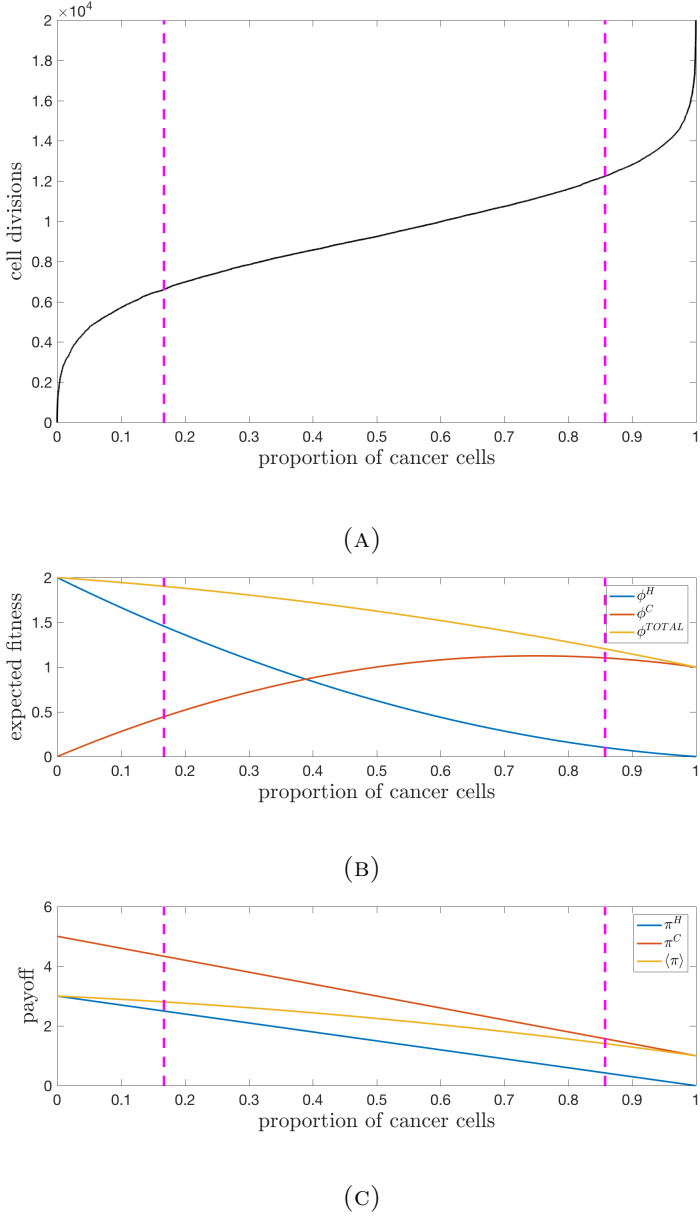
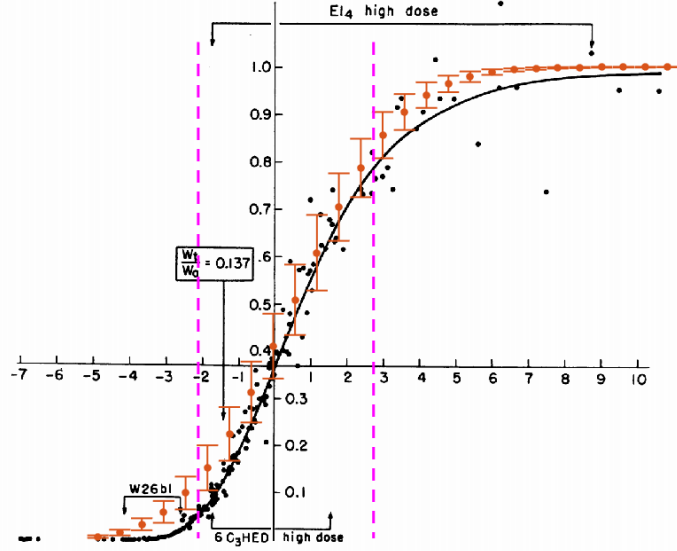


FIGURE 2.4: **Tumor fitness drives tumor growth** — (a) The average of 25 stochastic simulations ( $N = 1000$  cells,  $w = 0.5$ ,  $m = 0.1$ ) is plotted for 20,000 cell divisions to show the cancer cell population (defectors) saturating. The pink lines delineate the regions of tumor growth (defined by the maximum and minimum points of the second-derivative of  $i(t)$ ). (b) Fitness of the healthy population, cancer population, and total population plotted for the range cancer cell proportion. (c) Average payoff of a single healthy cell, cancer cell, and all cells plotted for the range cancer cell proportion.

although the literature is complicated by the fact that different parts of the growth curve have vastly different growth rates [4, 83], and it is nearly impossible to follow the growth

of a population of cancer cells *in vivo* from the first cancer cell through to an entire tumor made up of  $O(10^9 - 10^{12})$  cells. Growth rates are typically measured for a short clinical time period [4, 83], and then extrapolated back to the first renegade cell, and forward to the fully developed tumor population.



**FIGURE 2.5: Moran Process fit to Gompertzian Growth Data** — The mean and deviation of 25 stochastic simulations ( $N = 10^3$  cells,  $w = 0.7$ ,  $m = 0.3$ ) is overlaid on data from a “normalized” Gompertzian [4, 83]. Values for  $m$  and  $w$  were chosen by implementing a least-squares fit to the data over a range of  $m$  ( $0 \leq m \leq 1$ ), and  $w$  ( $0 \leq w \leq 1$ ). Pink lines delineate regions of growth (defined by the maximum and minimum points of the second-derivative of  $i(t)$ ).

#### 2.4.3 Heterogeneity drives growth

Insights into the process by which growth rates vary and conspire to produce a Gompertzian shape can be achieved by positing that growth is related to molecular and cellular heterogeneity of the developing population [36, 48, 85]. Indeed, an outcome of the model is that molecular heterogeneity (i.e. the dynamical distribution of the 4-digit binary string

0000—1111 making up the population of cells) drives growth. Consider entropy [86, 87] of the cell population as a measure of heterogeneity:

$$E(t) = - \sum_{i=1}^N p_i \log_2 p_i \quad (2.9)$$

(here,  $\log$  is defined as base 2). The probability  $p_i$  measures the proportion of cells of type  $i$ , with  $i = 1, \dots, 16$  representing the distribution of binary strings ranging from 0000 to 1111. We typically course-grain this distribution further so that cells having strings ranging from 0000 up to 1010 are called ‘healthy’, while those ranging from 1011 to 1111 are ‘cancerous’. Then growth is determined by:

$$\frac{dn_E}{dt} = \alpha E(t) \quad (2.10)$$

It follows from (3.9) that the cancer cell proportion  $n_E(t)$  can be written in terms of entropy as:

$$n_E(t) = \alpha \int_0^t E(t) dt \quad (2.11)$$

This relationship between growth of the cancer cell population and entropy is pinned down and detailed in [82]. We consider it to be one of the key emergent features of our simple model.

A typical example of the emergence of genetic heterogeneity in our model system is shown in the form of a phylogenetic tree in Figure 2.6. This particular tree is obtained via

a simulation of only 30 healthy phenotypic cells (0000), which during the course of a simulation expand out (radially in time) to form a much more heterogeneous population of cells at the end of the simulation. In our model, the genetic time-history of each cell is tracked and the population can be statistically analyzed after the simulation finishes.

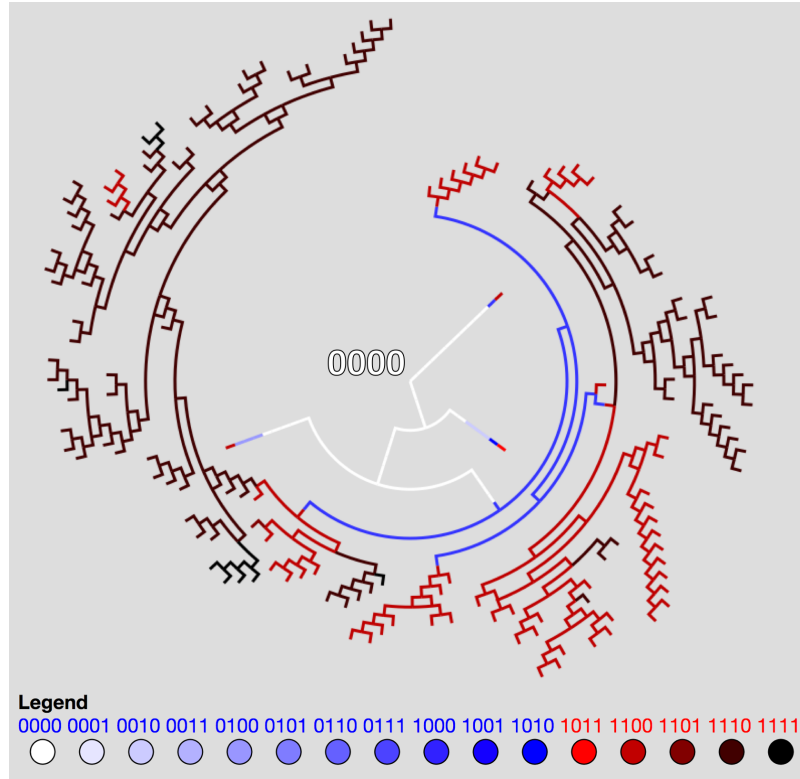


**FIGURE 2.6: Sample Dendritic Phylogenetic Tree** — Sample dendritic phylogenetic tree tracking point mutations as time extends radially, depicting the emergence of molecular heterogeneity. The tree shows a simulation of 30 cells (all with genetic string 0000 at the beginning of the simulation) with strong selection ( $w = 1, m = 0.2$ ). Pathways are color coded to indicate genetic cell type.

## 2.5 Simulated drug dosing strategies and therapeutic response

Figure 2.7 shows the clear advantage of early stage therapy in our model system. We compare the effect of therapy given at an early stage, mid-stage, and late stages of the Gompertzian growth of the tumor. The dashed black Gompertzian curve is the freely growing cancer cell population. In each of the figures, we depict the effect of a range of drug dose densities,  $D$ , where

$$D = c \cdot t. \quad (2.12)$$

The dose density is the product of the drug concentration,  $c$ , and the time over which the therapy is administered,  $t$ , (2.12). Here, the drug concentration value is a weighting ( $0 \leq c \leq 1$ ) which determines the intensity of the drug treatment. A higher value of  $c$  will alter the selection pressure in favor of healthy cells (and to the disadvantage of cancer cells) more dramatically.

Figure 2.7 varies the drug dose density by varying the drug concentrations ( $c = 0.2, 0.4, 0.6, 0.8, 1.0$ ) administered for a constant time ( $t = 5000$  cell divisions, black arrow). The colored curves show the subsequent decline of the cancer cell population under therapeutic pressure. Clearly, to obtain the desired effect of driving the cancer cell population down to manageable levels, one needs to (i) use a sufficient dose density, and (ii) initiate therapy early enough in the growth history. These figures are meant to paint a broad brush with respect to the simulated advantages of early therapy and to show the capability of the model with

respect to addressing questions of this type in a quantitative way. A detailed investigation is left for a separate publication.

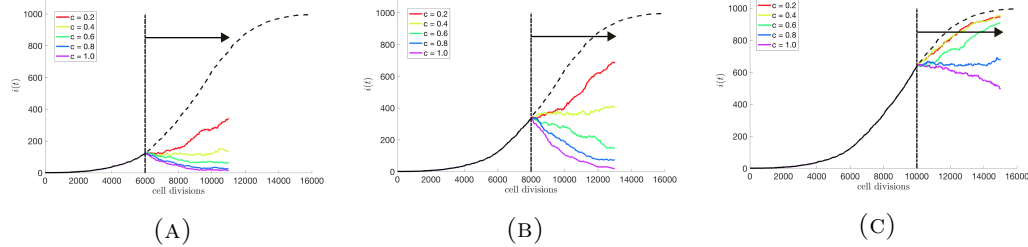


**FIGURE 2.7: Effects of varied dose density for early-stage, mid-stage, and late-stage therapies** — An average of 25 stochastic simulations of unperturbed tumor growth ( $N = 10^3$  cells,  $w = 0.5$ ,  $m = 0.1$ , no therapy) is plotted (black dashed line). The effect of varied drug dose density (eqn. 2.12), is shown by administering a range of drug concentration values ( $c = 0.2, 0.4, 0.6, 0.8, 1.0$ ) for constant length of time ( $t = 5000$  cell divisions, black solid arrows). This process is repeated for (a) high growth, early-stage, (b) linear growth, mid-stage, and (c) slowed growth, late-stage. The kill effect is highest for high drug concentration values (i.e. high dose density) and early therapy.

An established empirical law which relates drug dose density to its effectiveness in killing off cancer cells is known as the ‘log-kill’ law [9]. The log kill law states that a given dose of chemotherapy kills the same fraction of tumor cells (as opposed to the same number of tumor cells), regardless of the size of the tumor at the time the therapy is administered [9], a consequence of exponential growth with a constant growth rate. This effect is best illustrated on a dose-response curve, plotting the dose density,  $D$ , with respect to the probability of tumor cell survival,  $P_S$ . Thus, the log-kill law states the following:

$$\log(P_S) = -\beta D. \quad (2.13)$$

As an example, if there are 1000 cancer cells in a tumor population, and the first therapy dose kills off 90% of them (i.e.  $\beta = 0.9$ ), then after the first round of therapy there will

be 100 cancer cells remaining. If a second round of therapy is administered, exactly as the first round, starting soon enough so that no new cancer cells have formed, then this next round will also kill off 90% of the cells, leaving 10 cells, and so on for each future round of therapy. In a sense, since the first round killed 900 cells, while the second identical round killed only 90 cells, the population gets increasingly more difficult to kill off using the same treatment on each cycle. The log-kill law, a fundamentally static law (it does not say anything about the relationship of the fraction of cells killed vs. the growth rate of the tumor), is verified in our model system, as shown in the dose response curve in Figure 2.8d. On the x-axis, we increase the dose density  $D$ , and we plot the number of surviving cancer cells. The slope of this straight line (verifying the log-kill law) is the rate of regression of the tumor,  $\beta$ . Alternatively,  $\beta$  can be estimated using an exponential fit of  $i(t)$  during therapy (i.e.  $i(t) = i_0 \exp(-\beta(t - t_0))$ ), where  $i_0$  is the initial tumor size and  $t_0$  is the time therapy is initiated).

So how is the rate of regression,  $\beta$ , related to the growth rate of the tumor,  $\gamma$ ? This is relevant, since we know from the shape of the Gompertzian curve, the growth rate is highest (exponential) at the beginning stage of tumor development and lowest at the late saturation stage. Figure 2.8a shows therapy is more effective (i.e. a higher rate of regression,  $\beta$ ) for earlier stage therapy. These early stage therapies correspond to a higher growth rate, shown in 2.8b. The Norton-Simon hypothesis [7, 88, 88] states that the rate of regression is proportional to the instantaneous growth rate for an untreated tumor of that size at the time therapy is first administered. A faster growing tumor (early stage) should show a higher rate of regression than a more slowly growing tumor (late stage). This hypothesis is also verified in our model system, and shown clearly in Figure 2.8c.

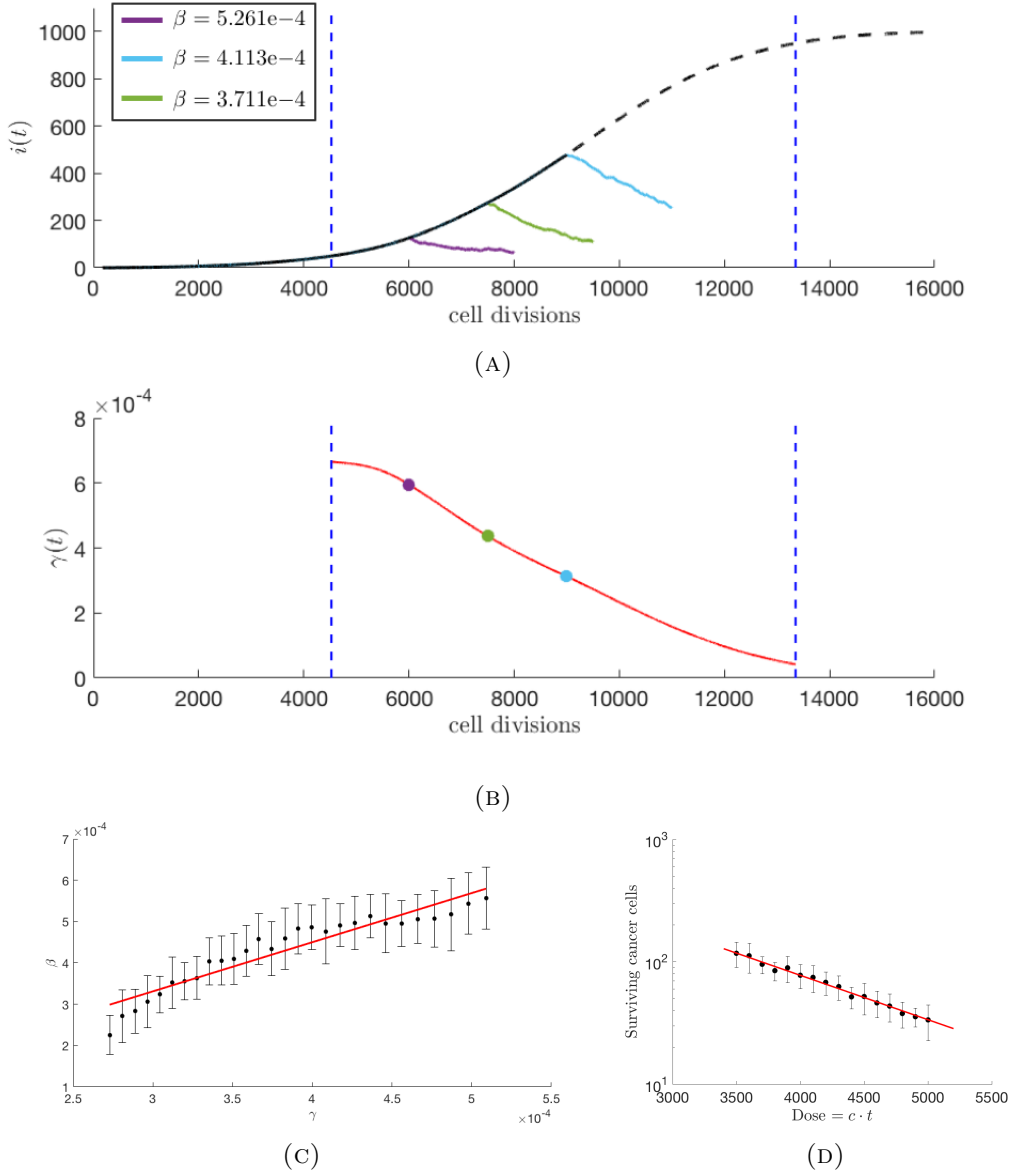


**FIGURE 2.8: Growth-dependent tumor regression** — (a) An average of 25 stochastic simulations of unperturbed tumor growth ( $N = 10^3$  cells,  $w = 0.5$ ,  $m = 0.1$ , no therapy) is plotted (black dashed line) with (b) corresponding instantaneous growth rate,  $\gamma(t)$ , of the unperturbed tumor (red). Tumor regression,  $\beta$ , (estimated using an exponential fit of  $i(t)$  during therapy, shown in legend) during therapy (constant dose density:  $c = 1.0$ ,  $t = 2000$ ) is calculated for a high growth, early-stage therapy (purple), linear-growth, mid-stage therapy (green), and late-stage, slowed growth (light blue); (c) This process is repeated for a full range of growth rates (between vertical blue dashed lines). Average values of  $\beta$  are plotted with standard deviations. Regression is proportional to growth rate (linear fit in red), with higher regression rates associated with high growth rates of early stage tumors. (d) Tumor regression,  $\beta$ , can also be calculated as the slope of a dose response curve (red), where therapy is administered for a range of dose densities ( $0.7 \leq c \leq 1.0$ ) for a single timepoint, 8000 cell divisions (i.e. single growth rate).

The reality of this growth-dependent tumor regression rate effect (where early stage faster growing tumors are more vulnerable to therapy than later stage, slowly growing tumors) dramatically reinforces the need to administer drug treatment early in tumor progression when growth rates are high and there are fewer cancer cells to kill off.

## 2.6 Mathematical modeling and tumor analytics

It is important to keep in mind that no mathematical model captures all aspects of reality, so choices must be made which involve prioritizing the features that are most essential in capturing the essence of a complex process and which are not. Most experts now agree that the evolutionary processes in a tumor played out among subpopulations of competing cells are key to understanding aspects of growth and resistance to chemotherapy, which will ultimately lead the way toward a quantitative understanding of tumor growth and cancer progression [10, 49, 53]. The paradigm of the cancer cell subpopulation and the healthy cell subpopulation competing as the defectors and cooperators in a Prisoner's Dilemma evolutionary game has been useful in obtaining a quantitative handle on many of these processes and frames the problem in an intuitive yet predictive way.

Nonetheless, the mathematical ‘taste’ of the modeler plays a role in what techniques are selected and ultimately where the spotlight shines. This fact makes clinicians uncomfortable and can lead to deep suspicion of the mathematical modeling enterprise as a whole. Aren’t the outcomes and predictions of mathematical models a straightforward consequence of the model assumptions? Once those choices are made, isn’t the cake already baked? So why should we be surprised if you tell us it tastes good? Why not simply use tried and

true statistical tools like regression methods to curve-fit the data directly, with no built in assumptions, and be satisfied with uncovering correlations and trends? Clinicians (and experimentalists, in general) feel that they are dealing directly with reality, so why mess around with ‘toy’ systems based on possibly ‘ad hoc’ or incorrect assumptions that create artificial realities that may or may not be relevant? To a theoretician, calling their assumptions ad hoc, as opposed to natural, is as insulting as calling a clinician sloppy and uncaring (try this for yourself at the next conference you go to! But please use the term ‘somewhat ad hoc’ to lessen the blow.) And if you want to deliver an even harsher insult, you could comment that the model seems like an exercise in curve fitting.

But the usefulness of mathematical models built on simplified assumptions is well established in the history of the physical sciences, as detailed beautifully in Peter Dear’s book, *The Intelligibility of Nature: How Science Makes Sense of the World* [89]. Bohr’s simple model of the structure of the atom was crucial in moving the community forward towards a deeper understanding of cause and effect, and ultimately pushing others to develop more realistic atomic models. The same could be said for many other important, but ultimately discarded models of reality (e.g. the notion of aether used as a vehicle to understand the mysterious notion of action-at-a-distance [89]) now relegated to footnotes in the history of the physical sciences.

Lessons from this history highlight the importance of using the principle of Occam’s razor (law of parsimony) as a heuristic guide in developing models: (1) keep things simple, but not too simple; (2) see what can be explained by using a given set of assumptions, and try to identify what is either wrong or cannot be explained; (3) add complexity to the model, but do this carefully. Since ultimately, the model will always be wrong (with respect to

some well chosen and specific new question being posed about a system), it is important that it be *useful as a vehicle of intelligibility* [89] associated with the set of questions surrounding the phenomena it was built to explain. Answers to some new questions will be found using the model as a temporary crutch, and new questions will emerge in the process that had not yet been asked, as their relevance had never previously been realized. A new quantitative language will emerge in which aspects of the model will be associated with the underlying reality it is attempting to describe, predictions will be easier to frame and test, and shortcomings will be exposed. In his famous article [90], Eugene Wigner writes compellingly that ‘the miracle of the appropriateness of the language of mathematics for the formulation of the laws of physics is a wonderful gift which we neither understand nor deserve. We should be grateful for it and hope that it will remain valid in future research and that it will extend, for better or for worse, to our pleasure, even though perhaps also to our bafflement, to wide branches of learning.’

In general, the more complex the model (as measured, for example, by the number of independent parameters associated with it), the less useful it will be, and the less likely it is to be adopted by the community at large. After all, if the model is as complex as the phenomena it was built to understand, why not stick with reality? Effective models can be thought of as *low-dimensional approximations of reality*, surrogates that help us bootstrap our way forward. They arise as the outcome of a complex balancing act between simplicity of the ingredients, and complexity of the reality the model is meant to describe. They generally do not arise in a vacuum, but are built in the context of informed and sustained discussions among people with different expertise. In the context of medical

oncology, this means physical scientists developing ongoing interactions with clinical oncologists, radiologists, pathologists, molecular and cell biologists and other relevant medical specialists.

Appropriate data is a necessary ingredient in developing and testing any successful model, and treasure troves of medical data sit unexamined in patient files and government databases across the country waiting to be put to good use. There is no doubt that they are telling an interesting and important story that we have yet to fully understand. It is not currently possible for the computer to simulate all of the complex, relevant, and systemic ingredients at play to faithfully recreate all aspects of cancer progression and treatment response in patients. It is hard to imagine that a deep and actionable understanding can ever be obtained without the combined use of data, models, and computer simulations to help guide us and highlight some of the underlying causal mechanisms of this complex and deadly disease.

## Chapter 3

# An evolutionary model of tumor cell kinetics and the emergence of molecular heterogeneity driving Gompertzian growth

Jeffrey West, Zaki Hasnain, Paul Macklin, Paul K. Newton

An Evolutionary Model of Tumor Cell Kinetics and the Emergence of Molecular

Heterogeneity Driving Gompertzian Growth [82]

SIAM Review 58:4, 716-736 (2016)

### 3.1 Abstract

We describe a cell-molecular based evolutionary mathematical model of tumor development driven by a stochastic Moran birth-death process. The cells in the tumor carry molecular information in the form of a numerical genome which we represent as a four-digit binary string used to differentiate cells into 16 molecular types. The binary string is able to undergo stochastic point mutations that are passed to a daughter cell after each birth event. The value of the binary string determines the cell fitness, with lower fit cells (e.g. 0000) defined as healthy phenotypes, and higher fit cells (e.g. 1111) defined as malignant phenotypes. At each step of the birth-death process, the two phenotypic sub-populations compete in a prisoner's dilemma evolutionary game with the healthy cells playing the role of cooperators, and the cancer cells playing the role of defectors. Fitness, birth-death rates of the cell populations, and overall tumor fitness are defined via the prisoner's dilemma payoff matrix. Mutation parameters include passenger mutations (mutations conferring no fitness advantage) and driver mutations (mutations which increase cell fitness). The model is used to explore key emergent features associated with tumor development, including tumor growth rates as it relates to intratumor molecular heterogeneity. The tumor growth equation states that the growth rate is proportional to the logarithm of cellular diversity/heterogeneity. The Shannon entropy from information theory is used as a quantitative measure of heterogeneity and tumor complexity based on the distribution of the 4-digit binary

sequences produced by the cell population. To track the development of heterogeneity from an initial population of healthy cells (0000), we use dynamic phylogenetic trees which show clonal and sub-clonal expansions of cancer cell sub-populations from an initial malignant cell. We show tumor growth rates are not constant throughout tumor development, and are generally much higher in the subclinical range than in later stages of development, which leads to a Gompertzian growth curve. We explain the early exponential growth of the tumor and the later saturation associated with the Gompertzian curve which results from our evolutionary simulations using simple statistical mechanics principles related to the degree of functional coupling of the cell states. We then compare dosing strategies at early stage development, mid-stage (clinical stage), and late stage development of the tumor. If used early during tumor development in the subclinical stage, well before the cancer cell population is selected for growth, therapy is most effective at disrupting key emergent features of tumor development.

### 3.2 Introduction

At the molecular and cellular levels, cancer is an evolutionary process [10, 91, 91, 91] driven by random mutational events [91–94] responsible for genetic diversification which typically arises via waves of clonal and sub-clonal expansions [24, 25], operating over an adaptive fitness landscape in which Darwinian selection favors highly proliferative cell phenotypes which in turn drive rapid tumor growth [4, 95, 96]. The tumor environment should be

viewed as a complex Darwinian adaptive eco-system consisting of cell types which have evolved over many years [10]. As a result, all but the most well designed and tailored therapeutic strategies often deliver disappointing outcomes and potentially introduce a potent new source of selective pressure for the proliferation of variant cells which develop an enhanced ability to resist future therapeutic assaults [56, 97–100]. The prospects for influencing and controlling such a system are likeliest at the emerging early stages of tumor development when the cell population has not yet been selected for growth and survival, and the tumor size is small. But by the time a typical tumor becomes clinically detectable (often after several years of growth), it already contains  $O(10^8)$  or more malignant cells (and potentially occupies a volume of  $1 - 2 \text{ mm}^3$ ), some of which may have entered the blood circulation [95]. Since there is very little human data available in this early subclinical stage of tumor development, computational models can serve as a useful surrogate in this critical developmental stage which clearly influences and determines many important emergent features of the tumor at later stages.

Our goals in this paper are to describe a mathematical model for stochastic cell kinetics in the beginning stages of tumor development (from a single malignant cell) that includes cell reproduction and death, mutations, evolution, and the subsequent emergence of genetic heterogeneity well documented in many soft-tissue tumors [35, 48, 101–107]. The model is a computational one, driven by a stochastic Moran (birth-death) process with a finite cell population, in which birth-death rates are functions of cell fitness. The fitness is determined by the cell’s numerical genome in the form of a four-digit binary string capable of undergoing point mutational dynamics with one digit in the string flipping values stochastically. The corresponding numerical value of the binary string determines whether the cell is

healthy (low-fitness) or cancerous (high fitness). These two classes of cells compete against each other at each birth-death event, with fitness calculated according to the payoff matrix associated with the prisoner’s dilemma evolutionary zero-sum game [14, 15, 18, 22]. The healthy cells play the role of cooperators, while the cancer cells play the role of defectors [14, 15]. Our goal is to understand how the model parameters: passenger ( $m_p$ ) and driver mutation rates ( $m_d$ ), selection strength ( $w$ ), birth and death rates, affect tumor growth characteristics, such as tumor growth rates, fixation probabilities of malignant and healthy cell types, saturation rates of cancer cells, and the emergence of genetic heterogeneity in a tumor at later stages of development when the tumor is clinically detectable.

An important outcome of the model is that growth of the cancer cell population is directly influenced by the intratumor heterogeneity (represented as the distribution of the 4-digit binary strings throughout the cell population), with high heterogeneity driving more rapid growth. The connection between heterogeneity and growth has been discussed in the literature [83, 85, 107–110]. We quantify heterogeneity in a tumor using tools from information theory [37, 87], as well as quantitative analysis of phylogenetic trees associated with clonal and sub-clonal expansions [48, 111] in the developing tumor. Because our numerical simulations are carried out from initial conditions corresponding to a homogeneous population of healthy cells (0000) all the way to a saturated population of cancer cells, we can use the model to test basic dose and scheduling strategies [112, 113] at the very early stages of tumor development in the subclinical range, well before a tumor would be clinically detectable by current technology. Our point of view is that this emerging subclinical tumor should be more amenable (and potentially vulnerable) to a well planned therapeutic assault than a more mature tumor comprised (on average) of larger numbers of cells with

more aggressive proliferative capabilities (having undergone generations of selection), that are potentially in the early stages of migration to other organs. More complex features that might influence early stage dynamics, like human-immune response [108] and the tumor microenvironment [114] are not included in this model in order to keep things as simple and clear as possible.

### 3.3 Description of the model

The ingredients in our model includes a stochastic birth-death process that is the engine which drives tumor growth, with heritable mutations operating over a fitness landscape so that natural selection can play out over many cell division timescales. Genetic mutations (point mutations) are modeled using a four-digit binary string of information that each cell carries with it.<sup>1</sup> This simple sequence divides the cells into 16 different “genotypes”, ranging from 0000 up to 1111, and this information is passed on to the daughter cell during a birth event. The birth-death replacement process is based on a fitness function defined in terms of interactions quantified by the prisoner’s dilemma payoff matrix which operates on two general classes of cells: healthy (the cooperators), and cancerous (the defectors). Natural selection acts on each generation of the cell population as the computational simulation proceeds on a cell division timescale. In this version of the model we typically simulate up to  $O(10^{11})$  cell divisions, so our mutation rates are chosen to be relatively high to

---

<sup>1</sup>To be clear, the four digit sequence is not meant as a bare-bones representation of the full human genome, but as a simple representation of the *relevant differences* in genetic information contained in different cells, allowing us to course-grain the cells into 16 different categories based on their genetic/epigenetic profiles.

accommodate these somewhat modest timescales. See [93] for discussions on mutation rates in cancer.

### 3.3.1 The Moran birth-death process

The stochastic engine [115] that drives tumor growth in our model is a finite cell-based Moran process consisting of a population of  $N$  cells, divided into two sub-populations consisting of  $i$  cancer cells, and  $N - i$  healthy cells. In all of our simulations,  $N$  is large enough so that there is not a significant difference between the results from our finite-cell model and the (deterministic) replicator equation approach for infinite populations, a connection that is discussed in detail in [116]. At each time-step in the simulation, one cell is chosen for reproduction and one cell is chosen for elimination. The cells are chosen randomly, based on their prevalence in the population pool which, in turn, is weighted by the fitness function based on a chosen payoff matrix. The probability of choosing a cancer cell at any given step is  $i/N$ , while the probability of choosing a healthy cell is  $(N - i)/N$ . As it unfolds, the process is a stochastic birth-death process where the total population size,  $N$ , stays constant and the number of cancer cells in the population,  $i$ , is the stochastic state variable. At any given step, the probability of transitioning from  $i$  cancer cells to  $j$  cancer cells is denoted  $P_{ij}$ , with  $j = i + 1$  or  $j = i - 1$ . These probabilities are determined by the birth/death rates associated with the cancer cell population, which in turn are determined by a cell population fitness function. Each cell carries with it a binary string in the form of a four digit binary sequence from 0000 up to 1111. This defines 16 different cell types, which are course-grained into two groups: healthy cells (0000 - 1010), and cancer cells (1011-1111). These two sub-populations interact at each birth-death time-step with

fitness defined in terms of the prisoner's dilemma payoff matrix. The algorithmic details are shown in the appendix Figure 3.10. To set the stage for more complex simulations, Figure 3.1 shows the result of a stochastic simulation (depicting  $i$ ) driven by the Moran process alone, with no mutations, and no selection. Figure 3.1 shows three different simulations, one leading to the elimination of all cancer cells via random drift (red), another fluctuates between a mixed cell population after 10,000 cell divisions (yellow), and a third leading to fixation of the cancer cell population (blue) after around 5000 cell divisions. The average of 25 stochastic simulations is also plotted (note that the average will converge to half cancer cells and half healthy cells by the law of large numbers). The mean time to fixation of the cancer cell population which starts with ' $i$ ' cells in this simple setting (no mutations, no selection) is given by

$$k = N \left[ \sum_{j=1}^i \frac{N-i}{N-j} + \sum_{j=i+1}^{N-1} \frac{i}{j} \right]. \quad (3.1)$$

With no mechanism for natural selection, there is no shape to the growth curves.

### 3.3.2 The prisoner's dilemma payoff matrix

To introduce the effect of selection which will regulate cell birth and death rates, we use the prisoner's dilemma evolutionary game in which two players compete against each other for the best payoff. Each has to decide whether to cooperate (healthy cell) or defect (cancer cell) and each receives a payoff determined from the prisoner's dilemma payoff matrix<sup>2</sup>, A:

---

<sup>2</sup>What defines a prisoner's dilemma matrix are the inequalities  $c > a > d > b$ . The chosen values in (3.2) are relatively standard, but not unique. More discussion of why the prisoner's dilemma matrix, which models the evolution of defection, is a useful paradigm for cancer can be found in [45] and some of the references therein.

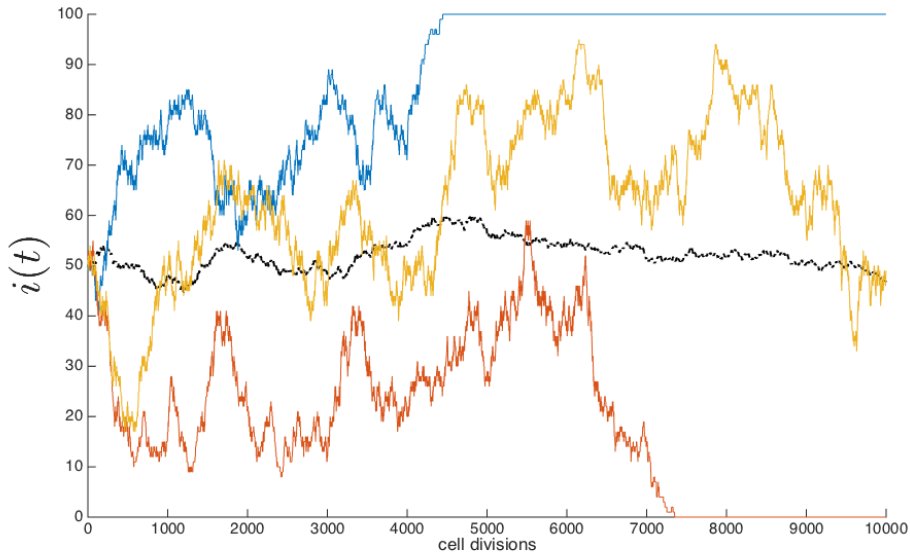


FIGURE 3.1: **Stochastic Moran birth-death process** — Cancer cell population,  $i(t)$ , during three stochastic simulations of the Moran birth-death process in a population of 100 cells and an initial condition of  $i = 50$  cells. The blue curve leads to fixation of the cancer cell population, the red curve leads to elimination of the cancer cell population, and the yellow curve remains fluctuating in a mixed population of cells after 10,000 cell divisions. An average of 25 stochastic simulations (black dashed line) is also plotted.

$$A = \begin{pmatrix} a & b \\ c & d \end{pmatrix} = \begin{pmatrix} 3 & 0 \\ 5 & 1 \end{pmatrix}. \quad (3.2)$$

The essence of the prisoner's dilemma game is the two players compete against each other, and each has to decide what best strategy to adopt in order to maximize their payoff. This  $2 \times 2$  matrix assigns the payoff (e.g. reward) to each player on each interaction. My options, as a strategy or, equivalently, as a cell type, are listed along the rows, with row 1 associated with my possible choice to cooperate, or equivalently my cell type being healthy, and row 2 associated with my possible choice to defect, or equivalently my cell type being cancerous. Your options are listed down the columns, with column 1 associated

with your choice to cooperate (or you being a healthy cell), and column 2 associated with your choice to defect (or you being a cancer cell). The analysis of a rational player in a prisoner's dilemma game runs as follows. I do not know what strategy you will choose, but suppose you choose to cooperate (column 1). In that case, I am better off defecting (row 2) since I receive a payoff of 5 instead of 3 (if I also cooperate). Suppose instead you choose to defect (column 2). In that case, I am also better off defecting (row 2) since I receive a payoff of 1 instead of 0 (if I were to have cooperated). Therefore, *no matter what you choose, I am better off (from a pure payoff point of view) if I defect.* What makes this game such a useful paradigm for strategic interactions ranging from economics, political science, biology [45], and even psychology [15] is the following additional observation. *You will analyze the game in exactly the same way I did (just switch the roles of me and you in the previous rational analysis), so you will also decide to defect no matter what I do.* The upshot if we both defect is that we will each receive a payoff of 1, instead of each receiving a payoff of 3 if we had both chosen to cooperate. The defect-defect combination is a Nash equilibrium [22], and yet it is sub-optimal for both players and for the system as a whole. Rational thought rules out the cooperate-cooperate combination which would be better for each player (3 points each) and for both players combined (6 points). In fact, the Nash equilibrium strategy of defect-defect is the worst possible system wide choice, yielding a total payoff of 2 points, compared to the cooperate-defect or defect-cooperate combination, which yields a total payoff of 5 points, or the best system-wide strategy of cooperate-cooperate yielding a total payoff of 6 points.

The game becomes even more interesting if it is played repeatedly [14, 15, 18, 22], with each player allowed to decide what strategy to use on each interaction so as to accumulate

a higher payoff than the competition over a sequence of  $N$  games. In order to analyze this kind of an evolving set-up, a fitness function must be introduced based on the payoff matrix  $A$ . Let us now switch our terminology so that the relevance to tumor cell kinetics becomes clear. In this case, we randomly select pairs of cells out of the total population at each step, and subject them to a birth-death process, basing our birth rates and death rates on the prisoner's dilemma payoff matrix. Thus, in our context, it is not the strategies that evolve, as cells cannot change type based on strategy (only based on mutations), but the prevalence of each cell type in the population is evolving, with the winner identified as the sub-type that first reaches fixation in the population. As the populations evolve, the fitness of the two competing sub-populations can be tracked, as well as the overall fitness of the combined total population of cells.

### 3.3.3 The fitness landscape

Let us start by laying out the various probabilities of pairs of cells interacting and clearly defining payoffs when there are  $i$  cancer cells, and  $N - i$  healthy cells in the population. The probability that a healthy cell interacts with another healthy cell is given by  $(N - i - 1)/(N - 1)$ , whereas the probability that a healthy cell interacts with a cancer cell is  $i/(N - 1)$ . The probability that a cancer cell interacts with a healthy cell is  $(N - i)/(N - 1)$ , whereas the probability that a cancer cell interacts with another cancer cell is  $(i - 1)/(N - 1)$ . The payoffs associated with the healthy cells and cancer cells, obtained by weighting the payoff matrix values with appropriate probabilities, are given by (following notation in [116]):

$$\pi^H = \frac{3(N-i-1) + 0i}{N-1}, \quad (3.3)$$

$$\pi^C = \frac{5(N-i) + 1(i-1)}{N-1}. \quad (3.4)$$

This gives rise to the average payoff associated with the population of cells:

$$\langle \pi \rangle = \frac{\pi^H(N-i) + \pi^C(i)}{N}. \quad (3.5)$$

Based on these formulas, we define the fitness of the healthy cells as:

$$f^H = 1 - w_H + w_H \pi^H, \quad (3.6)$$

and the fitness of the cancer cells as:

$$f^C = 1 - w_C + w_C \pi^C. \quad (3.7)$$

Here,  $(w_H, w_C)$  are ‘selection strength’ parameters,  $0 \leq w_H \leq 1, 0 \leq w_C \leq 1$ , that measure the strength of selection pressure on each of the population of cells. If  $w_H = 0$ , there is no natural selection acting on the healthy cell population and the dynamics is driven purely by the Moran process. When  $w_H = 1$ , the selection pressure on the healthy cell population is strongest and the prisoner’s dilemma payoff matrix has maximum effect. Likewise for the

parameter  $w_C$  and how it controls selection pressure in the cancer cell population. Since therapy imposes selection pressure on different sub-populations of cells,  $w_H$  and  $w_C$  are the two parameters we alter to administer simulated therapeutic responses. We discuss this in section §3.5.

The expected fitness of each of the sub-populations are:

$$\phi^H = \frac{N-i}{N} f^H, \quad (3.8)$$

$$\phi^C = \frac{i}{N} f^C, \quad (3.9)$$

with total expected fitness:

$$\phi = \phi_i^H + \phi^C. \quad (3.10)$$

From these formulas, we can define the transition probability of going from  $i$  to  $i+1$  cancer cells on a given step:

$$P_{i,i+1} = \frac{if^C}{if^C + (N-i)f^H} \frac{N-i}{N}. \quad (3.11)$$

The first term represents that probability that a cancer cell is selected for reproduction (weighted by fitness), and a healthy cell is selected for death. Likewise, the transition probability of going from  $i$  to  $i - 1$  cancer cells on a given step is:

$$P_{i,i-1} = \frac{(N-i)f^H}{if^C + (N-i)f^H} \frac{i}{N}. \quad (3.12)$$

Here, the first term is the probability healthy cell is selected for reproduction (weighted by fitness), and a cancer cell is selected for death. The remaining transition probabilities are as follows:

$$P_{i,i} = 1 - P_{i,i+1} - P_{i,i-1}; \quad P_{0,0} = 1; \quad P_{N,N} = 1. \quad (3.13)$$

It is these simple formulas that drive the subsequent dynamics of the competing populations of cells and determine the emergent features of the forming tumor (cancer cell population). A typical set of simulations of the evolving fitness of the healthy cell population,  $\phi_H$ , the cancer cell population  $\phi_C$ , and the total fitness,  $\phi$ , is shown in Figure 3.2 as the selection parameter varies from 0 to 1 ( $w_H = w_C \equiv w$ ). As the population evolves, the fitness of the healthy cell population decreases, the fitness of the cancer cell population increases (sometimes reaching a maximum point), while the total population fitness decreases.

### 3.3.4 Passenger and driver mutations

Two remaining parameters in our model are the passenger mutation rate,  $m_p$  and the driver mutation rate,  $m_d$  [93]. Passenger mutations confer no fitness advantage, hence  $m_p$  controls point mutations that act on the digit strings that define the 11 levels of healthy cells 0000-1010, and the 5 levels of cancer cells 1011-1111. A mutation diagram is shown in Figure 3.3 depicting all of the possible point mutation transitions at each step. Mutations

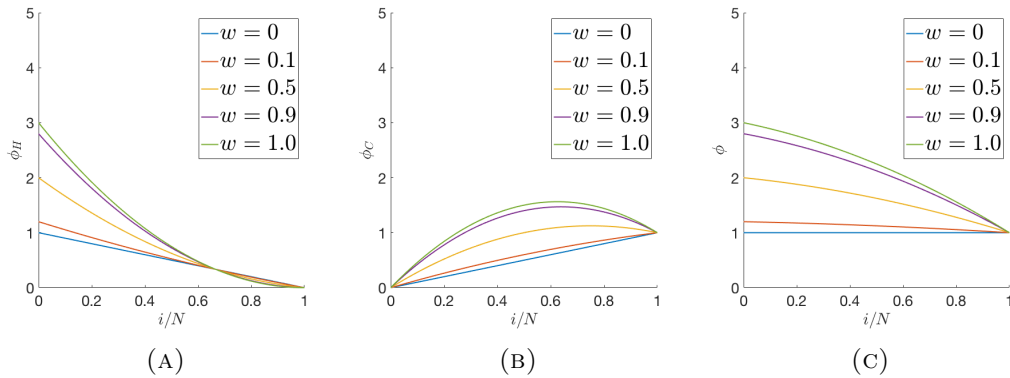


FIGURE 3.2: **Fitness as a function of the selection parameter  $w \equiv w_H \equiv w_C$**  — (a) Monotonically decreasing fitness of healthy cell sub-population  $\phi_H$ ; (b) Fitness of cancer cell sub-population  $\phi_C$ . Note that  $\phi_C$  has a maximum at  $i = \frac{N}{2} + \frac{(N-1)}{8w}$ , which is between 0 and  $N$  for  $w > \frac{1}{4}(1 - 1/N)$ ; (c) Monotonically decreasing fitness of the total population,  $\phi$ .

that stay within either of those two ranges do not alter the cell fitness. On the other hand, the driver mutation parameter controls mutations that take a binary string from a healthy cell and, via a point mutation, alter it so that the string becomes a cancer cell<sup>3</sup>. A simple example would be a mutation that alters 1010 (healthy) to 1011 (cancer) by stochastically flipping the first digit from 0 to 1. The interested reader can consult the flow diagram in Figure 3.10 of the Appendix for more details of the algorithm. The full code is available from the authors upon request.

### 3.4 Results

Gompertzian growth arising from multicellular systems occurs in many settings with different physical and biological constraints acting in concert. Hence it appears as if this

<sup>3</sup>In our simulations, we assume that driver mutations cannot revert to passenger mutations, i.e. once a cancer cell is born, it stays in that category. We do not know of any evidence in the literature that shows the reversion of a cancer cell to a healthy cell, nor is this particularly a focus of this manuscript.

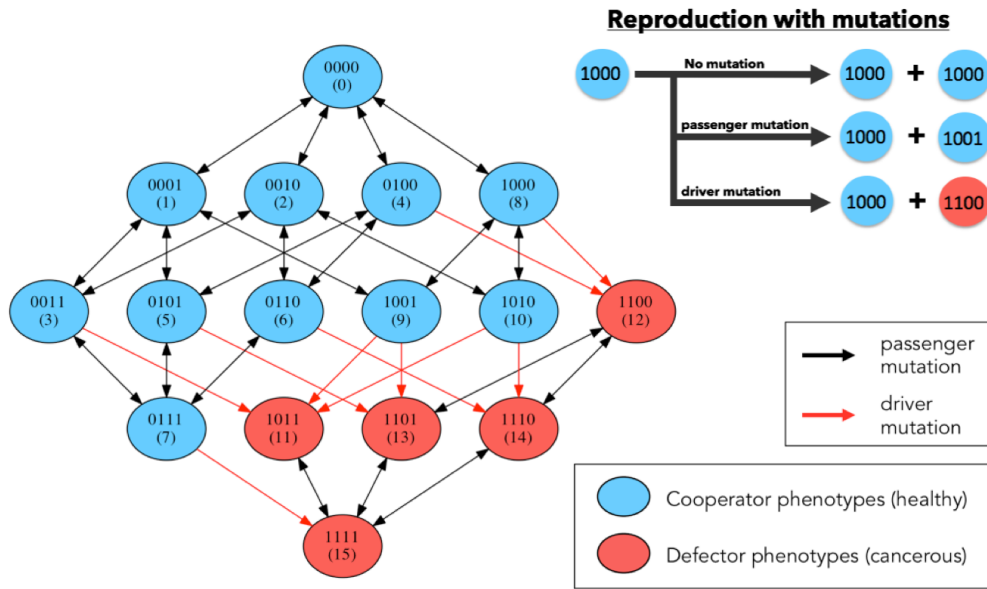


FIGURE 3.3: **Markov Point Mutation Diagram** — Left: diagram shows 16 genetic cell types based on 4-digit binary string and the effect of a point mutation on each cell type. Blue indicates healthy cell type (0000 — 1010), red indicates cancerous cell type (1011 — 1111). Black arrows indicate passenger mutations (healthy to healthy or cancer to cancer), red arrows indicate driver mutations (healthy to cancer). Top right: 3 scenarios may occur during the reproduction process: no mutation, passenger mutation, or driver mutation.

universal growth curve does not depend on specific physical mechanisms (e.g. oxygen diffusion, blood supply, tumor microenvironment, etc.) but more on multi-cellularity and the ability for populations of cells to assume a heterogeneous distribution of functional states, as was described most clearly in Kendal's 1985 paper [85] and documented clinically in breast [113] and other tumor types. Alternative bio-mechanistic models of tumor growth at the cellular level have been developed (see [114, 117–121]) although do not generally include molecular information or evolutionary effects. Features of the Gompertzian growth curve defined by eqns (3.14), (3.15) allow us to clearly describe three distinct growth regimes, the earliest being subclinical and the most critical regime in which to influence future tumor kinetics, the second being the clinical regime where growth measurements

are typically obtained [95], and the third being the lethal burden phase where growth saturates. The growth equation, (3.22), relates tumor heterogeneity to growth rates, and we quantify heterogeneity via the Shannon entropy [37, 87] of the cellular population. One of the main features of our evolutionary simulations is to show how it (i) leads to Gompertzian growth, (ii) how growth is driven by heterogeneity quantitated via Shannon entropy, (iii) how the initiation of heterogeneity and fitness can be tracked via dynamic phylogenetic trees, and (iv) how tumor kinetics can be influenced via therapeutic strategies that target heterogeneity best in earlier growth regimes. In keeping consistent with the notation of the Gompertzian growth curve, we now represent the tumor growth as the proportion of cancer cells in the population,  $n_G(t)$ .

### 3.4.1 Gompertzian tumor growth and three growth regimes

The basic (top-down) equations giving rise to pure Gompertzian growth [122–125] are the coupled equations:

$$\frac{dn_G}{dt} = \gamma n_G, \quad (3.14)$$

$$\frac{d\gamma}{dt} = -\alpha\gamma. \quad (3.15)$$

Here, is the proportion of growing cancer cells in the mixed population, which grows exponentially according to (3.14), but with a time-dependent growth rate which is exponentially decaying according to (3.15). It is straightforward to integrate (3.14) to obtain:

$$n_G(t) = N_0 \exp \left[ \left( \frac{1}{t} \int_0^t \gamma dt \right) \cdot t \right]. \quad (3.16)$$

Then, (3.15) is solved with:

$$\gamma(t) = \gamma_0 \exp(-\alpha t). \quad (3.17)$$

Plugging (3.17) into (3.16) and integrating yields the Gompertzian curve:

$$n_G(t) = N_0 \exp \left[ \frac{\gamma_0}{\alpha} (1 - \exp(-\alpha t)) \right], \quad (3.18)$$

where in the long-time limit , the population saturates to the value

$$n_\infty = N_0 \exp(\gamma_0/\alpha), \quad (3.19)$$

which we normalize to one (without loss of generality). The key features of Gompertzian growth are shown in Figure 3.4. As the cancer cell proportion  $n_G(t)$  increases (Figure 3.4a), there are three distinct growth regimes defined by the inflection point on the  $n_G$  growth curve (maximum of  $\dot{n}_G$  and  $d^2 n_G/dt^2 = 0$ ), and the two inflection points on the growth-velocity curve  $\ddot{n}_G$  (maximum/minimum of  $\ddot{n}_G$  and  $d^3 n_G/dt^3 = 0$ ). As shown in Figure 3.1(a), there are three points that divide the growth curve into four distinct regions. For convenience, and symmetry, we lump the second and third regions together and define three basic growth regimes:

- **Regime 1 (Subclinical):** Increasing velocity  $\dot{n}_G$ , increasing acceleration  $d^2n_G/dt^2$ .  
Cell population and tumor volume grows at an exponential rate;
- **Regime 2 (Clinical):** In this regime,  $\dot{n}_G$  reaches its maximum value. In the early part of the regime,  $\dot{n}_G$  is increasing while  $d^2n_G/dt^2$  decreases. In the later part of the regime,  $\dot{n}_G$  is decreasing and  $d^2n_G/dt^2$  becomes negative (deceleration). Growth rates are clinically typically measured as linear;
- **Regime 3 (Saturation/Lethal):** Decreasing tumor velocity  $\dot{n}_G$  with decreasing deceleration. Growth rate rapidly slows towards full saturation of the cancer cell population.

Regime 1, generally speaking, is the subclinical growth regime where the developing tumor has substantially fewer than  $10^8$  malignant cells with a tumor size smaller than 1 or 2  $\text{mm}^3$ . Typically, the clinically measurable regime is Regime 2, while the lethal stage when the tumor saturates is associated with Regime 3. In reality, the boundaries of these regimes are, of course, not sharp and depend on tumor type and location which influence detectability. But the clarity of the pure Gompertzian curve gives a useful framework which delineates the three distinct growth regimes based on clear principles associated with growth, velocity, and acceleration. The growth rate curve is shown in Figure 3.4c, with its derivatives shown in Figure 3.4d. It is most instructive to show the average growth rates defined in each of the three regimes, also shown in the Figure 3.4c. The average growth rate in the time interval from  $t_1$  to  $t_2$  is defined as:

$$\gamma_{ave} = \frac{1}{t_2 - t_1} \int_{t_1}^{t_2} \gamma(t) dt \quad (3.20)$$

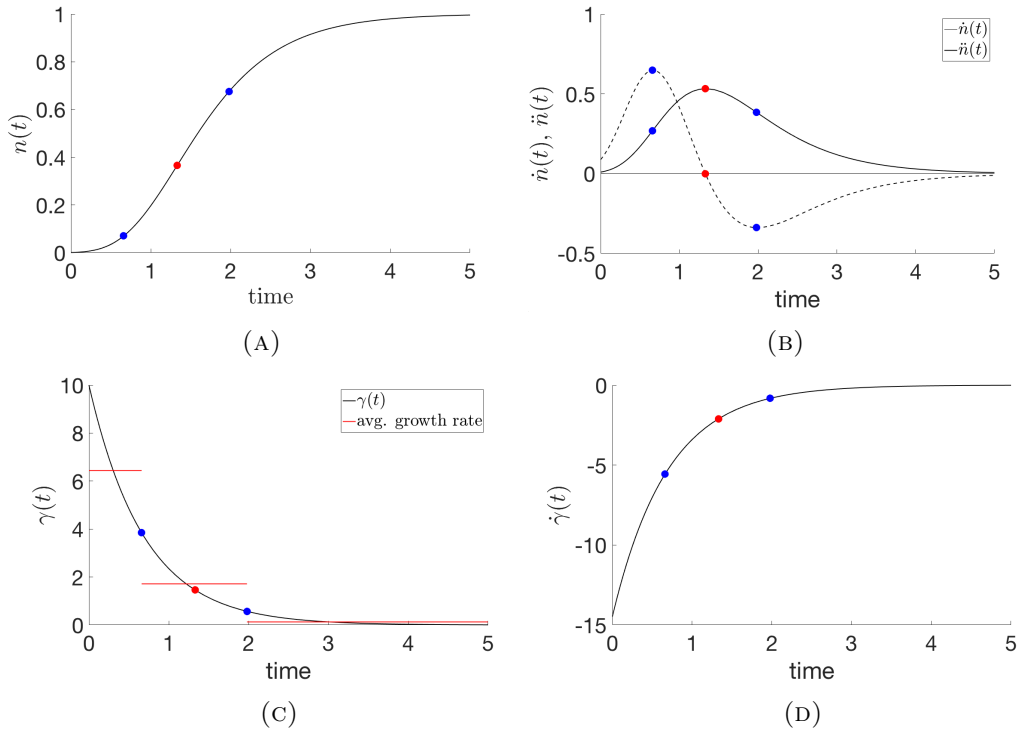


FIGURE 3.4: **Gompertzian equation** — Numerical simulation of the Gompertzian equation (3.14), (3.15) with parameters  $N_0 = 0.001$ ,  $\gamma_0 = 10$ , and  $\alpha = 0.2895$ . The three regimes of tumor growth are demarcated by the blue dots in each subfigure, representing the maximum and minimum of the second-derivative. (a) Cancer cell proportion,  $n(t)$ , over time; (b) First- and second-derivatives of the tumor growth curve; (c) Growth rate,  $\gamma(t)$ , over time, with the average growth rate in regimes 1, 2, 3 plotted in red; (d) First derivative of growth rate.

The subclinical regime 1 has the highest average growth, whereas regime 2, where tumor growth is typically measured, average growth rates are lower, followed by the lowest average growth in the clinically lethal regime 3. This implies that clinically measured growth rates typically *underestimate* growth rates that preceded it in the subclinical stage. It also implies that linear extrapolation back from clinically measured growth rates to estimate tumor initiation times (see [4, 95, 96]) will systematically overestimate the amount of time the tumor has been developing before being measured. While this might generally be seen as good news (since the cancer initiation event was more recent than estimated via linear

extrapolation), it also gives the clinician a shorter window of time in which to act.

### 3.4.2 Heterogeneity and growth via statistical mechanics

Kendal [85] lays out a clear argument of how this growth curve arises from a purely statistical mechanics point of view. In a nutshell, his argument can be explained by considering a population of  $n$  cells, let the  $j$ th cell ( $j = 1, 2, 3, \dots, n$ ) have the potential to assume one of  $q_j$  possible states. The number of combinations of states possible within the population,  $P$ , can be thought of as a measure of intra-neoplastic diversity:

$$P = q_1 q_2 q_3 \dots q_n, \quad (3.21)$$

and is related to the growth rate of a tumor via the equation:

$$\frac{dn}{dt} = \alpha \log P, \quad (3.22)$$

where  $n(t)$  is the number of cells capable of proliferation at a given time  $t$  and  $\alpha$  is a parameter that sets the timescale of growth <sup>4</sup>. There are two basic cases to consider. First, suppose the cells have no interaction at all, say in the earliest stages of tumor development,

---

<sup>4</sup>Kendal's formulation [85] assumes a cell population made up of three sub-groups: (1) proliferative cells; (2) nonproliferative and nonclonogenic cells; (3) nonproliferative but clonogenic cells, with an assumption that the neoplasm's growth rate is influenced by the proportion of proliferating to nonproliferating cells and an expression of each clone's growth potential. The log is chosen based on the fact that heterogeneity is measured as the multiplicative combination of achievable states in the tumor, and the requirement that  $G(P_1 \cdot P_2) = G(P_1) + G(P_2)$  for any two sub-populations  $P_1, P_2$  and growth function  $G$ . The discussion of the relationship between tumor heterogeneity and growth is an ongoing topic in the current literature [48, 101, 102, 104, 106].

and let each of the  $n$  cells have the ability to assume one of  $m$  possible states. Then,

$P = m^n$ , and the growth equation becomes

$$\frac{dn}{dt} = \alpha n \log m = (\alpha \log m)n. \quad (3.23)$$

The solution to this equation is the exponentially growing population:

$$n(t) = N_0 \exp((\alpha \log m)t). \quad (3.24)$$

Thus, early stage development is characterized by exponential growth (regime 1), with a growth rate proportional to the log of the number of assumable states of the cells comprising the tumor population. This stage is characterized by the Gompertzian curve shown in Figure 3.4a to the left of the first blue dot, in regime 1. Contrast this with later stages of tumor growth, when the sub-populations of cells communicate and influence each other's growth characteristics, either via competition, or cooperation (regime 3) within the tumor microenvironment. In effect, this will constrain (reduce) the number of assumable states of each cell, since the population is effectively coupled. In the extreme, suppose  $P = m^n/n^n$ . In other words, suppose  $P$  is now inversely related to the total number of possible intercellular interactions. Inserting this into (3.22) yields

$$\frac{dn}{dt} = \alpha \log \left( \left( \frac{m}{n} \right)^n \right) = \alpha n [\log m - \log n]. \quad (3.25)$$

$m_d$	$m_p$	$t_{Emax}$	$t_{SAT}$	$n_d$	$n_p$	$\gamma_{ave,1}$	$\gamma_{ave,2}$	$\gamma_{ave,3}$
0.4	0.1	5.50e+5	1.830e+6	1.289e+4	4.68e+4	3.14e-5	3.68e-6	1.448e-7
0.3	0.2	4.88e+5	1.753e+6	1.682e+4	8.26e+4	4.04e-5	4.31e-6	1.677e-7
0.2	0.3	4.85e+5	1.761e+6	1.715e+4	1.230e+4	3.86e-5	4.41e-6	1.729e-7
0.1	0.4	5.40e+5	1.426e+6	1.362e+4	1.836e+4	3.04e-5	3.81e-6	1.658e-7

TABLE 3.1:  $m_d$ : driver mutation rate;  $m_p$  : passenger mutation rate;  $t_{Emax}$ : time to maximum entropy;  $t_{SAT}$ : time to saturation;  $n_d$ : number of driver mutations;  $n_p$ : number of passenger mutations;  $\gamma_{ave,1}$ : average growth rate in regime 1;  $\gamma_{ave,2}$ : average growth rate in regime 2;  $\gamma_{ave,3}$ : average growth rate in regime 3.

The solution to this equation is exactly the Gompertzian growth curve (3.18) and accounts for regimes 2 and 3 previously discussed in which tumor growth slows down. The growth equation (3.22) which relates cancer cell population growth to tumor heterogeneity is capable of producing a family of growth curves, depending on details of intercellular coupling, which of course is influenced by details of the biological and physical constraints influencing the tumor microenvironment. Thus, the growth equation (3.22) has the ability to produce different detailed shapes based on assumptions associated with intercellular coupling. Table 3.1 shows the average growth rates in the three regimes as a function of the key parameters in the model.

### 3.4.3 Quantitative measures of tumor heterogeneity and growth

For our purposes, we measure heterogeneity using the Shannon entropy from information theory [37]:

$$E(t) = - \sum_{i=1}^N p_i \log_2 p_i, \quad (3.26)$$

(here, log is defined as base 2). The probability  $p_i$  measures the proportion of cells of type  $i$ , with  $i = 1, \dots, 16$  representing the distribution of binary strings ranging from 0000 to 1111. We then course-grain this distribution further so that cells having strings ranging from 0000 up to 1010 are called “healthy”, while those ranging from 1011 to 1111 are “cancerous”<sup>5</sup>. The growth equation (3.22) then becomes

$$\frac{dn_E}{dt} = \alpha E(t). \quad (3.27)$$

It follows from (3.27) that the cancer cell proportion  $n_E(t)$  can be written in terms of entropy as:

$$n_E(t) = \alpha \int_0^t E(t) dt. \quad (3.28)$$

The panel in Figure 3.5 shows the results from our cell-based simulations. Figure 3.5a shows the Gompertzian curve associated with the proportion of cancer cells in the population, while Figure 3.5b shows the velocity and accelerations associated with growth, and can be compared with Figure 3.4b. In Figure 3.5c we show the entropy during a typical simulation, marking the maximum entropy point which peaks relatively early in the simulation before the entropy returns back down to zero, reflecting the fact that cancer cells have reached fixation and have saturated the population. Figure 3.5d shows the fitness of the cancer cell sub-population, healthy cell sub-population, and the overall tumor fitness ( $w_H = w_C \equiv w = 0.5$ ). As a typical simulation proceeds, the cancer cell sub-population fitness increases,

---

<sup>5</sup>Our results are relatively insensitive to where we draw the dividing line between healthy and cancerous.

the healthy cell sub-population fitness decreases, while the overall tumor fitness decreases.

Figure 3.5e, 3.5f shows the Gompertzian growth curves as the selection pressure increases (Figure 3.5e) and as the mutation rate increases (Figure 3.5f). High values for either of these parameters leads to a very steep growth curve, as is expected.

Figure 3.6 shows the growth curves linearly extrapolated back to give a prediction of when the first driver mutation occurred that initiated tumor growth. The growth rates from regime 2 (linear regime) are used to extrapolate back to the initiation event. Since the actual growth rate in regime 1 is much faster than linear, the linear extrapolation extends the event too far back in time as compared to when the event actually occurred. The inset of Figure 3.6 shows histograms of the average growth rates in each of the three regimes as a function of the mutation rate  $m$  (here, we take  $m_p = m_d = m$ ).

A typical stochastic simulation showing the evolution of all 16 possible cell types is shown in Figure 3.7. We also show  $E(t)$ , where entropy is computed using the most extreme coarse-grained two-state system comprised of the two sub-populations of healthy cells and cancer cells. We compare in Figure 3.7 the Gompertzian growth curve (eqn. (3.18)) and the corresponding curve obtained from eqn. (3.28) to the stochastic simulation and the agreement is excellent. Likewise, we also show a comparison of  $dn/dt$  with eqn. (3.27) and eqn. (3.14) with  $E(t)$  normalized so that limiting values match the stochastic simulation, and the agreement is also excellent. In the beginning, entropy is zero, since the population consists purely of healthy cells, and in the end of the simulation, entropy is again zero as the population consists purely of cancer cells. Entropy peaks somewhere early in the simulation when the mixture of cell types is equally distributed over cancer and healthy

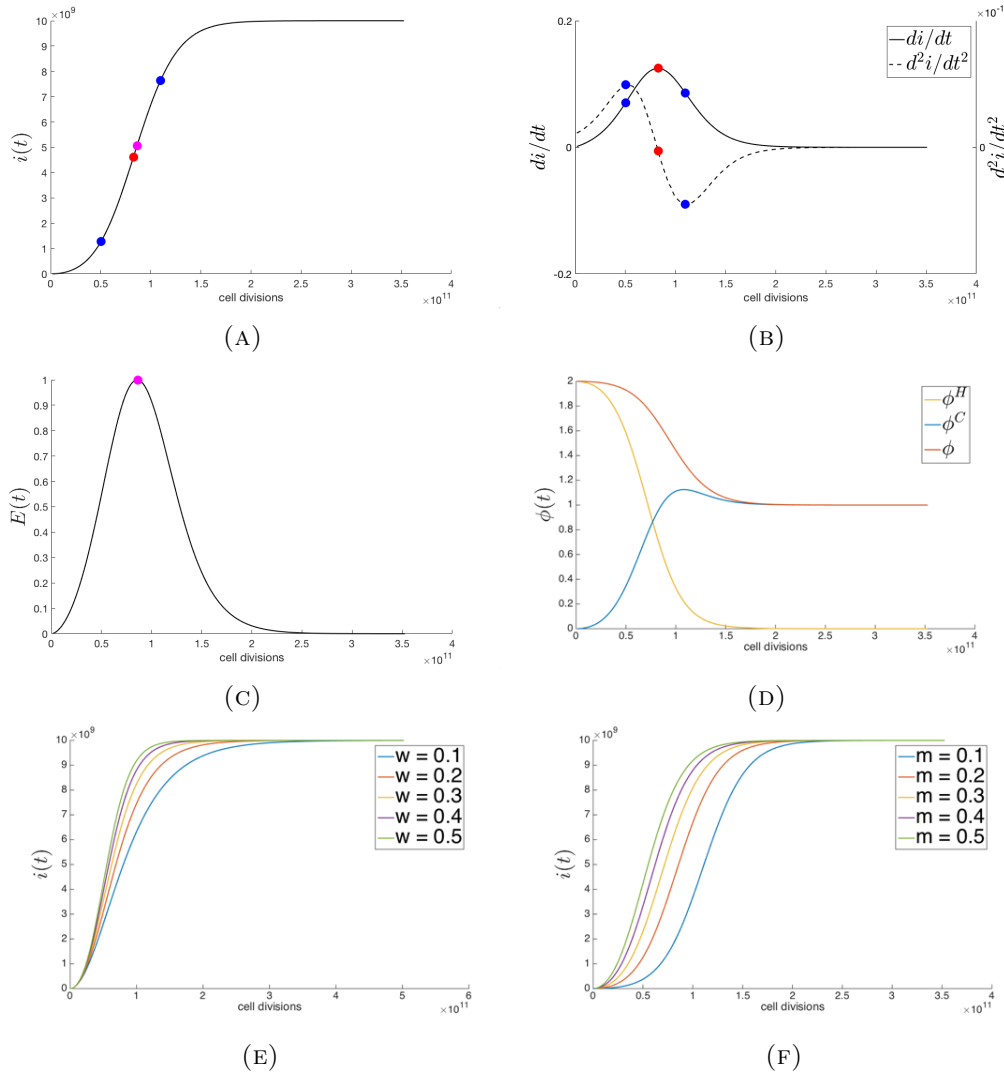


FIGURE 3.5: **Moran birth-death process with selection** — (a) Cancer cell population,  $i(t)$  ( $w = 0.5$ ,  $m = 0.2$ ,  $N = 10^{10}$ ) plotted with a spline curve connecting 200 data points from a single stochastic simulation; (b) First- and second-derivatives of the tumor growth curve in (a) are plotted with maximum and minimum of second-derivative indicated (blue); (c) Entropy of the cell population from eqn. (3.26) as it relates to the growth equation (3.27); (d) Fitness of healthy cell population and cancer cell population and total fitness as defined by eqns. (3.8), (3.9), (3.10); (e) Simulations of cancer cell population,  $i(t)$ , for a range of selection parameter values; (f) Simulations of cancer cell population,  $i(t)$ , for a range of mutation rate values.

types. It is this intermediate but important heterogeneously distributed state that is the key driver of growth, as is clear from eqn. (3.27).

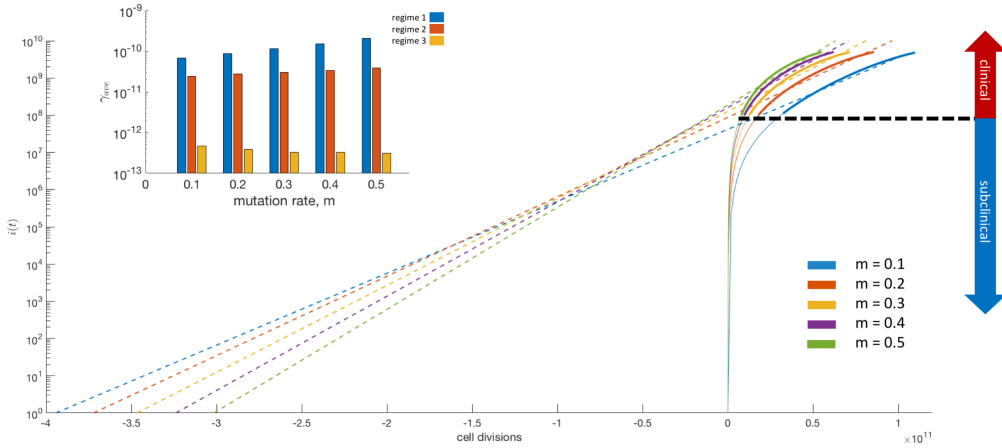


FIGURE 3.6: **Tumor initiation prediction** — Five sample stochastic simulations of tumor growth ( $N = 10^{10}$  cells,  $w = 0.5$ ,  $m = 0.1, 0.2, 0.3, 0.4, 0.5$ ) plotted on a log-linear graph where the model output ( $i(t)$ , solid lines) is fit in the clinical regime (greater than  $10^8$  cells) using an exponential growth equation and extrapolated backwards in simulation time (dashed lines). The inset bar graph shows the average growth rate in each regime.

### 3.4.4 Dynamic phylogenetic trees and evolution of fitness

To track the initiation of cellular heterogeneity from an initially homogeneous state, we follow all of the mutations that take place during the course of a simulation, and organize this in the form of a phylogenetic tree in Figure 3.8 showing the typical size of the genotypic space and the evolution of the genotypic landscape. As the simulation proceeds, the phylogenetic tree dynamically branches out into an increasingly complex structure, with fitness characteristics color coded in Figure 3.8a. We also show the bins associated with each of the 16 cell types, the number of cancer cells  $i(t)$ , and the entropy associated with the sub-population of cell types as a simulation proceeds, in Figure 3.8b. Knowing exactly the types of cells comprising the tumor at any given time allows us to target cell distributions for simulated therapies to test different strategies, which we describe next.

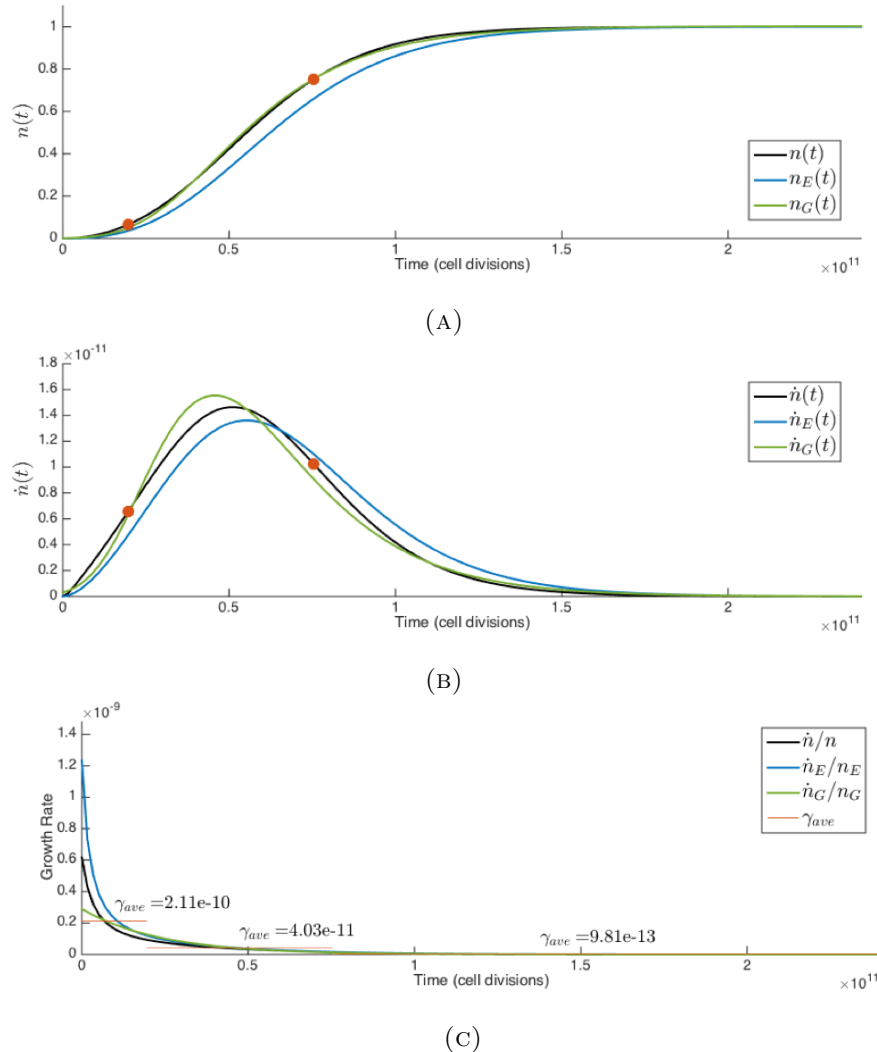


FIGURE 3.7: Comparison of stochastic Moran birth-death process, Gompertzian, and Shannon entropy growth curves — (a) A single stochastic simulation ( $N = 10^{10}$  cells,  $m = 0.5$ ,  $w = 0.5$ ,  $m_p = m_d = 0.25$ ) growth curve,  $n(t)$ , compared with the Gompertzian growth curve,  $n_G(t)$ , eqn. (3.18), and Shannon entropy growth curve,  $n_E(t)$ , eqn. (3.28). Growth curves  $n_G(t)$  and  $n_E(t)$  are normalized to equal one in the limit; (b) Comparison of first-derivatives of  $n(t)$ ,  $n_E(t)$ ,  $n_G(t)$ ; (c) Comparison of growth rates associated with  $n(t)$ ,  $n_E(t)$ ,  $n_G(t)$ , with average growth rates of  $n(t)$  plotted for each regime, eqn. (3.20).

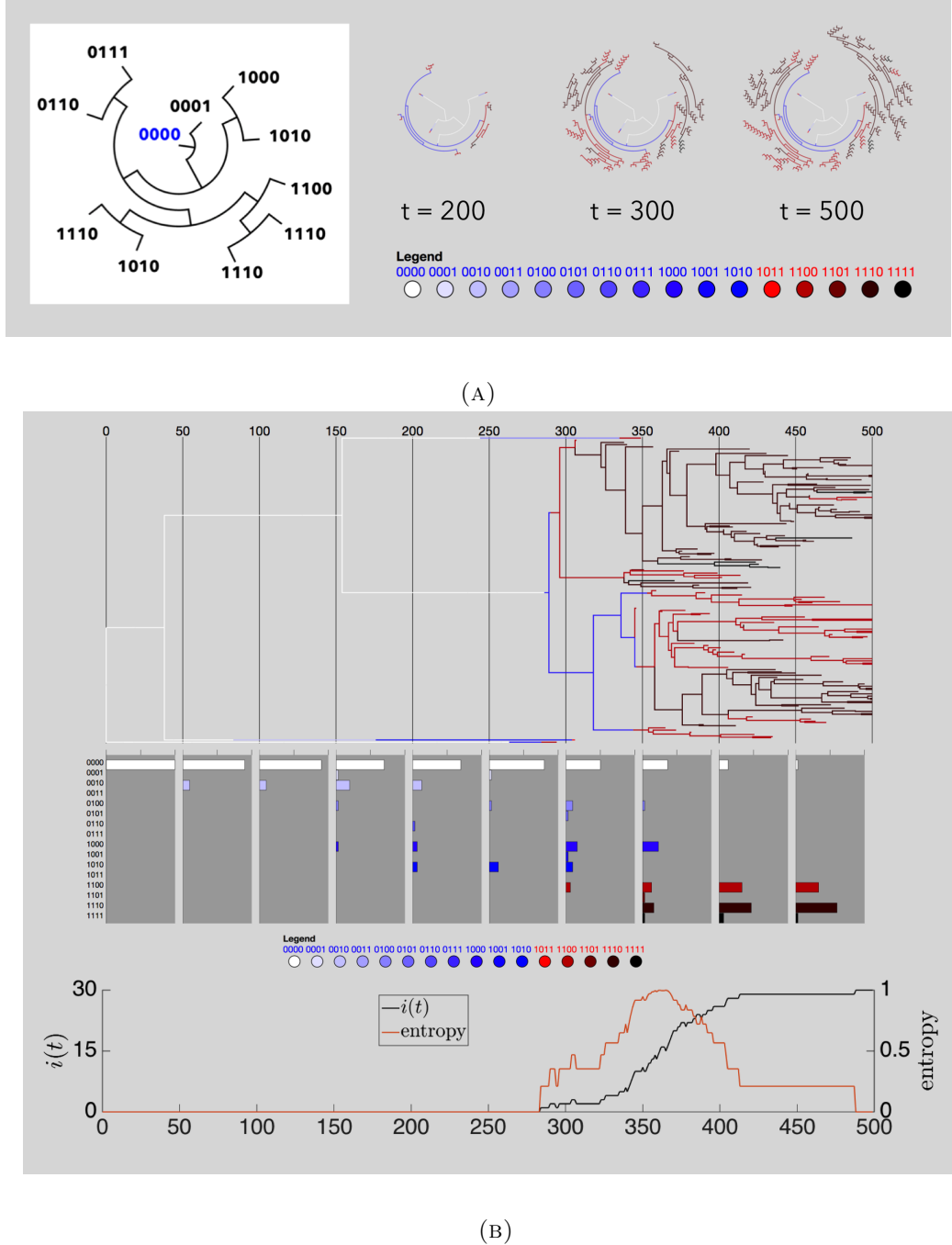


FIGURE 3.8: **Emergence of genetic heterogeneity** — (a) Left: sample dendritic phylogenetic tree tracking point mutations as time extends radially. Right: three snapshots in time of a dendritic tree in a simulation of 30 cells with strong selection ( $w = 1$ ,  $m_p = 0.1$ ,  $m_d = 0.2$ ). Pathways are color coded to indicate genetic cell type; (b) Linear phylogenetic tree of the same stochastic simulation shown in (a) along with histogram plots of the distribution of genetic cell types and a plot of the cancer cell population  $i(t)$  and entropy.

### 3.4.5 A comparison of early vs. late therapy

In Figure 3.9 we show the results from asking the simple question of how early therapy (administered in regime 1) compares with therapy in the middle stages of tumor development (regime 2), or in the later stages of development (regime 3). Eqns (3.11), (3.12) are the governing equations controlling birth/death rates of the cancer cell, healthy cell sub-populations as natural selection plays out. Since the proliferation of cancer cells can be thought of as an imbalance of selection pressures on the competing sub-populations in favor of the cancer sub-population, the goal of any therapeutic intervention is to alter this complex imbalance in favor of the healthy cell sub-population. We implement this by adjusting the selection pressure parameters ( $w_H, w_C$ ) in the formulas (3.6), (3.7). In particular, when therapy is ‘on’, we choose  $w_C = 0$ , and  $w_H = 1$ , tilting the selection pressure in favor of the healthy cell sub-population. When therapy is ‘off’, the two parameters return to their original baseline values, which here we take as  $w_H = 0.1$ ,  $w_C = 0.1$ . Figure 3.9 depicts the proportion of cancer cells in the population both in the absence of therapy, and when therapy is administered. As a comparative tool, in each case, we administer the therapy until a fixed number of cancer cells remains (in each case, we take this threshold number to be 25 cancer cells), and we compare the amount of time,  $\Delta t$ , it takes to achieve this low level. The figure clearly shows  $\Delta t_1 < \Delta t_2 < \Delta t_3 < \Delta t_4$ , while if therapy is administered too late, as in  $\Delta t_5$ , the low threshold is never achieved. The simulations show that a shorter therapeutic time-period is needed if administered earlier to gain the same level of success. The topic of how best to optimize computational therapies is complex, and these simulations are only meant as a confirmation and quantification of how early stage therapy is more effective than late stage therapy.

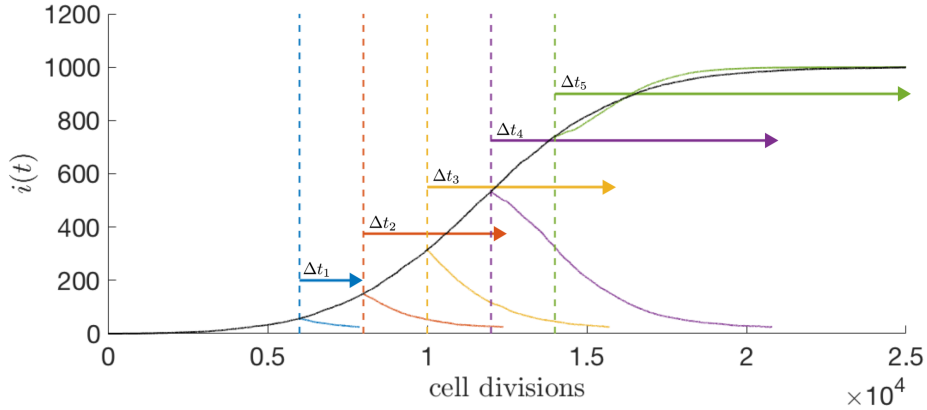


FIGURE 3.9: **Simulated therapy** — An average of 25 stochastic simulations ( $N = 10^3$  cells,  $w = 0.5$ ,  $m = 0.1$ ) where therapy ( $w_H = 1$ ,  $w_C = 0$ ) is administered at different time points ( $t = 6000, 8000, 10000, 12000, 14000$  cell divisions) until all cancer cells are eliminated below a small threshold value (25 cells). Time required ( $\Delta t$ ) for tumor elimination increases as the tumor volume increases (i.e.  $\Delta t_1 < \Delta t_2 < \Delta t_3 < \Delta t_4$ , blue, red, yellow, purple arrows respectively), until, at later simulation time points, therapy is unable to regress tumor size ( $\Delta t_5$ , green arrow).

### 3.5 Discussion

To summarize the main points forming the framework of our model:

- (i) A tumor is a complex Darwinian ecosystem of competing cells operating on an adaptive fitness landscape driven by mutational dynamics and shaped by evolutionary pressures;
- (ii) The basic competitors in an evolutionary game theory model of tumor development are cell populations with a broad distribution of fitness characteristics course grained into two types: healthy cells (cooperators) and cancer cells (defectors). Each of these cell sub-populations attempts to maximize its own fitness;

(iii) Cell fitness is associated with reproductive prowess and in this respect, healthy cells are less fit than cancer cells;

(iv) Primary tumors initiate from a single malignant cell that has undergone the appropriate mutational steps and subsequently undergoes clonal and sub-clonal expansion.

Polyclonality and heterogeneity are thus seen as emergent features of tumor development;

(v) Parameters and distributions measured in the detectable range of tumor growth, such as tumor growth rates and fixation probabilities, are emergent features that have developed from a monoclonal state via cell kinetics and evolutionary development taking place in the subclinical regime;

(vi) Tumor growth is driven by molecular heterogeneity of the cell population comprising the tumor and reflected in the growth equation (3.22);

(vii) Tumor cell populations are more amenable to therapeutic strategies in the early stages of development, before selection for growth and survival have shaped the environment.

We believe the simple evolutionary model described in this paper, driven by a Moran process and shaped by heritable mutations with a fitness landscape based on the prisoner's dilemma evolutionary game is useful in helping to understand early stage tumor growth and how it is influenced by the interplay of a few select small number of key parameters. When a malignant tumor cell population has already exceeded  $O(10^8 - 10^{10})$  cells, some of which may have entered the circulation or lymphatics and migrated to other sites, the opportunity to control or even shape future events may be limited. Attacking tumor heterogeneity as soon as it develops seems to be a useful strategy, particularly if heterogeneity is the driver of growth, as in eqn. (3.22). Whether these concepts can be developed in the more general

context when cell dissemination to other sites is included in the model, and then translated into actionable clinical strategies is a challenge for the future.

### 3.6 Appendix

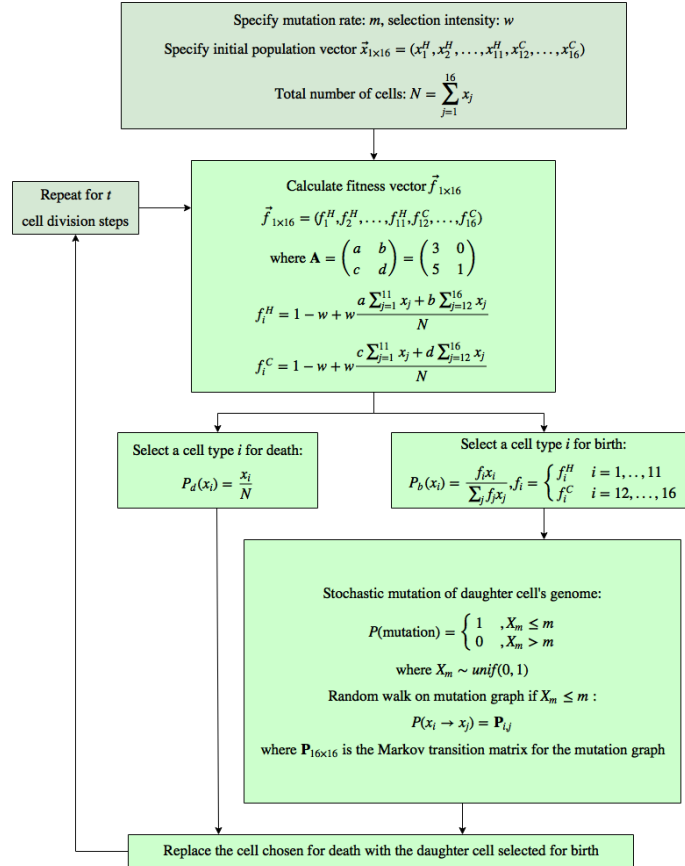


**FIGURE 3.10: A flow chart of the Moran process with selection and mutation algorithm** — Box 1: mutation rate  $m$  (where  $m = m_p + m_d$ ), selection pressure  $w$  and the initial state vector  $x$  containing  $N$  total cells are the inputs for a simulation. Box 2: the prisoner's dilemma game ( $a = 3$ ;  $b = 0$ ;  $c = 5$ ;  $d = 1$ ) is used to calculate the fitness of each healthy and cancer cell type, which is a function of the payoff values and the state vector,  $x$ . Box 3, 4: a single cell is chosen for death according to the relative proportion of the cell type in the cell population. Simultaneously, a single cell is selected for birth according to the relative proportion, weighted by cell fitness. Box 5: During the replication process, the daughter cell inherits a replica of the parent cell's genetic string, with errors occurring at a rate of  $m$ . A single bit of the daughter cell's genetic string may flip during each cell division. The possible mutations can be thought of as a single step random walk on the Markov diagram shown in Figure 3.3.

## Chapter 4

# Chemotherapeutic dose scheduling based on tumor growth rates: the case for low dose metronomic high entropy therapies

Jeffrey West, Paul K. Newton

Chemotherapeutic dose scheduling based on tumor growth rates:

*the case for low dose metronomic high entropy therapies [40]*

USC Preprint

#### 4.1 Abstract

We use a stochastic Moran process model of tumor cell kinetics, coupled with a prisoner's dilemma game-theoretic cell-cell interaction model to design chemotherapeutic strategies tailored to different tumor growth characteristics. Using the Shannon entropy as a novel tool to quantify dosing strategies, we contrast maximum tolerated dose (MTD) strategies as compared with low dose, high density metronomic strategies (LDM) for tumors with different growth rates. Our results show that LDM strategies can outperform MTD strategies. The advantage is magnified for fast growing tumors that thrive on long periods of unhindered growth without chemotherapy drugs present and is not evident after a single cycle of chemotherapy, but grows after each subsequent cycle of repeated chemotherapy. The model supports the concept of designing different chemotherapeutic schedules for tumors with different growth rates and develops quantitative tools to optimize these schedules for maintaining low volume tumors.

#### Major Findings

Model simulations show that metronomic (low dose, high density) therapies can outperform maximum tolerated dose (high dose, low density) therapies. This is due to the fact that tumor cell reduction is more sensitive to changes in dose density than changes in dose concentration, especially for faster growing tumors. This effect is negligible after a single cycle of chemotherapy, but magnified after many cycles. The model also allows for novel

chemotherapeutic schedules and quantifies their performance according to tumor growth rate.

## Quick Guide to Equations and Assumptions

### Assumptions of the model:

1. The model is a computational one, driven by a stochastic Moran (birth-death) process with a finite cell population, in which birth-death rates are functions of cell fitness.
2. Two classes of cells (healthy, cancer) compete against each other at each birth-death event, with fitness ( $f_H, f_C$ ) calculated according to the payoff matrix associated with the prisoner's dilemma evolutionary zero-sum game.
3. Chemotherapy is a selective agent that alters the selection pressure ( $w_H, w_C$ ) of each cell population, with two parameters: dose concentration ( $c$ ) and dose density ( $d$ ).

### Key equations:

In a Moran finite-population, birth-death process there are  $i$  cancer cells in a population of  $N$  total cells (where the number of healthy cells is denoted  $N - i$ ). At each time step in the stochastic evolutionary population dynamics model, a single cell is chosen for birth and a separate single cell is chosen for death. A tumor grows by increasing the number of cancer cells from  $i$  to  $i + 1$  in any given time step. The probability that a healthy cell interacts with another healthy cell is given by  $(N - i - 1)/(N - 1)$ , whereas the probability that a healthy cell interacts with a cancer cell is  $i/(N - 1)$ . The probability that a cancer

cell interacts with a healthy cell is  $(N - i)/(N - 1)$ , whereas the probability that a cancer cell interacts with another cancer cell is  $(i - 1)/(N - 1)$ . These probabilities, known as the Moran process, can be extended to include a fitness landscape where natural selection can play out over many cell division timescales.

The probabilities outlined above are weighted by the “payoff” in order to determine the fitness function for each subpopulation: healthy ( $f_H$ ) and cancer ( $f_C$ ), below. The payoff values ( $a, b, c, d$ ) are associated with the prisoner’s dilemma evolutionary game [14, 75]. The prisoner’s dilemma is defined by the payoff inequalities such that  $c > a > d > b$ , but here we assume the relatively standard (but not unique) values of  $a = 3, b = 0, c = 5$ , and  $d = 1$ .

$$f_H = 1 - w_H + w_H \left( \frac{a(N - i - 1) + bi}{N - 1} \right) \quad (4.1)$$

$$f_C = 1 - w_C + w_C \left( \frac{c(N - i) + d(i - 1)}{N - 1} \right) \quad (4.2)$$

Here, ( $w_H, w_C$ ) are “selection strength” parameters,  $0 \leq w_H \leq 1, 0 \leq w_C \leq 1$ , that measure the strength of selection pressure on each of the population of cells. If  $w_H = 0$ , there is no natural selection acting on the healthy cell population, and the dynamics is driven purely by the Moran process (i.e. random drift). When  $w_H = 1$ , the selection pressure on the healthy cell population is strongest, and the prisoner’s dilemma payoff matrix has maximum effect.

From these formulas, we can define the transition probability of going from  $i$  to  $i+1$  cancer cells on a given step ( $P_{i,i+1}$ ) or from  $i$  to  $i-1$  on a given step ( $P_{i,i-1}$ ).

$$P_{i,i+1} = \frac{if_C}{if_C + (N-i)f_H} \frac{N-i}{N} \quad (4.3)$$

$$P_{i,i-1} = \frac{(N-i)f_H}{if_C + (N-i)f_H} \frac{i}{N} \quad (4.4)$$

The first term in each equation represents the probability that a cell is selected for reproduction (weighted by fitness). The second term represents the probability that a cell is selected for death. The probability of the number of cancer cells remaining the same ( $P_{i,i}$ ) is given by the following. There are two absorbing states ( $P_{0,0}$ ,  $P_{N,N}$ ).

$$P_{i,i} = 1 - P_{i,i+1} - P_{i,i-1}; \quad P_{0,0} = 1; \quad P_{N,N} = 1 \quad (4.5)$$

## 4.2 Introduction

Low dose metronomic chemotherapy (LDM) is the systematic and frequent delivery of chemotherapeutic agents at doses lower than the maximum tolerated dose paradigm (MTD) [38, 39]. It is typically given at a low dose between 1/10th and 1/3rd of the maximum tolerated dose, without a long period of time between subsequent doses, hence it is also associated with higher dose densities [38]. Important features of low dose, high density metronomic chemotherapy include: regular administration of chemotherapy without any interruptions using an optimized dose; preference for oral drugs; low incidence of side

effects; low risk of developing resistance; lower cost. In addition, some elderly or frail patients may only be suited for lower dose chemotherapy. Residual toxicity from previous treatment may also reduce consideration for MTD chemotherapy [39]. Metronomic chemotherapy regimens have been associated with lower cost of inexpensive oral drugs such as cyclophosphamide and result in fewer side-effect associated expenditures. Several phase II studies have shown promises of metronomic-like chemotherapy and its excellent safety profiles [39]. The lower doses of metronomic chemotherapy regimens are now thought to not only reduce the harmful side effects of toxicity delivered to the patient but perhaps also improve anti-tumor effects [126], by killing endothelial cells in addition to its cytotoxic effect on cancer cells [127, 128] in an uninterrupted schedule for prolonged treatment periods. Metronomic chemotherapy has been shown to be effective in preclinical trials where cancer cells have developed resistance to the same chemotherapeutics [126]. These LDM regimens are also suited to combination or additive strategies to new targeted and relatively non-toxic anticancer drugs recently developed.

While the advantages of LDM chemotherapy may be wide ranging with respect to toxicity, resistance, and anti-angiogenic effects (outside of the scope of our model), the goal of this article is to use an evolutionary mathematical model of cell/tumor growth with the ability to simulate chemotherapeutic scheduling to identify *growth regimes* where LDM would likely outperform MTD, and to test various scheduling protocols altering dose density and concentration. While there is no simple answer to the question of what types of tumors and growth regimes where LDM would be preferable to MTD, our results show that LDM chemotherapies with an adequate dose can outperform MTD, especially for fast growing tumors that thrive on long periods of drug-free rest with unhindered regrowth. This effect is

not evident after a single cycle of chemotherapy, but is magnified after each subsequent cycle of repeated chemotherapy. In the interplay of choosing between high dose chemotherapy (MTD) or low dose, high density chemotherapy (LDM), our results show that increasing dose has diminishing returns, so the higher densities afforded by LDM regimens are an ideal tradeoff. These results may have remained hidden even in the advent of helpful theoretical regression laws like Skipper's laws and the Norton-Simon hypothesis because these laws rely on instantaneous rates of regression, rather than the net result of the full chemotherapy cycle operating in an environment with variable growth rates. We explain how our results add to the understanding of these classic growth models and advocate the consideration of tumor growth rates when choosing chemotherapy scheduling.

#### **4.2.1 Administration of metronomic chemotherapy**

A systematic literature review of the MEDLINE, EMBASE, CENTRAL, and PubMed databases for LDM chemotherapy trials from 2000 to April 2012 performed by Lien et al. in 2013 [39] revealed a wide variety in dose delivered and dose schedules under the terminology of metronomic chemotherapies. From the 80 studies analyzed, 107 unique treatment regimens were found (including regimens where multiple drugs were used metronomically). 38 regimens used LDM only (monotherapy n = 24, doublet LDM therapy n = 14). Of the monotherapy, the relative dose intensity (RDI: measured with respect to the maximum tolerated dose) ranged from 0.27 to 1.58 (median 1.02) and dose density (percentage of days drug is delivered) ranged from 32% to 100% [39]. RDI is calculated by dividing the dose intensity (DI; the sum of the doses given each day of the chemotherapy cycle) for a chemotherapy regimen by the baseline DI value of the conventional MTD

schedule. A chemotherapy may deliver a greater overall DI than the MTD (i.e. RDI > 1) if a lower dose is delivered more often, achieving a greater total dose over the course of the full chemotherapy cycle. The lower dose reduces toxicity, allowing for more frequent dosing, a key idea behind the metronomic schedules.

For a low dose metronomic chemotherapy, any schedule that administers a lower dose at more frequent intervals (higher dose density) could be classified as “low dose metronomic.” But, as seen above, in clinical practice the relative dose intensity delivered and the density of the scheduled are varied without clear consensus. In fact, only one monotherapy treatment regimen kept the RDI constant, balancing the lower dose with an equivalent increase in dose density. Of the remaining 23 regimens about half increased RDI ( $n = 12$ ) while half decreased RDI ( $n = 11$ ). It is evident that many of the quantitative details of LDM chemotherapy are unresolved including patient selection, choice of drug (or combinations of drugs and treatments), and optimal dose and treatment intervals [39]. With this in mind, the goal of this manuscript is very targeted. We wish to quantify the relationship between *dose* and *dose density* delivered using the Shannon entropy index [37] as a quantitative scheduling and dosage tool. We will first briefly review the prisoner’s dilemma evolutionary game theory model of primary tumor growth that we use to carry out our computational trials [32, 129] as well as the notion of Shannon Entropy as an index to compare chemotherapeutic regimens in order to show that high entropy schedules (with an adequate dose intensity) outperform low entropy schedules.

#### 4.2.2 The classic tumor regression laws

Benzekry et al.[130] chronicle that, despite a rise in personalized and precision medicine, currently chemotherapeutic agents are often still administered in the maximum tolerated dose paradigm. The author predicts that the forthcoming development of metronomic chemotherapy may pave the way for implementing “*computational oncology at bedside, because optimizing metronomic regimen should only be achieved thanks for modeling support.*” This prediction characterizes a growing field sometimes referred to as computational or mathematical oncology [100, 131]. First, however, in order to properly understand how alternative dosing schedules like the metronomic regimens fit into the future of chemotherapy scheduling, it is important to remember the reasons that led to the advent and continued use of MTD paradigms.

##### 4.2.2.1 Skipper’s Laws

The relationship between dose and tumor cytotoxicity is linear-log (i.e. exponential decay) [6]. Skipper et al. [8] were the first to develop a set of theoretical laws governing the behavior (and imply the design) of chemotherapy schedules in cancer in the late 1970’s. Our understanding of the Gompertzian growth of tumors have made the application of these laws more complex, but the fundamentals of these laws still apply today [3].

In a tumor that grows exponentially (eqn. 4.6 and 4.7) with a constant exponential rate, the first law states that the tumor volume doubling time is constant over the life of the

tumor ( $d_t = \log(2)/\alpha$ ),

$$\dot{n} = \alpha n \quad (4.6)$$

$$n(t) = n_0 \exp(\alpha t) \quad (4.7)$$

The second of Skipper's laws is that the percentage of cells killed by a given drug dose,  $D$ , is constant, therefore a linear increase in dose causes a log increase in cell kill [100]. As an example, a drug dose,  $x$ , that shrinks tumor size from  $10^6$  to  $10^5$  cells results in a 90% decrease of tumor population. An identical subsequent drug dose (a total dose of  $2x$ ) will further reduce tumor population size according to that same kill constant, to  $10^4$ . A third dose results in  $10^3$  cells, a fourth,  $10^2$ , and so on. The kill law is known as a the 'log' kill because the constant fraction is a constant logarithmic amount. Skipper's log-kill law indicates that subsequent dosing has a diminishing return; the last few remaining cells are the most difficult to eliminate. This log-linear relationship can be formulated as follows:

$$\log P_S = -\beta D. \quad (4.8)$$

#### 4.2.2.2 Norton-Simon Hypothesis

One important reason the Skipper-Schabel-Wilcox model is so meaningful is that it conceptualizes the tumor growth model (e.g. exponential) and tumor regression (log-kill). Norton and Simon realized the importance of extending these observations to a Gompertzian growth model (eqn. 4.11). The log-kill law, a fundamentally static law does not

say anything about the relationship between the fraction of cells killed and the growth rate of the tumor, only the relationship between the rate of tumor regression and the dose. In effect, Skipper's second law assumes a constant growth rate, and therefore, a constant regression rate. In Gompertzian growth, the non-constant growth rate results in a range of log-kill rates ( $\beta$ ) corresponding to the instantaneous growth rate ( $\gamma(t)$ ). Gompertzian growth is given by the following coupled ordinary differential equations.

$$\dot{n} = \gamma n \quad (4.9)$$

$$\dot{\gamma} = -\alpha\gamma \quad (4.10)$$

The Gompertz function reduces to the exponential function when  $\alpha = 0$ . These coupled ordinary differential equations may be directly solved, as follows.

$$n(t) = n_0 \exp \left[ \frac{\gamma_0}{\alpha} (1 - \exp(-\alpha t)) \right] \quad (4.11)$$

The Norton-Simon hypothesis states that tumor regression is positively (linearly) correlated with the instantaneous growth rate just before the treatment of the unperturbed tumor [7, 88]. Generally, smaller tumors are associated with higher growth rates (and therefore, higher regression rates). Mathematically, the Norton-Simon Hypothesis can be formulated,

$$\dot{n} = f(n(t))(1 - L(t)) \quad (4.12)$$

where  $n(t)$  is the growth rate model of the tumor at time  $t$ ,  $f(n(t))$  is the growth dynamics associated with the unperturbed tumor (i.e. exponential growth or Gompertzian growth), and  $L(t)$  is the loss function of cells resulting from treatment. The growth function  $f(n(t))$  may be assumed to be exponential, (eqn. 4.7) or Gompertzian, (eqn. 4.9 and 4.10). Remembering that Skipper's second law states that cell kill follows first-order kinetics, we may assume for the time being that  $L(t) \equiv \text{const.}$ , or that the rate of cell removal due to treatment is constant. In other words, each dose of chemotherapy is associated with some value of  $L$ . The goal is to find the optimal dose concentration and dose density that maximize the loss rate of cell kill,  $L$ .

#### 4.2.3 The Implications of the Norton-Simon Hypothesis

Norton and Simon hypothesized that chemotherapy will only be effective in targeting cells that are in active proliferation (and as such are directly contributing the growth of the tumor in equation 4.12). Their model demonstrated ability to fit data preclinical experiments [112] and predict future tumor growth and regression after a few initial measurements and data from clinical trials in breast cancer [7].

The model has several key implications. First, the model predicts a higher regression for higher dose delivered. The highest dose tolerable to the patient should be chosen. Second, tumor regrowth during rest periods of chemotherapy necessitates a shorter rest period and subsequently, a shorter time of tumor regrowth. The next round of a dose dense chemotherapy will attack a smaller tumor (with higher growth rate) and lead to higher regression. Both implications give rise to the invention of the MTD paradigm to attack the

tumor with the highest dose, coupled with shortest rest. These predictions were confirmed by clinical trials in which chemotherapy schedules were densified from 21 to 14 days [132]. The hypothesis also predicts that tumors with an identical tumor burden may have varied responses. The growth rate of the tumor determines the response to chemotherapy. As such, early administration is important, implying a better response when the tumor is in initial stages of high growth. Similar models using the ratio of tumor volume to the host-influenced tumor carrying capacity (which corresponds inversely to the instantaneous growth rate of the tumor) has been shown to inversely predict radiotherapy response [133].

Fundamentally however, the Norton-Simon hypothesis provides no predictions for the effect of dose and dose density on regression. The Norton-Simon hypothesis (equation 4.12) conceals the fact that the rate of cell-kill,  $L(t)$  will be dependent on two factors: drug concentration and the number of days the drug is administered. The goal of this manuscript is to extend the classical and well-accepted predictions of Norton-Simon hypothesis from instantaneous regression rates (i.e. the derivative) to the cumulative effect (i.e. the integral) over one (or many) cycles of chemotherapy. Chemotherapy “strategies,” or schedules are quantified using the Shannon entropy [37] by their total cell reduction (TCR) over the course of the full schedule, rather than the initial regression rate ( $\beta$ ). The evolutionary model we introduce in this paper is compared with regression data from murine models (see figure 4.3) and shown to be in good agreement.

## 4.3 Materials and methods

### 4.3.1 Chemotherapeutic agents alter the fitness landscape

It is now well established that cancer is an evolutionary and ecological process [10, 11].

Studying cancer as a disease of clonal evolution has major implications on tumor progression, prevention and therapy [24, 25]. The evolutionary forces at play inside the tumor such as genetic drift with heritable mutations and natural selection operating on a fitness landscape are influenced by tumor microenvironment and the interactions between competing cell types. Increased selection will influence the rates of proliferation and survival, which cause the population of cells within a tumor to progress toward more invasive, metastatic, therapeutic resistant cell types. The role of chemotherapeutic agents is to kill proliferating cancer cells, which can be modelled as altering the evolutionary trajectory of the tumor: the relative fitness of the surrounding healthy cell subpopulation is greater than the targeted proliferating cancer cells.

In order to model these complex evolutionary forces in cancer, many theoretical biologists have used an evolutionary game theory (EGT) framework, pioneered by Nowak, to study cancer progression (see [14, 15, 17, 19, 134]). Evolutionary game theory provides a quantitative framework for analyzing contests (competition) between various species in a population (via the association of ‘strategies’ with birth/death rates and relative sub-clonal populations) and provides mathematical tools to predict the prevalence of each species over time based on the strategies [17, 64, 66, 72]. More specifically, the framework of EGT allows the modeler to track the relative frequencies of competing subpopulations with different

traits within a bigger population by defining mutual payoffs among pairs within the group. From this, one can then define a fitness landscape over which the subpopulations evolve.

#### 4.3.2 The model

The model presented in [32, 129] and used in this paper to carry out our computational trials is a framework of primary tumor growth used to test the effect of various chemotherapeutic regimens, including MTD and LDM. The model is a stochastic Moran (finite-population birth-death) process [115] that drives tumor growth, with heritable mutations [50] operating over a fitness landscape so that natural selection can play out over many cell division timescales (described in more detail in [32, 129]). The birth-death replacement process is based on a fitness landscape function defined in terms of stochastic interactions with payoffs determined by the prisoner’s dilemma game [14, 75]. This game incorporates two general classes of cells: healthy (the cooperators) and cancerous (the defectors) [135, 136]. During tumor progression, each cell is binned into one of two fitness levels, corresponding to their proliferative potential: healthy (low fitness) and cancer (high fitness). In our model, we can think of a cancer cell as a formerly cooperating healthy cell that has defected and begins to compete against the surrounding population of healthy cells for resources and reproductive prowess. The model demonstrates several simulated emergent ‘cancer-like’ features: Gompertzian tumor growth driven by heterogeneity [36, 48, 85], the log-kill law which (linearly) relates therapeutic dose density to the (log) probability of cancer cell survival, and the Norton-Simon hypothesis which (linearly) relates tumor regression rates to tumor growth rates, and intratumor molecular heterogeneity as a driver of tumor growth [129].

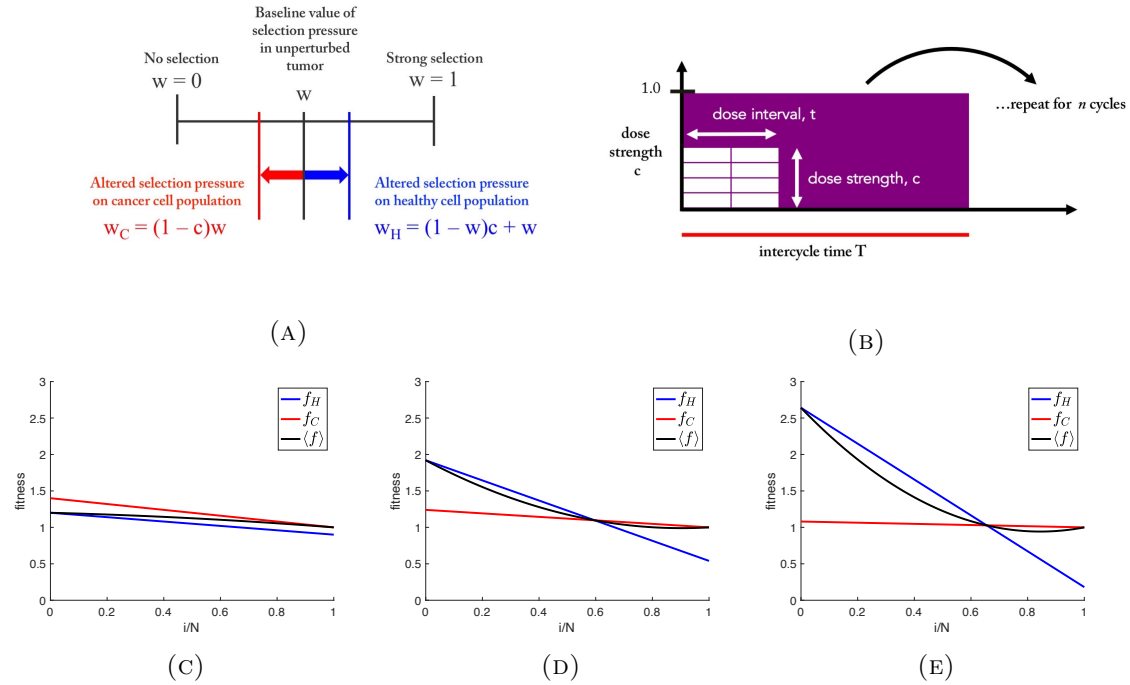


**FIGURE 4.1: Chemotherapy is a selective agent that alters the fitness landscape of cells** — (a) The dose strength parameter,  $c$ , ( $0 \leq c \leq 1$ ), alters the selection pressure parameter,  $w$ , ( $0 \leq w \leq 1$ ), in favor of the healthy cell population ( $w_H > w$ ) and to the disadvantage of the cancer cell population ( $w_C < w$ ). (b) Total dose density delivered in the one chemotherapeutic cycle,  $D$ , is the product of the dose strength ( $c$ ,  $0 \leq c \leq 1$ ) and dose interval ( $d$ ,  $0 \leq d \leq 1$ ) such that  $D = ct$  (eqn. 4.13 ( $0 \leq D \leq 1$ )). (c,d,e) Plots showing the fitness of the healthy cell subpopulation ( $f_H$ , blue) and the cancer cell subpopulation ( $f_C$ , red) for no therapy, low dose therapy, and high dose therapy.

Others have presented mathematical models to study evolutionary dynamics of tumor response to targeted therapy [113] in either combination or sequential therapy [34, 137], and optimal drug dosing schedules to prevent or delay the emergence of resistance or optimize tumor response [138–140]. We are interested testing “strategies,” or drug schedules that control the number of cancer cells,  $i$ , in a population of  $N$  cells comprising the simulated tissue region. (Note: the size of the tumor population,  $i$ , is variable and changing according to the fitness landscape, detailed in equations 4.1 through 4.5. The carrying capacity,  $N$ , is a parameter in the model, but all plots shown here are normalized by  $N$ , so the proportion of cancer cells,  $i/N$ , is used to track tumor growth, without loss of generality.) The model

presented here uses a parameter,  $w$ , to control the effect of selection pressure. A value of  $w = 0$  corresponds to neutral drift (no selection) and a value of  $w = 1$  corresponds to strong selection. We break  $w$  into two separate parameters,  $w_H$ , the selection pressure on the healthy population, and  $w_C$ , the selection pressure on the cancer population (see figure 4.1a). Each dose of chemotherapy is associated with a dose concentration,  $c$ , which alters the selection pressure as indicated in figure 4.1a. Here, we assume drug concentration will be measured as a fraction of the conventional maximum tolerated dose (MTD) dosages, hence  $0 \leq c \leq 1$  (see Figure 4.1b). As  $c$  increases, the selection pressure is altered in favor of the healthy cells ( $w_H > w$ ) and to the detriment of cancer cells ( $w_C < w$ ) as shown in Figure 4.1a. Before therapy, the fitness landscape of an untreated tumor is that of a prisoner's dilemma (Figure 4.1c), where the fitness of the cancer subpopulation is greater than the healthy population for the entire range of cancer proportion,  $i/N$ . The change in fitness landscape for a moderate value of  $c$  ( $c = 0.4$ ) is shown in Figure 4.1d, which gives the healthy cell population a fitness advantage over the cancer population. The advantage is lessened as the tumor size ( $i/N$ ) increases (which contributes to the emergence of the Norton-Simon model in Figure 4.2, explained in detail below). For a strong dose of therapy (such as  $c = 0.8$ , shown in Figure 4.1e), the effect on the fitness landscape is exaggerated. Thus, a higher dose leads to a higher kill rate of cancer cells.

In literature, two models have been proposed to model loss functions due to a drug: 1) non-cycle specific (where the loss function is linear with tumor size) [141] and 2) cycle-specific (where loss function is linear with tumor growth rate) [7, 8]. Cycle-specific drugs are considered here, and thus a model of regression that is linear with tumor growth rate is chosen. The loss function of the Norton Simon hypothesis in equation 4.12 shows an

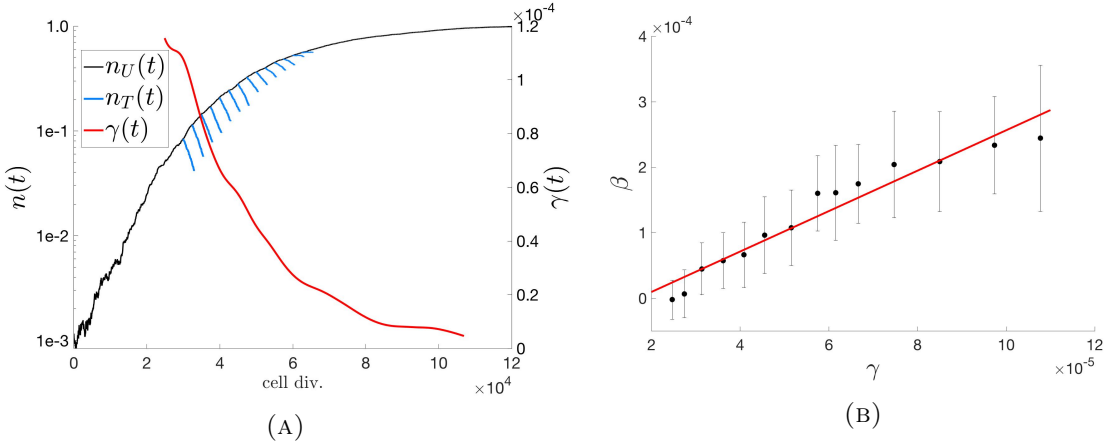


**FIGURE 4.2: Classical Tumor Regression Laws** — (a) The Norton-Simon hypothesis states that tumor regression is proportional to the growth rate of an unperturbed tumor of that size. Unperturbed tumor growth,  $n_U(t)$  (black) in a representative population of  $N = 10^3$  cells, and growth rate,  $\gamma(t)$  (red) is shown. Therapy is administered at various timepoints in the growth of the tumor and then regression,  $n_T(t)$ , is plotted (blue). Rate of regression,  $\beta$ , is the best-fit slope on the log-plot. (b) The average regression rate was calculated for 25 stochastic simulations, and plotted as a function of  $\gamma$  at the time of therapy with error bars indicating the standard deviation of values. A linear best fit (predicted to be linear by the Norton-Simon hypothesis) is calculated to be  $\beta(t) = 3.0865\gamma + -5.2359e - 05$ .

example of cycle-specific drug modeling.

The instantaneous growth rate (i.e.  $\gamma$ ) of a stochastic Moran process model (see equations 4.1 through 4.5) is proportional to the selection pressure,  $w$ . This indicates that varying  $w$  linearly with dose concentration  $c$  (shown in figure 4.1a) is comparable to the previous cycle-specific drug models. This linearity is confirmed by plotting instantaneous regression rates throughout the life of a tumor in figure 4.2. Identical, continuous chemotherapy is administered at different time points in the life of the tumor, corresponding to different instantaneous growth rates (figure 4.2a). A linear relationship between the instantaneous growth rate ( $\gamma$ ) and instantaneous regression rate ( $\beta$ ) (figure 4.2b) emerges from the model, comparable to the predictions of the Norton-Simon hypothesis.

A separate justification of the linear model of the effect of drug concentration on selection

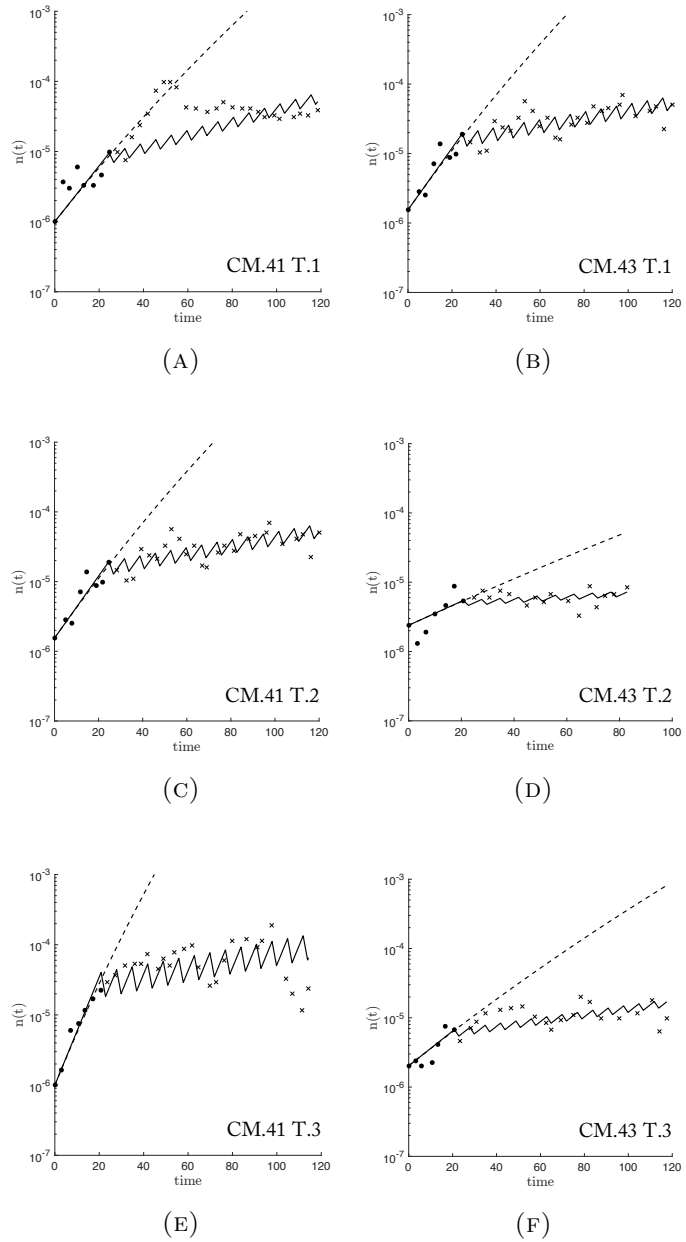


**FIGURE 4.3: Response of murine tumors to 5-Fluorouracil (5-FU) treatment with model best-fit** — Data (reproduced from [142]) from two treated mice: CM.41 (left panel) and CM.43 (right panel), receiving doses of 50mg/kg or 100mg/kg, respectively, on 2 days out of 7 (biweekly). Biweekly measurements of tumor volume are recorded for untreated (black circles) until 3-4mm in size and treated volumes (black x's) are measured until tumor reaches 1cm size. A Gompertzian function is best-fit (dashed line) and the Prisoner's dilemma model is fit using  $w$  and  $c$  as parameters (solid line). The model fit performs well for the wide range of tumor growth rates found in six tumors ( $w = [0.18, 0.08, 0.21, 0.08, 0.35, 0.12]$  and  $c = [0.30, 0.49, 0.34, 0.34, 0.36, 0.32]$  left to right, top to bottom, respectively).

pressure is shown in figure 4.3. A best-fit was performed to find the optimal parameters of  $w$  and  $c$  to fit data reproduced from mouse models quantifying inter-mouse and intra-mouse variability and response to 5-Fluorouracil (5-FU) in two treatment groups: 50mg/kg (figure 4.3 left panel) and 100mg/kg (figure 4.3 right panel) [142]. Tumor size measurements were taken from visibility until a mouse tumor reached 3 to 4 mm in size, and drug treatment was administered weekly until 1cm in size. The prisoner’s dilemma model (black solid lines) appears to accurately capture both the growth dynamics (solid black circles) and the treatment dynamics (black x’s). The dashed lines are Gompertzian best-fit functions of the unperturbed pre-treatment data (black circles), showing good agreement with the prisoner’s dilemma (black solid lines). Previously, we have reported the model’s success in capturing current unperturbed growth models (i.e. Gompertzian growth) as an emergent phenomena of this evolutionary model [129].

#### 4.3.3 Dose concentration versus dose density

Despite a growing trend toward personalized and precision medicine, treatment goals have shifted from complete cure to an optimization of long term management of the disease; rather than trying to find the silver bullet, we might utilize the advances in mathematical models to optimize existing therapeutic options [130, 143]. For this reason, we have decided to test the merit of various chemotherapeutic regimens by comparing the total tumor cell reduction (TCR). Presumably, a therapy regimen with a higher value of TCR will provide a greater level of tumor control, a longer time to relapse, and better prognosis.

A drug dose,  $D$ , (equation 4.13) is generally measured in units of  $\text{mg}/\text{m}^2/\text{week}$  (here, average body surface area assumed to be  $1.8\text{m}^2$ ). Yet, dose  $D$  consists of two components: dose concentration (parameter  $c$  in our model) and dose time factor (parameter  $t$  in our model). The time factor, called the dose density when normalized by the intercycle time, represents the percentage of days a dose is administered. In order to compare the importance of each term on tumor cell reduction, we hold one term constant and vary the other in Figure 4.4.

$$D = ct. \quad (4.13)$$

Clearly seen in Figure 4.4a, there is a diminishing return on increasing the dose strength of a given chemotherapy regimen. Although there is a positive relationship (an increase in dose leads to a higher regression) that relationship lessens as the dose is increased further. However, in Figure 4.4b, the relationship between dose density and regression is linear, showing no signs of diminishing returns of increasing density.

The point has an important subtlety: the dose cannot be continually lowered in favor of density. The dose must be sufficient to overcome the growth rate of the tumor; some doses are not adequate for tumor regression regardless of the density. This is seen for values below the dotted line in Figure 4.4a and 4.4b.

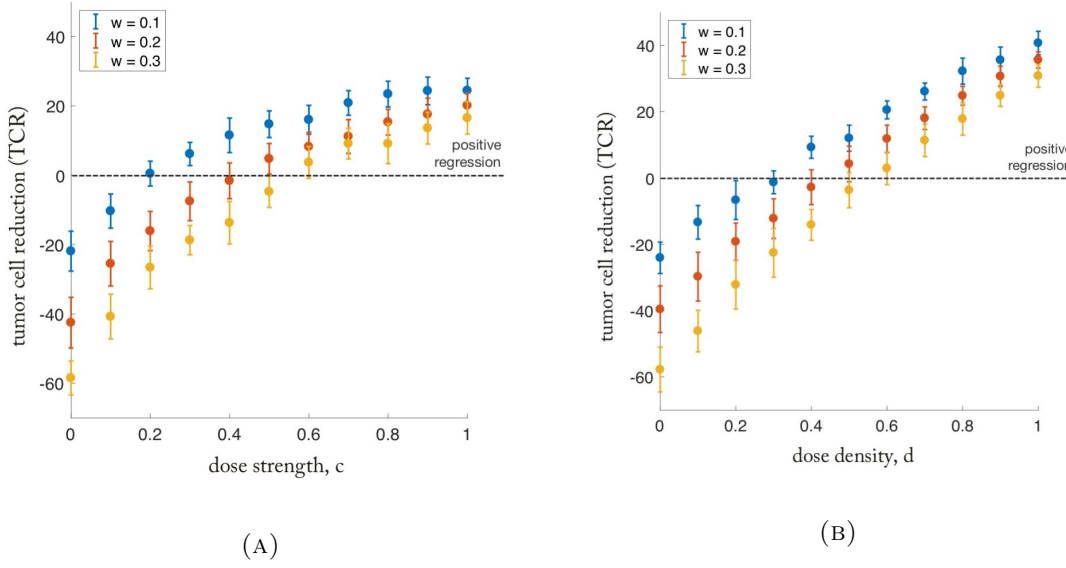


**FIGURE 4.4: Diminishing returns of dose escalation compared to linear relationship of dose density** — (a) Dose Escalation: The percent regression of a tumor for a range of dose strength (constant dose interval:  $t = 10$  days,  $T = 14$  days) are shown for a range of selection pressure:  $w = 0.1$  (blue),  $w = 0.2$  (red), and  $w = 0.3$  (yellow). For each subsequent increase in dose strength, the dose escalation approach to chemotherapy shows diminishing returns in percent tumor regression. (b) Dose Density: The percent regression of a tumor for a range of dose interval (constant dose strength:  $c = 1.0$ ) are shown for a range of selection pressure:  $w = 0.1$  (blue),  $w = 0.2$  (red), and  $w = 0.3$  (yellow). Dose density shows a linear relationship between densifying chemotherapy and percent tumor regression.

## 4.4 Results

### 4.4.1 Quantifying chemotherapeutic strategies via entropy metric

In clinical practice today, there are three common chemotherapy regimens in use considered here: Maximum Tolerated Dose (MTD), Low Dose Metronomic weekly (LDMw) and Low Dose Metronomic daily (LDMd). These three chemotherapy strategies are shown in Figure 4.5, left. Each regimen consists of identical cycles that are repeated until the tumor is eradicated. The MTD (left, top) regimen delivers the maximum dose on a single day, repeated once every 2 weeks. The LDMw (left, middle) regimen lowers the dose, but

doubles the dose density from 1 to 2 days out of 14. The LDMd (left, bottom) regimen has the highest density (there is a dose administered on 100% of the days), but the lowest dose.

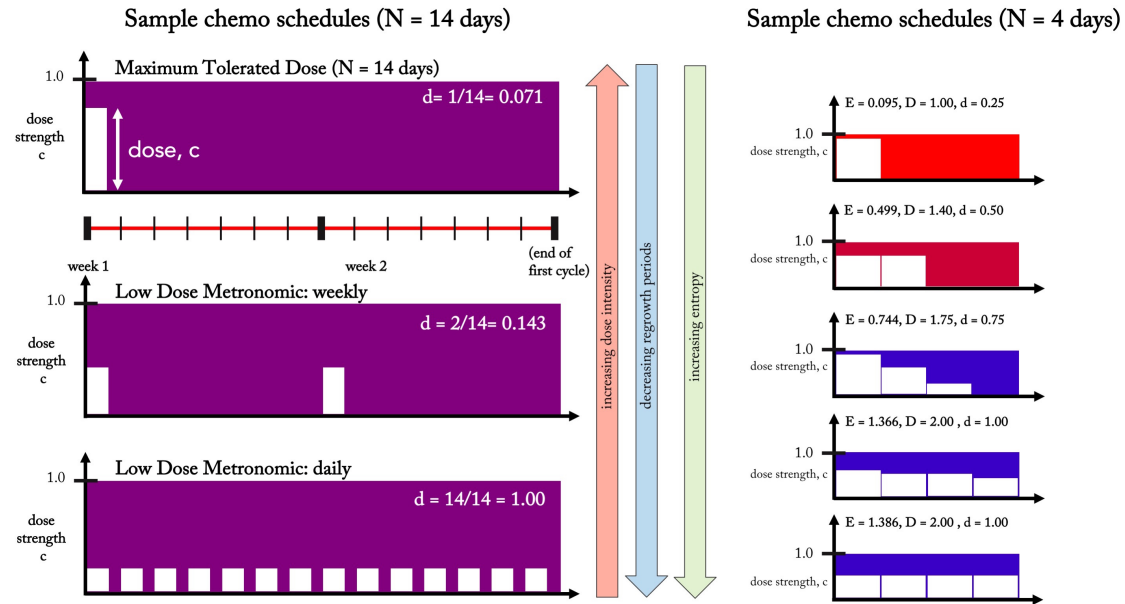


**FIGURE 4.5: Shannon entropy as an index to compare treatment strategies**

— **Left:** 3 common chemotherapy schedules are shown for one cycle ( $N = 14$  days). Maximum Tolerated Dose (left, top) is a high dose (administered once at the beginning of every 2 week cycle) and low dose density ( $d = 0.071$ , see equation 4.16) regimen. Low Dose Metronomic Weekly (left, middle) is a lower dose, higher density ( $d = 0.143$ ) regimen, while Low Dose Metronomic Daily is the lowest dose, highest density ( $d = 1.00$ ). **Right:** Similarly, chemotherapy regimens can be simulated for a range of dose, density, and entropy values. Pictured from top to bottom are a range of representative regimens from low entropy (i.e. high dose, low density) to high entropy (i.e. low dose, high density) for a cycle of  $N = 4$  days. On each  $i$ th day, treatment of dose  $c_i$  is administered. The treatment strategy's Shannon Entropy,  $E$ , is calculated according to equation 4.14 and the total dose delivered is calculated according to equation 4.15. All treatment strategies are front loaded (monotonically decreasing) regimens. It should be noted that LDM-like regimens correspond to a high entropy value (bottom, left and right).

There are hundreds of such choices of chemotherapy regimens when considering varying doses across many days or weeks (Figure 4.5, right), each varying the total dose delivered,

$D$ , and the density,  $d$ . We propose using a Shannon Entropy index,  $E$ , of a given chemotherapy schedule as a measure that can quantify and synthesize information of both the dose on a given day and the distribution of unique, daily doses across the entire chemotherapy regimen into a single metric. The entropy is calculated as follows, where  $c_i$  is the dose strength (often simply referred to as ‘dose’) on day  $i$ .

$$E = - \sum_{i \in c_i > 0}^N c_i \log c_i \quad (4.14)$$

The assumption in equation 4.13 that an identical dose is delivered every day can be relaxed, and the total dose delivered is found by summing the dose on each  $i$ th day ( $c_i$ ) multiplied by the length of the dose in days ( $t_i$ ). We assume that the smallest resolution of discrete times between doses,  $t_i$  is a single day, or  $t_i = 1$  for all  $i$ .  $N$  is the number of days between cycles, also known as the intercycle time.

$$D = \sum_{i=1}^N c_i t_i = \sum_{i=1}^N c_i \quad (4.15)$$

The dose density of a regimen can be found by summing the number of days where a non-zero dose is delivered, and dividing by the intercycle time in days,  $N$ . Thus, the density will be a non-dimensionalized parameter such that ( $0 \leq d \leq 1$ ).

$$d = \sum_{i \in c_i > 0}^N \frac{t_i}{N} \quad (4.16)$$

The Shannon entropy metric,  $E$ , is an ideal metric for comparing chemotherapy regimens because it separates the existing cases already in clinical practice today: MTD (low entropy, characterized by high doses with long periods of rest), metronomic regimens (high entropy, characterized by low doses with short or no periods of rest), as well as any arbitrary strategy of varied doses administered in a cycle of arbitrary length of days. All of the simulated therapy regimens were assumed to be frontloaded (non-increasing, with the highest dose on day 1 and equal or lower subsequent doses). Backloaded regimens give similar but slightly disadvantageous results, because backloaded regimens often start with a period of rest, giving the tumor time to grow to a larger tumor, which is associated with a lower growth rate (and therefore lower regression).

#### 4.4.2 LDM versus MTD chemotherapies

Computational simulations of 1000 unique chemotherapy schedules were run with identical initial conditions ( $N = 1e6$  cells;  $i/N = 1e3$ ). Mean values of tumor cell regression percentage for 50 simulations were calculated and plotted in a pictorial histogram according to regression percentage (Figure 4.6). Both slow growing tumors ( $w = 0.1$ ) and fast growing tumors ( $w = 0.2$ ) were simulated.

Each block represents a chemotherapy regimen, which has an associated Shannon entropy index (eqn. 4.14). The background color of the blocks of the chemotherapy regimens are color-coded from red (low entropy) to blue (high entropy). The smaller white squares within each block indicate the strength of the therapy dose for each day ( $c_i$ ). Pictured are 1000 combinations of  $N = 4$  day chemotherapy schedules, but similar trends are seen for

chemotherapy schedules of longer length of days. All regimens are equivalent total dose ( $D = 0.3$ ), non-increasing, and are repeated for 8 cycles of chemotherapy and the tumor cell regression (TCR) is recorded. The histograms clearly show a color-shift from red toward blue for low TCR toward high TCR. This indicates that high entropy (blue) therapies outperform low entropy therapies and consistently lead to higher tumor cell reduction. These high entropy regimens are low dose, more dose-dense chemotherapies, characteristic of LDM chemotherapy.

In Figure 4.7, the analysis is repeated for varied tumor growth rates (i.e. varied selection pressure) for  $w = 0.1$ , (blue)  $w = 0.2$ , (red) and  $w = 0.3$  (yellow). The difference in reduction is shown for 1 cycle, 8 cycles, and 16 cycles. Fast growing tumors have a high slope on a least-squares linear fit approximation of the entropy-TCR plot, which means that high entropy therapies (LDM) are more effective for fast growing tumors than for slow growing tumors. By contrast, slow growing tumors have a lower slope on the entropy-regression plot, which means that all regimens have relatively similar performance outcomes. Fast growing tumors, therefore, have a higher likelihood of benefiting from a more LDM-like chemotherapy, provided the dose is adequate to lead to tumor regression.

The effect is almost negligible after a single cycle (Figure 4.7a). The appeal of the implication of Norton-Simon toward an MTD approach to chemotherapy lies in the high initial response of tumors to a high dose. The metronomic chemotherapies take more cycles to overtake the initial quick response of the MTD, but after the 8 cycles (Fig. 4.7b) and 16 cycles (Fig. 4.7c), the cumulative effect is evident and metronomic chemotherapies outperform MTD therapies. For each growth rate (i.e. selection pressure), there is a corresponding optimal chemotherapy schedule. In each case, the optimal solution corresponds to the

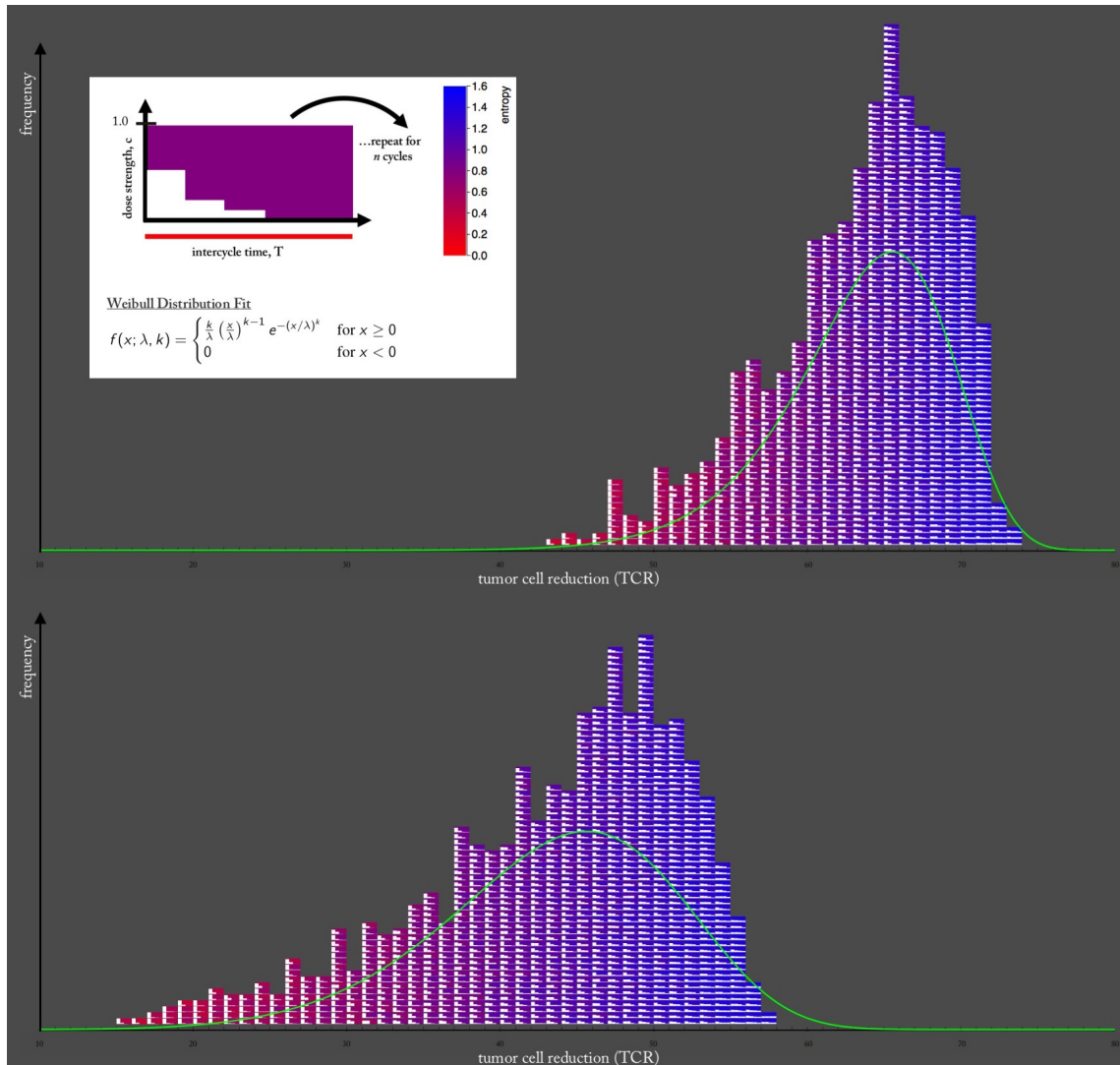


**FIGURE 4.6: High entropy, LDM-like chemotherapies outperform low entropy MTD-like chemotherapies** — Two pictorial histograms are plotted where each block (color-coded from red: low entropy to blue: high entropy) represents a chemotherapy regimen. The top histogram is for a slow-growing tumor ( $w = 0.1$ ) and the bottom histogram is faster growth ( $w = 0.2$ ). All regimens are equivalent total dose ( $D = 0.3$ ), monotonically decreasing, and are repeated for 8 cycles of chemotherapy and the tumor cell reduction (TCR) is recorded. The dose density,  $d$ , and dose concentration,  $c_i$ , are varied between regimens. The histogram clearly shows a color-shift from red toward blue for low TCR, ineffective therapies toward high TCR, effective therapies. High entropy (blue) therapies outperform low entropy therapies. The data was fit to a Weibull distribution (shown in upper left panel; top:  $k = 14.251, \lambda = 65.882$ , bottom:  $k = 6.647, \lambda = 46.758$ ), overlaid in green.

highest entropy (which corresponds to the low-dose metronomic chemotherapy schedule).

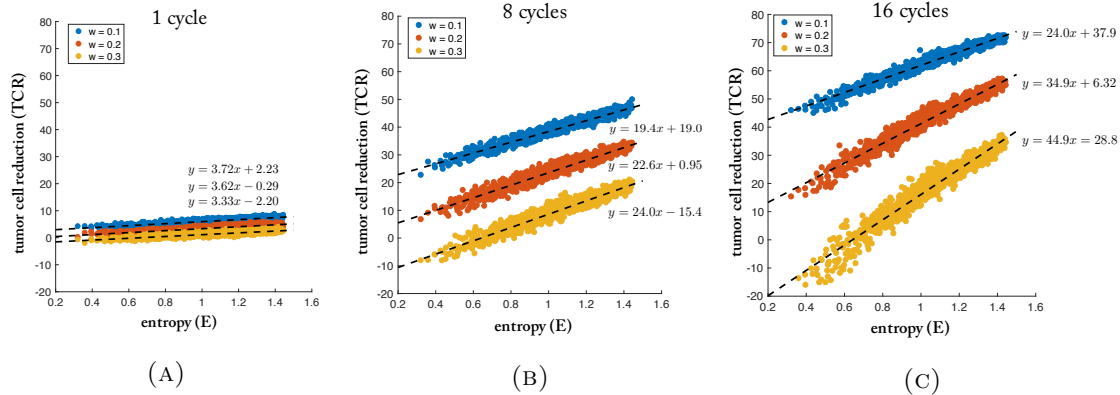


**FIGURE 4.7: High entropy strategies lead to an increase in tumor regression —** The relationship between tumor cell reduction (TCR) and entropy ( $H$ ) is shown for a single cycle of chemotherapy (a), 8 cycles (b), and 16 cycles (c). The simulations (averages of 25 stochastic simulations for total dose delivered  $D = 0.3$ ) are repeated for slow ( $w = 0.1$ , blue), medium ( $w = 0.2$ , red), and fast growing tumors ( $w = 0.3$ , yellow). The low slope value in (a) indicates negligible advantage of high entropy strategies after only a single cycle. After many cycles, the advantage of high entropy strategies is apparent (b,c). Also note that the slope associated with faster growing tumors (yellow) is higher than those of slower growing tumors (blue). This indicates that at high entropies, TCR for the fast growing tumors is closer to those for slow growing tumors, as compared with low entropies.

## 4.5 Discussion

We use a stochastic Moran process model coupled with a prisoner’s dilemma evolutionary game (cellular interactions) to contrast LDM and MTD chemotherapies with respect to their effect on tumor growth. The Shannon entropy was identified as a useful metric to compare chemotherapy strategies. The metric is useful in quantifying LDM strategies (which correspond to high entropy values), MTD strategies (low entropy), as well as novel strategies with intermediate entropy values.

Our results show that high dose chemotherapy strategies outperform low dose, although there are some subtleties associated with the growth rates of the tumors. Dosing consists of

a product of concentration and density and our results show that an increase in density is more effective than the same percentage increase in concentration. In other words, higher dose concentrations shown diminishing returns. The effectiveness of density in leading to a higher tumor cell reduction allows the LDM chemotherapies (which are more dose dense) to outperform MTD strategies. This effect is magnified for fast growing tumors that thrive on long periods of unhindered growth without chemotherapy drugs present. This effect is not evident after a single cycle of chemotherapy, but is magnified after each subsequent cycle of repeated chemotherapy. We could ask if there is any evidence of this effect in the literature on clinical trials already performed. We first point to a paper comparing different chemotherapeutic schedules for prostate tumors [144] (relatively slow-growth rates). In this phase 3 study, docetaxel dosing given every three weeks was compared to dosing every week. The mean survival was only slightly higher for the first group (three weeks) compared with the second (weekly), showing no obvious benefit to a low-dose high density treatment. By contrast, a phase 2 trial for small cell lung cancer (SCLC) [145] was performed, a tumor with typically higher growth rates than prostate tumors. For this group, the drug topotecan was administered on a higher dose weekly basis with disappointing results, pointing out the advantages of the LDM therapies for this fast-growing tumor type.

Thus our model points to the benefits of choosing dosing strategies based on tumor growth rates, something not currently done in medical practice. The concept of choosing dosing schedules based on tumor growth rates could well be a fruitful avenue to test further in clinical trials focused on this question. Others have attempted to estimate prospective patient-specific tumor growth rates to make clinical decisions about treatment scheduling and fractionization, using measurements at diagnosis and first day of treatment [133, 146].

Furthermore, the promise of LDM chemotherapy on mitigating the risk of resistance [126] and metastasis [130] could be a separate line of future investigation.

## Chapter 5

# Harnessing the evolutionary cost of chemotherapeutic resistance by shaping the fitness landscape of a tumor

Jeffrey West, Yongqian Ma, Paul K. Newton

Harnessing the evolutionary cost of chemotherapeutic resistance by shaping the fitness  
landscape of a tumor [41]

USC Preprint

## 5.1 Abstract

Pre-existing resistant clones present in a tumor at the start of treatment remains a major problem in cancer therapeutics today. Tumor relapse and the development of chemotherapeutic resistance is now thought largely to be a consequence of the mechanism of “competitive release” of pre-existing resistant cells in the tumor which are selected for growth after chemotherapeutic agents attack the sub-population of chemo-sensitive cells which had previously dominated the collection of competing sub-clones in the tumor. We present an evolutionary game theory model based on the replicator equation to describe the clonal competition according to a fitness landscape, where the less fit resistant clone is released from competition after continuous chemotherapy, leading to a resistant tumor upon relapse. We explain the important parameters (cost of resistance and initial fraction of resistance) in anticipating the evolutionary adaptations of the tumor in order to design therapies that exploit or mitigate the harmful effects of potential future adaptions. As the tumor is growing according to Darwinian principles, so must our treatment schedules be designed with these same Darwinian principles in mind. Tumor adaptations only adapt to local and current selection forces and never anticipate the future. In contrast, treatment protocols must be dynamic and models must be evolutionary in scope, so we present a dynamic adaptive therapy control paradigm to indirectly control the resistant population to shape the fitness landscape by carefully choosing the timing of “on” and “off” chemotherapy periods.

## 5.2 Introduction

In his now classic 1961 study of competition for space between two species of barnacles in the intertidal zone off the Scottish coast, Joseph Connell [147] discovered something interesting. The blue barnacles *Balanus* normally occupied the intertidal zone, while the brown barnacles *Chthamalus* occupied the coast above high tide. Despite the commonly held belief that each occupied their own niche because of different adaptations to local micro-conditions, Connell hypothesized that the colonization of the intertidal zone by *Balanus* was actually preventing *Chthamalus* from inhabiting this region. To test this, he removed the blue barnacles from the intertidal zone and tracked the subsequent penetration of *Chthamalus* into this region. He concluded that *Chthamalus* had undergone *relief from competition* with *Balanus* which allowed it to flourish where previously it could not. The point, he emphasized, was there was nothing *inherent* about the micro-environment of the intertidal zone that was preventing *Chthamalus* from occupying this region. It was simply the competition against a more dominant species that was holding it back. Without the presence of that species, *Chthamalus* happily claimed both zones as fundamental niches. Thus, the important notion of *competitive release* was formulated (see Grant [148]). When two (or more) sub-species compete for the same resources, with one species dominating the other, if the dominant species is removed, this can provide the needed release from competition that can allow the less dominant species to flourish. The mirror image of competitive release is the related notion of *character displacement* developed by Brown and Wilson [149] in which competition can serve to displace one or more morphological, ecological, behavioral, or physiological characteristics of two closely related species that

develop in close proximity. These concepts are now well established as part of the overall framework of co-evolutionary ecology theory.

Since co-evolution among competing sub-clones is now a well established [10, 11, 24, 25] phylogenetic process in malignant tumors, the mechanism of competitive release should be expected to play a role and affect the chemotherapeutic strategies one might choose to eliminate or control tumor growth [150]. Indeed, tumor relapse and the development of chemo-therapeutic resistance is now thought largely to be a consequence of the mechanism of competitive release of pre-existing resistant cells in the tumor which are selected for growth after chemotherapeutic agents attack the sub-population of chemo-sensitive cells which had previously dominated the collection of competing sub-clones. Anticancer therapies strongly target sensitive cells in a tumor, selecting for resistance cell types and, if total eradication of all cancer cells is not accomplished, the tumor will recur as derived from resistant cells that survived initial therapy [3, ch. 1]. Subsequent application of identical therapies will have a diminished effect. A recent (2012) systematic literature analysis of cancer relapse and therapeutic research showed that while evolutionary terms rarely appeared in papers studying therapeutic relapse since 1980 (< 1%), the language usage has steadily increased more recently, due to a huge potential benefit of studying therapeutic relapse from an evolutionary perspective [151].

Our goal in this paper is to describe an evolutionary mathematical model of competitive release in a tumor in order to better quantify and understand what we feel is a key mechanism responsible for the evolution of chemotherapeutic resistance with the hope that understanding it could ultimately prove crucial for controlling and harnessing the evolutionary engine that drives its growth. We also describe quantitative tools to shape the

fitness landscape of a tumor using chemotherapeutic strategies that are as dynamic as the tumor.

### **5.2.1 Pre-existing resistance**

Cancer therapies have shown success in reducing tumor burden for significant time periods, but eventual relapse and resistance have led many to use evolutionary principles and mathematical modeling to answer whether resistance arises *de novo* during therapy or is pre-existing before therapy. Pre-existing resistant sub-clones should generally be present in all patients with late-stage metastatic disease (for single point mutations which confer resistance) as told by probabilistic models [152] and from samples taken prior to treatment [153, 154] which have been reported for melanoma [155], prostate cancer [156], colorectal cancer [157, 158], ovarian cancer [159], and medulloblastoma [160]. This implies that treatment failure is not due to evolution of resistance but rather pre-treatment presence of resistant phenotypes that are relatively sheltered from the toxic effects of therapy [161].

Pre-existing resistance has important therapeutic implications. If we assume no pre-existing resistance then most models predict maximum dose-density therapy will reduce the probability of resistance (because this treatment minimizes the number of cell-divisions, thereby minimizing the risk of *de novo* resistance) [161]. To be clear, when curative therapy is possible: treatment strategy must be designed to achieve that result. But in pre-existing resistance scenarios, the maximum dose-density therapy strategy lends itself to competitive release due to the evolutionary nature of tumor progression. Most preclinical efforts that aim to maximize the short-term effect of the drug on sensitive cells does not significantly

affect the long-term control of cancer [152]. This is because the phenomenon of competitive release can occur via the harsh selective pressure imposed by the tumor microenvironment after cancer therapies diminish the presence of the dominant (i.e. the chemo-sensitive) clone, or the process of metastasis may allow a resistant subclone in the primary tumor to emerge to higher frequencies [150].

These pre-existing mutations that are responsible for conferring resistance may be deleterious and may be associated with a phenotypic cost, or a reduced fitness, compared to sensitive cells. Even with this fitness cost, deleterious mutations are still expected to be present in late-stage metastatic cancers [162]. This cost can come in many ways, such as an increased rate of DNA repair or an active pumping out of the drug across cell membrane. All these strategies use up energy that would otherwise be available for invasion into non-cancerous tissues or proliferation. Tumors that have not yet undergone treatment may possess resistant cells in small numbers because a fitness disadvantage allows the sensitive population to suppress the resistant population to a smaller population. During drug therapy, the rapid removal of chemo-sensitive cells permits unopposed proliferation of the resistant cell population, an evolutionary phenomenon known as competitive release.

A graphical representation of clonal competition within a growing tumor known as a “fishplot” (sometimes known as a Muller plot) was first utilized in cancer to compare modes of clonal evolution in acute myeloid leukemia (see [163]). A fishplot shows the tumor burden (vertical axis) over time (horizontal axis) and the clonal lineages (a subclone is encased inside of the founding parent clone in the graph). A sample fishplot, seen in figure 5.1, displays a schematic of unhindered tumor growth after the first driver mutation (figure 5.1, left). Before diagnosis, the tumor grows exponentially, during which time a resistant

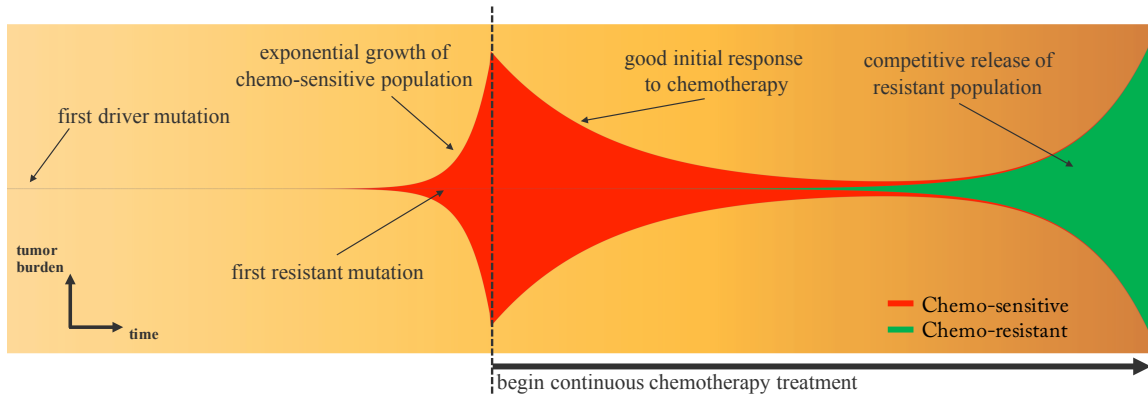


**FIGURE 5.1: Clonal evolution of competitive release** — A fishplot (sometimes known as a Muller plot), showing the tumor size (vertical axis) and composition (sensitive: red; resistant: green) over time (horizontal axis, left to right) with important events annotated. After first driver mutation (left), initial exponential growth of sensitive population occurs until diagnosis (dashed line). Continuous therapy targeting the chemo-sensitive population responds well with a decrease in tumor burden. In the absence of sensitive cells, the resistant population (existing in small numbers before the start of therapy) grow to become the dominant clone at relapse, albeit with lower exponential growth rate.

mutation occurs (figure 5.1, middle). After diagnosis, a regimen of continuous chemotherapy shows initial good response and tumor regression the resistant population grows back (although at a slower growth rate) unhindered by competition, leading to relapse (figure 5.1, right).

### 5.2.2 Using evolutionary principles to model chemotherapy

There is a need for a change in strategy in the war on cancer: eradicating most disseminated cancers may be impossible, undermining the typical goal of cancer treatment of killing as many tumor cells as possible [143]. The underlying assumption of this approach has been that a maximum cell-kill will either lead to a cure or, at worst, the maximum life extension. Taking cues from agriculturists who have long abandoned the goal of complete eradication of pests in favor of applying insecticides only when infestations exceeds a threshold in

the name of “control” over “cure,” so we must also change from the cure paradigm in cancer treatments to a control paradigm [143]. The first step in this paradigm shift is viewing tumor progression from an evolutionary lens. As such, any therapeutic methods should take the following parameters into account: the pre-existing fraction of the resistant population in the tumor before therapy and the relative growth rates (i.e. the fitness cost) of resistant subclones.

Several treatment strategies have been proposed to exploit or predict the evolutionary trajectory of tumor growth and adaptations, such as targeting the trunk driver events that are present in every tumor cell, target parallel evolutionary events, forcing the tumor down a specific evolutionary path, resulting in acquired sensitivity (sequential therapy), and dynamic therapies that maintain a stable population of treatment-sensitive cells [150]. Some have proposed modelling tumorigenesis as a process by which the homeostasis that characterizes healthy tissue is disrupted, explaining how the order of treatments can take advantage of an evolutionary double bind [26, 29, 139], thereby predicting tumor adaptations and exploiting that prediction using fundamental evolutionary principles. Regaining homoeostasis might not mean tumour eradication but instead may represent a new state where we live with cancer as a controllable, yet chronic disease. Treatments can be synergized such that evolving resistance to a single drug will increase susceptibility to a different drug. Others are modeling and planning “evolutionary enlightened” therapies, known as “adaptive therapies” that respond to the tumor’s adaptations in order to make future treatment decisions. A theoretical framework for these adaptive therapies first developed by Gatenby [42], leverages that pre-existing resistance is typically present only in small population numbers due to a cost of resistance. This less fit phenotype is suppressed in

the Darwinian environment of the *untreated* tumor but treatments that are designed to kill maximum numbers of cells remove the competition for the resistant population and ultimately select for that population during tumor relapse. (It's important to note that both high-dose, maximum tolerated dose schedules and low-dose, metronomic dose schedules have this cumulative goal of achieving maximum cell-kill over the course of many cycles of treatment.) In contrast, the goal of an adaptive therapy is to maintain a stable tumor burden that permits a significant population of chemo-sensitive cells for the purpose of suppressing the less fit but chemo-resistant populations. It takes an evolutionary strategy to combat an evolutionary tumor. An optimal treatment will indeed maintain a stable population of chemo-sensitive cells that suppress resistant populations when therapy is absent. In other words, any treatment with either the explicitly or implicitly stated goal of eliminating the maximum amount of tumor cells will likely never achieve cure or the maximum survival time.

These ideas were tested experimentally using mouse models to optimize adaptive strategies designed to maintain a stable, controllable tumor volume [164, 165]. The two-phase adaptive therapy involved an initial high-dose phase to treat the exponential growth of the tumor and a second phase designed for stable tumor control using a variety of strategies (such as decreasing doses or skipping doses when stability is achieved). Findings suggest that adaptive therapies based on evolutionary treatment strategies that maintain a residual population of chemo-sensitive cells may be clinically viable, and is currently extended to an on-going clinical trial for metastatic castration resistant prostate cancer patients (NCT02415621).

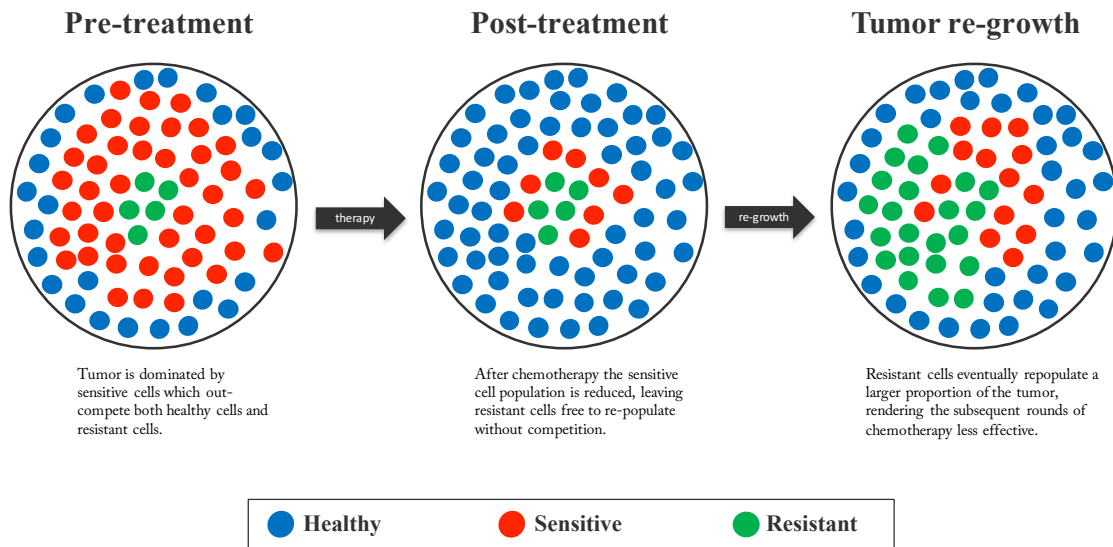


**FIGURE 5.2: Schematic of competitive release in a tumor** — Prior to treatment (left), a tumor consists of a large population of sensitive cells (red) and a small population of less fit resistant cells (green) competing for resources with the surrounding healthy cells (blue). Chemotherapy targets the sensitive population (middle), selecting for the less fit resistant population that thrives in the absence of competition from the sensitive population. Upon regrowth, the tumor composition has larger numbers of resistant cells, rendering the subsequent rounds of treatment less effective.

The goal of this manuscript is to introduce an evolutionary framework to model the important parameters of competitive release (cost, initial fraction of pre-existing resistance) and use that framework to better understand therapeutic implications of the tumor evolution, then present a few sample simulations of adaptive therapy techniques and ideas. A schematic of the three compartment model of competitive release is shown in figure 5.2, where the tumor consisting of sensitive and resistant cells is competing with the surrounding normal/healthy tissue. At diagnosis (see figure 5.2, left), the tumor is dominated by sensitive cells (red) which outcompetes the surrounding healthy population (blue) during unhindered tumor progression. A small portion of resistant cells (green) remains in small

numbers, suppressed by the larger sensitive population. After several rounds of chemotherapy, the tumor shrinks, leaving the resistant population largely unaffected (figure 5.2, middle). Inevitably, the tumor relapses due to the small number of cancer cells remaining after therapy (figure 5.2, right). In the absence of competition from the dominant sensitive population, the resistant cells grow unhindered, rendering subsequent rounds of chemotherapy less effective. In the next section, we will introduce the details of the three compartment model using the replicator equation dynamics and introduce the idea of shaping the fitness landscape of the evolving tumor in order to combat the competitive release phenomena.

### 5.3 Materials and Methods

Previously, a model predicting and quantifying competitive release has been proposed to track the relative tumor volume,  $v(t)$ , after treatment as a function of the exponential death rate of the sensitive cells,  $d$ , the exponential growth rate of the resistant cells,  $g$ , and the initial fraction of resistant cells,  $f$  [152]. The model can be written as follows.

$$v(t) = (1 - f)e^{-dt} + fe^{gt} \quad (5.1)$$

This model, shown to be a good description of the changing tumor size during therapy for colorectal, prostate, and multiple myeloma cancers, identifies the important parameters in competitive release: initial fractional resistance ( $f$ ), and birth/death rates ( $g,d$ ) for each resistant and sensitive populations, respectively. The regrowth rate of the resistant population ( $g$ ) affects the effectiveness of a continuous therapy (see figure 5.3a). A greater

“cost” of resistance (reflecting by a lower regrowth rate,  $g$ ) leads to a longer time to relapse. Although the tumor might recur with a slower growth rate, subsequent treatment is ineffective due to resistant population in large numbers (again, see figure 5.1). The initial fraction of resistant cells present at the time of treatment,  $f$ , also affects treatment effectiveness (figure 5.3b). An increase in initial fraction leads to a shorter time to relapse. A small difference in resistant regrowth rate (two-fold decrease from  $g = 0.2$  to  $0.1$ ) leads to an earlier relapse time compared to a large difference in initial fractional resistant (hundred-fold increase from  $f = 10^{-6}$  to  $10^{-4}$ ), indicating that the regrowth rate parameter has a greater effect on the effectiveness of a continuous therapy (figure 5.3c). However, the model provides no evolutionary information or concepts, a keystone principle behind competitive release. The next section will outline a model that encompasses the same characteristics of competitive release, but using evolutionary modeling concepts in order to test adaptive, “evolutionary enlightened” chemotherapy strategies in the final section.

### 5.3.1 The Model

Evolutionary game theory (EGT, see [14, 15, 17, 19, 134]), which has been used extensively to study cancer progression, provides a quantitative framework for analyzing contests (competition) between various species in a population (via the association of ‘strategies’ with birth/death rates and relative sub-clonal populations) and provides mathematical tools to predict the prevalence of each species over time based on the strategies [17, 64, 66, 72, 166]. The framework defines mutual payoffs among pairs within the subclonal populations competing for resources in the tumor. From this, one can define a fitness landscape (related to population growth rates) over which the subclonal populations evolve in time. The aim

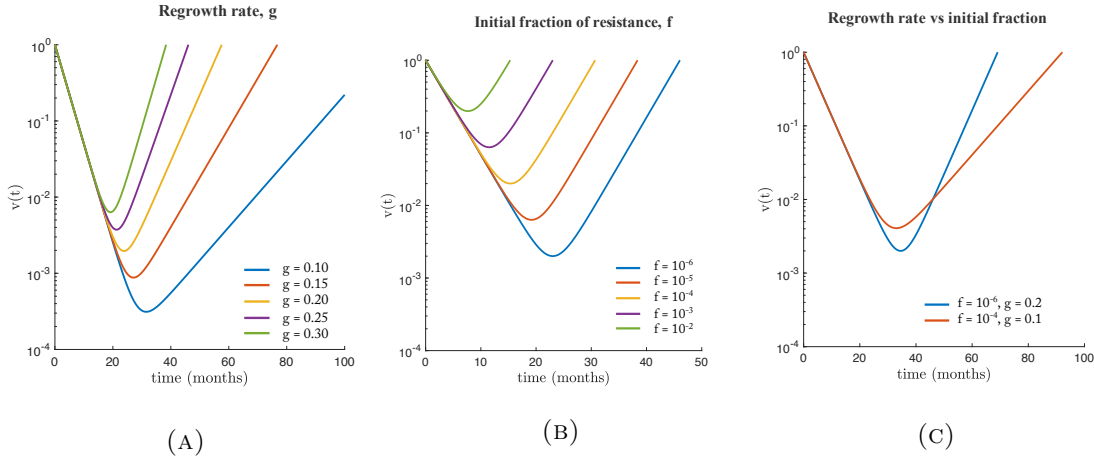


**FIGURE 5.3: Dynamics of competitive release under continuous therapy** — The dynamics described by the simple model of fraction,  $f$ , of resistant cells at the start of continuous therapy (equation 5.1). During therapy, sensitive cell population decreases at rate  $d$  and resistant population grows at rate  $g$ . Left: An increase in the resistant regrowth rate ( $g = [0.1, 0.15, 0.2, 0.25, 0.3]$  in equation 5.1) leads to decreased effectiveness of therapy ( $f = 1e-5; d = 0.3$ ). Middle: an increased initial fraction of resistance ( $f = [1e-6, 1e-5, 1e-4, 1e-3, 1e-2]$ ) also leads to decreased therapy effectiveness ( $g = d = 0.3$ ). Right: a small difference in resistant regrowth rate (two-fold decrease from  $g = 0.2$  to  $0.1$ ) compared to a large difference in initial fractional resistance (hundred-fold increase from  $f = 10^{-6}$  to  $10^{-4}$ ). The regrowth rate parameter has a greater effect on the effectiveness of a therapy.

of this research is to develop an evolutionary model based on the replicator equation dynamical framework (described below) of tumor progression and competitive release due to continuous chemotherapy, and use that model to identify and test treatment implications.

This work builds on previous work from the authors (see [32, 129]) used to carry out computational trials testing chemotherapy drug scheduling strategies (see [40]) where two cell types (a healthy and a cancerous cell type) compete according to a fitness landscape described by the evolutionary prisoner's dilemma game (see [14, 75]). This game incorporates two general classes of cells: healthy (the cooperators) and cancerous (the defectors) [135, 136]. Natural selection acts on each generation of the cell population as the computational simulation proceeds, selecting (on average) for cells with higher fitness [129],

leading to tumor growth and eventual saturation of the cancerous population. The work is extended to include a third player: the resistant cell type. The fitness landscape of interactions between all three players (healthy: blue; chemo-sensitive cancer cells: red; and chemo-resistant cancer cells: green) is depicted in figure 5.4 before therapy (top) and during therapy (bottom). In our model, we can think of a cancer cell (either a chemo-sensitive or chemo-resistant cancer cell) as a formerly cooperating healthy cell that has defected (via a driver mutation) and begins to compete against the surrounding population of healthy cells for resources and reproductive prowess. This is indicated in figure 5.4, showing the chemo-sensitive cancer cell as a higher fitness (red) than a healthy cell (blue). In the process of acquiring mutations during early tumor growth, a resistant cell may arise (green). As described previously, the development of a resistant-conferring mutation is modelled as a fitness cost; thus the resistant cell is placed further down on the fitness scale (figure 5.4, top: green) yet still a higher fitness than the healthy cell type.

In this way, the pre-treatment dynamics are described by 3 separate prisoner's dilemmas. The interactions between healthy and sensitive are described by the prisoner's dilemma (fitness of sensitive is greater than healthy, as the cancerous sensitive cells have a higher proliferative potential than the surrounding normal healthy cells). The interactions between healthy and resistant are also described by the prisoner's dilemma (fitness of resistant is greater than healthy). Finally, the sensitive population fitness is greater than resistant fitness (due to the cost of resistance): a third prisoner's dilemma.

During therapy, the fitness of chemo-sensitive cancer cells dramatically decreases and the healthy population fitness increases (see figure 5.4, bottom). The resistant cell type is unaffected by the chemotherapy treatment, leaving the fitness the same as prior to treatment

(figure 5.4, bottom: green).

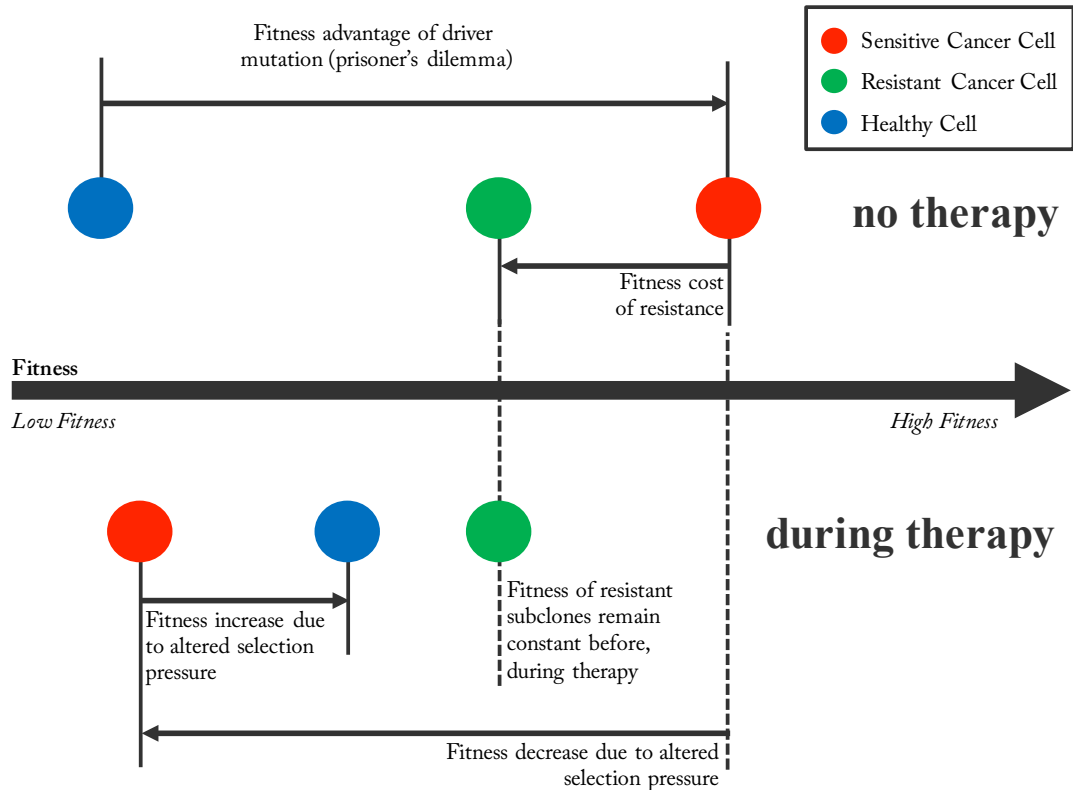


**FIGURE 5.4: Fitness landscape before and during therapy** — A schematic of the fitness of each subpopulation before therapy (top) and during therapy (bottom). A driver mutation leads to a fitness advantage of the cancer cell (red), determined by the prisoner’s Dilemma. A subsequent resistant-conferring mutation comes at a fitness cost (green). The fitness of the resistant population is unaffected by therapy’s selective pressure, but the healthy population is given an advantage over the chemo-sensitive population.

### 5.3.2 Replicator equation dynamics

The dynamics of the fitness landscape of the three competing cell types depicted in figure 5.4 are described by the replicator equation (see [116]). Each  $i$ th cell type ( $i = 1, 2, 3$ ) competes according to the replicator equation (eqn. 5.2, below), where  $x_1, x_2, x_3$  are the corresponding frequency of healthy, sensitive and resistant cells, respectively, such that

$\sum_i x_i = 1$ . The change in frequency of each cell type,  $\dot{x}_i$ , is a function of the proportion ( $x_i$ ) and fitness of that cell type ( $f_i$ ). The fitness is a function of the selection pressure,  $w_i; 0 \leq w_i \leq 1$ , and the payoff matrix,  $A$ . A value of  $w = 0$  corresponds to neutral drift (no selection) and a value of  $w = 1$  corresponds to strong selection.

$$\dot{x}_i = (f_i - \langle f \rangle)x_i \quad (5.2)$$

$$f_i = 1 - w_i + w_i(A\vec{x})_i \quad (5.3)$$

Here,  $\vec{x}$  is the vector  $\vec{x} = (x_1, x_2, x_3)^T$  and  $(Ax)_i$  is the  $i$ th element of vector  $Ax$ . The prevalence of each sub-population,  $x_i$ , changes over time according to the changing population fitness,  $f_i$ , and the average fitness of all populations  $\langle f \rangle = f_1x_1 + f_2x_2 + f_3x_3$ .

Before therapy, the selection pressure is constant across all cell type (i.e.  $w_i = w$ ). During therapy, the values of  $A$  remain constant (described in more detail below) and the selection pressure values are altered as shown in equations 5.4, 5.5, and 5.6 (see figure 5.4 for explanation of changing fitness landscape). Therapy can be administered at different doses (i.e. values of the drug concentration:  $c; 0 \leq c \leq 1$ ). A higher value of  $c$  indicates a stronger dose of chemotherapy drug (described in more detail in [40]). The selection pressure parameters are linear functions of the drug concentration, comparable to other cycle-specific drug therapy models [7, 8], explained in greater detail in our previous work here [40].

$$w_1 = (1 + c)w \quad (\text{healthy}) \quad (5.4)$$

$$w_2 = (1 - c)w \quad (\text{sensitive}) \quad (5.5)$$

$$w_3 = w \quad (\text{resistant}) \quad (5.6)$$

### 5.3.3 The pairwise prisoner's dilemmas

The fitness landscape is described by the entries of the payoff matrix, where each pairwise interaction is described by the row and column values, which are parameters in the population fitness, equation 5.3.

$$\begin{array}{ccc} & H & S & R \\ H & \left( \begin{array}{ccc} a & b & c \\ d & e & f \\ m & n & g \end{array} \right) & = & \left( \begin{array}{ccc} 1.2 & 1 & 1 \\ 1.2 + p_2 & 1.01 & 1.03 \\ 1.2 + p_3 & 1.01 - p_1 & 1.02 \end{array} \right) & = A \end{array} \quad (5.7)$$

As described previously, there are three pairwise games between healthy (H), sensitive (S), and resistant (R) populations: 1. (H,S), 2. (H,R), and 3. (R,S) which are all described as prisoner's dilemma (cooperators, defectors). The three pairwise prisoner's dilemmas necessitates the following inequalities:  $d > a > e > b$ ,  $m > a > g > c$ , and  $g > f > n > e$ . More discussion of why the prisoner's dilemma matrix, which models the evolution of defection, is a useful paradigm for cancer can be found in our previous work [32, 129]. Values are chosen as small perturbations from 1, consistent with the necessary inequalities.

Thus the 9 parameters of the payoff matrix,  $A$ , are reduced to 3 parameters:  $p_1, p_2, p_3$ . A new set of parameters ( $\gamma_2, \gamma_3$ , see equation 5.8) is defined such that  $\gamma_i = w_i p_i$ , where  $\gamma_i$  is the initial growth rate of the sensitive ( $\gamma_2$ ) and resistant ( $\gamma_3$ ) populations.

$$\left\{ \begin{array}{l} \dot{x}_2|_{x_3=0, x_2 \rightarrow 0} \approx w(d-a)x_2 = wp_1x_2 \stackrel{\Delta}{=} \gamma_1 x_2 \\ \dot{x}_3|_{x_2=0, x_3 \rightarrow 0} \approx w(m-a)x_3 = wp_2x_3 \stackrel{\Delta}{=} \gamma_2 x_3 \end{array} \right. \quad (5.8)$$

An important feature of the model is the cost of resistance. Strictly speaking, a slower growth rate of resistant cell population (i.e.  $\gamma_3 < \gamma_2$ ) implies a cost of resistance. Importantly, a second aspect of the cost must also be considered: the prisoner's dilemma between sensitive and resistant cells (i.e.  $p_1 > 0$ ) must be present in order for the sensitive population to suppress the resistant cell population in the absence of therapy. The rest of the work assumes a constant value of selection pressure ( $w = 0.1$ ) and a constant value for suppression ( $p_1 = 0.7$ ) in order to investigate the cost parameter (cost =  $\gamma_3 - \gamma_2$ ).

## 5.4 Results

The model of competitive release has two important parameters: the phenotypic cost of resistance (the difference between the unperturbed growth rates of the sensitive and resistant populations:  $\gamma_2 - \gamma_3$ ), and the initial fraction of resistance ( $f$ ). The effect of both parameters is shown in figure 5.5. An increased cost of resistance (figure 5.5a) decreases the regrowth rate and leads to a longer relapse time under continuous therapy. The initial regression rate is identical at the beginning of therapy, but the regrowth rate is diminished by the cost of resistance. An increase in initial fraction (figure 5.5b) of resistant at the

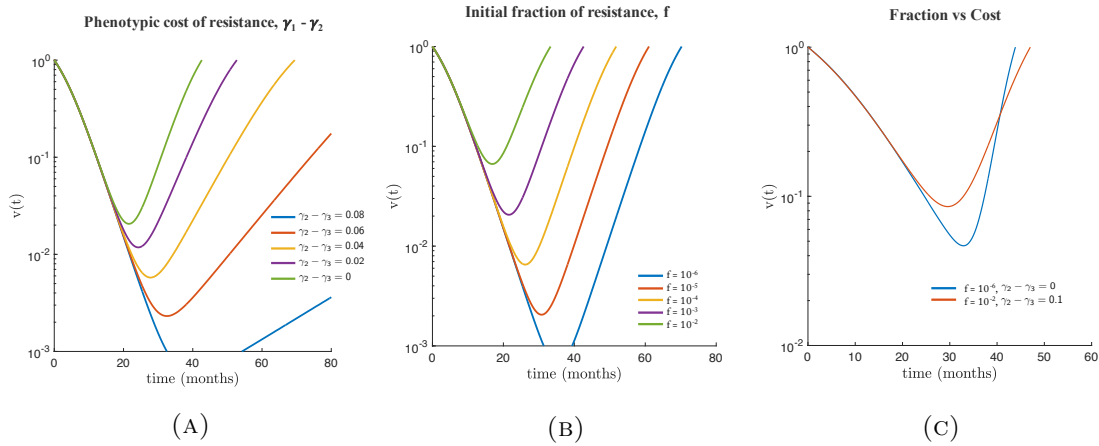


**FIGURE 5.5: The effect of growth rate, cost, and fractional resistance under continuous therapy** — (a) Increasing the phenotypic cost of resistance ( $\gamma_2 - \gamma_3$ ), results in an identical initial regression rate but extended relapse time ( $\gamma_2 = 0.02, f = 10^{-3}$ ). The slope of the regrowing tumor decreases with cost. (b) Increasing the fractional resistance results in an identical initial regression rate but extended relapse time ( $\gamma_2 = \gamma_3 = 0.02, f = 10^{-3}$ ). (c) Patient 1 (blue) has a low initial fractional resistance ( $f = 10^{-6}$ ) with no cost to resistance. Patient 2 (red) has four orders of magnitude greater fractional resistance ( $f = 10^{-2}$ ) with a relatively small cost ( $\gamma_2 - \gamma_3 = 0.1$ ) and yet has a shorter time to relapse. This implies that the cost of resistance (i.e. the diminished regrowth rate of the tumor) is more important to relapse than the initial fraction of resistance.

start of therapy leads to shorter relapse times. The initial regression rate and the regrowth rate are identical for all simulations but a small fractional resistance leads to a lower minimum tumor burden achieved and longer relapse times. Immediately, it is important to ask which of these parameters has the most significant effect on time to relapse. In figure 5.5c, the relapse times for two patients are compared. Patient 1 (blue) has a low initial fractional resistance ( $f = 10^{-6}$ ) with no cost to resistance. Patient 2 (red) has four orders of magnitude greater fractional resistance ( $f = 10^{-2}$ ) with a relatively small cost  $\gamma_2 - \gamma_3 = 0.1$  and yet has a shorter time to relapse. This implies that the cost of resistance (i.e. the diminished regrowth rate of the tumor) is more important to relapse than the initial fraction of resistance. Even a small cost of resistance leads to a significant change in tumor relapse dynamics. This is consistent with previous models, shown in figure 5.3c.

Evolutionary game theory models allow testing two different treatment paradigms: 1) treatments that target the strategies (or, subpopulations of cells) and 2) treatments that target the game, by anticipating or driving the evolutionary trajectory to more amenable dynamical spaces [167]. Traditional treatment methods (i.e. maximum tolerated dose schedules or low dose metronomic schedules) have the goal of complete eradication of all tumor cells (or, at least the eradication of all chemo-sensitive cells), encourage the competitive release phenomenon in the presence of pre-existing resistance. Figure 5.5 and 5.6 (below) detail the important outcomes of the first paradigm: targeting the strategies (i.e. indiscriminately targeting chemo-sensitive cells, without a view to tumor evolution). In the final section, figure 5.8 is a proof-of-concept adaptive strategy aimed at anticipating the evolutionary trajectory (i.e. “targeting the game”) to improve outcomes.

#### 5.4.1 Treating the strategy: competitive release

Figure 5.6 details the relationship between dose concentration and two important measures of therapy effectiveness: progression free survival (PFS) and time to relapse. Measuring the effectiveness of a chemotherapy based on the killing rate or progression free survival alone are not sufficient predictive measures of long-term cancer control [152]. As seen in figure 5.6, left, an increased dose (3 therapies are simulated on identical initial conditions:  $\gamma_2 = 0.020$ ,  $\gamma_3 = 0.018$ ,  $f = 10^{-3}$ ) corresponds to a slightly shorter PFS (an increase from blue to red to yellow), but an increased time to relapse to the initial tumor volume. However, despite the increase relapse times, none of these doses optimize tumor control, as seen in the fishplots (figure 5.6, right). At the point of relapse to the initial tumor volume, the tumor is dominated by the presence of resistant clones (green), rendering

future treatments ineffective. Oftentimes, the effectiveness of a new chemotherapy drug may be determined by PFS times when drugs that have high killing rates of sensitive cells may have *shorter* times to progression and lower total tumor burden at all times, everything else equal. The figure clearly shows that all treatments have similar progression free times but with a greater range of relapse times (even though continuous treatment always eventually leads to relapse).

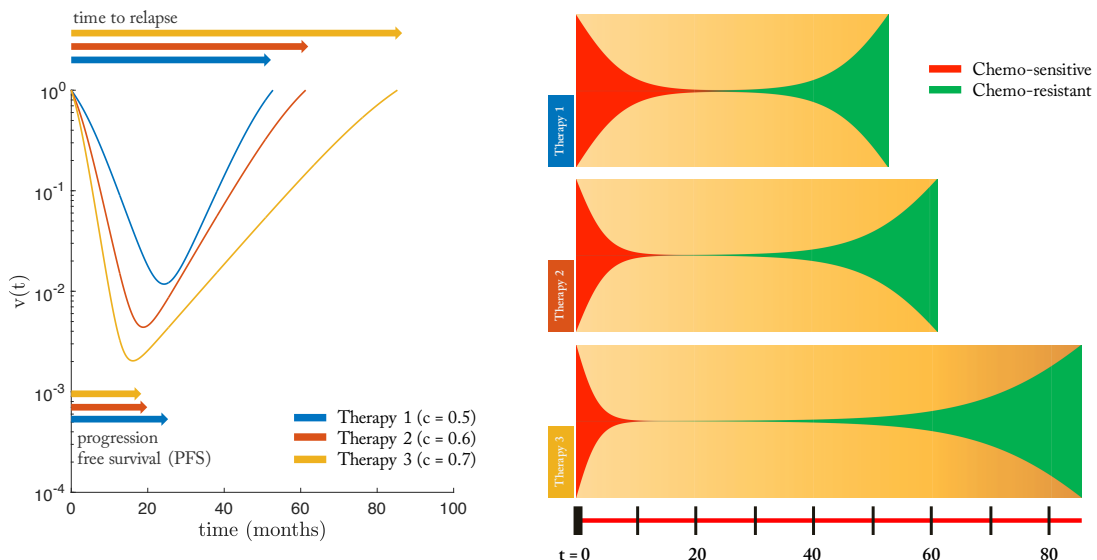


**FIGURE 5.6: The effect of dose on tumor relapse and progression free survival under continuous therapy** — Left: 3 therapies are simulated on identical initial conditions ( $\gamma_2 = 0.020$ ,  $\gamma_3 = 0.018$ ,  $f = 10^{-3}$ ,  $w = 0.1$ ). Time to relapse significantly increases with increasing dose while the progression free survival shows marginal, but decreasing, difference. Right: the same 3 therapies are shown in a fish plot, where the simulation is stopped at the point of relapse to initial tumor size (now consisting entirely of chemo-resistant population).

In order to better understand the dynamics of competitive release to anticipate the evolutionary trajectory of the tumor, dynamical state space diagrams are shown in Figure 5.7 for no therapy ( $c = 0$ ; 5.7a) and with therapy ( $c = 0.6$ ; top right triangle). A schematic explaining the tri-linear coordinates (sometimes referred to as barycentric coordinates where

$\sum_i x_i = 1$ ) of the triangular simplex (a representation of the phase space for every possible value of  $\vec{x}$ ) is shown in figure 5.7c. The corners represent saturation of a single cell type (e.g. the top corner represents  $\vec{x} = [1, 0, 0]$ , or all healthy cells).

First, let us consider the no treatment dynamics: the top left triangle in figure 5.7a. The healthy (H; top corner), sensitive (S; bottom left corner), and resistant (R; bottom right corner) populations compete according to equation 5.2 and follow trajectories shown (black). Instantaneous relative velocity is indicated by background color gradient (red to blue). All internal trajectories (pre-therapy) lead to tumor growth and eventual saturation of the sensitive population (bottom left corner of triangle). The resistant population nullcline (line of zero growth;  $\dot{x}_R = 0$ ) is plotted (dashed green line). After an initial slow positive growth, the resistant population is suppressed by the faster growing sensitive population; all trajectories lead to the bottom left corner: saturation of the sensitive population. The healthy population nullcline (dashed blue line) is also plotted. The healthy nullcline is the dividing line of positive tumor growth and negative tumor growth (with the tumor consisting of both the sensitive and resistant populations). The sensitive nullcline (dashed red line) is on the boundary of the triangle, indicated there is no internal point for which there is negative sensitive growth.

Chemotherapy alters the selection pressure to the disadvantage of chemo-sensitive cancer population and advantage of the healthy population (see equations 5.4, 5.5, and 5.6), altering dynamical outcomes: shown in the top right triangle in figure 5.7b. Internal solution trajectories (black) show initial trajectory toward healthy saturation (triangle top) but eventual relapse toward resistant population (bottom right of triangle) upon passing the resistant nullcline (dashed green line). Interestingly, the trajectories pass the resistant

nullcline before the healthy nullcline (dashed blue line), indicating the resistant population may have positive growth ( $\dot{x}_R > 0$ ) even though the tumor has positive regression ( $\dot{x}_H < 0$ ), indicated as region 3. The sensitive nullcline is also plotted (dashed red line), showing initial conditions where tumor burden is too large and the dose concentration is inadequate to achieve positive regression of the sensitive population (regions 1, 5, and 6 such that  $\dot{x}_S > 0$ ). The nullcline information will be used in the next section to determine timing schedules of adaptive therapy (see figure 5.8).

#### 5.4.2 Treating the game: adaptive therapy

In contrast to targeting a specific player in the game (i.e. heavily targeting the chemo-sensitive population), adaptive therapies take advantage of the important recognition that fitness is contextual and changes during therapy or on drug holidays. The mechanism for control is also contextual: the suppression of the growth of resistant cell population occurs during periods of rest or weaker doses of therapy (drug-sensitive cells have a fitness advantage in these conditions); suppression of the growth of the sensitive cell population occurs during treatment. Figure 5.8 shows how the idea of contextual fitness can be applied to therapeutic strategies.

A simple control paradigm is proposed to *indirectly* control the resistant population. Therapy targets only the chemo-sensitive cells, but the resistant population can be controlled by systematically choosing when to administer therapy and when to give drug holidays. Therapy “on” is for the purpose of killing sensitive cells. Therapy “off” is for the purpose of allowing a stable amount of sensitive cells to remain, in order to suppress the resistant

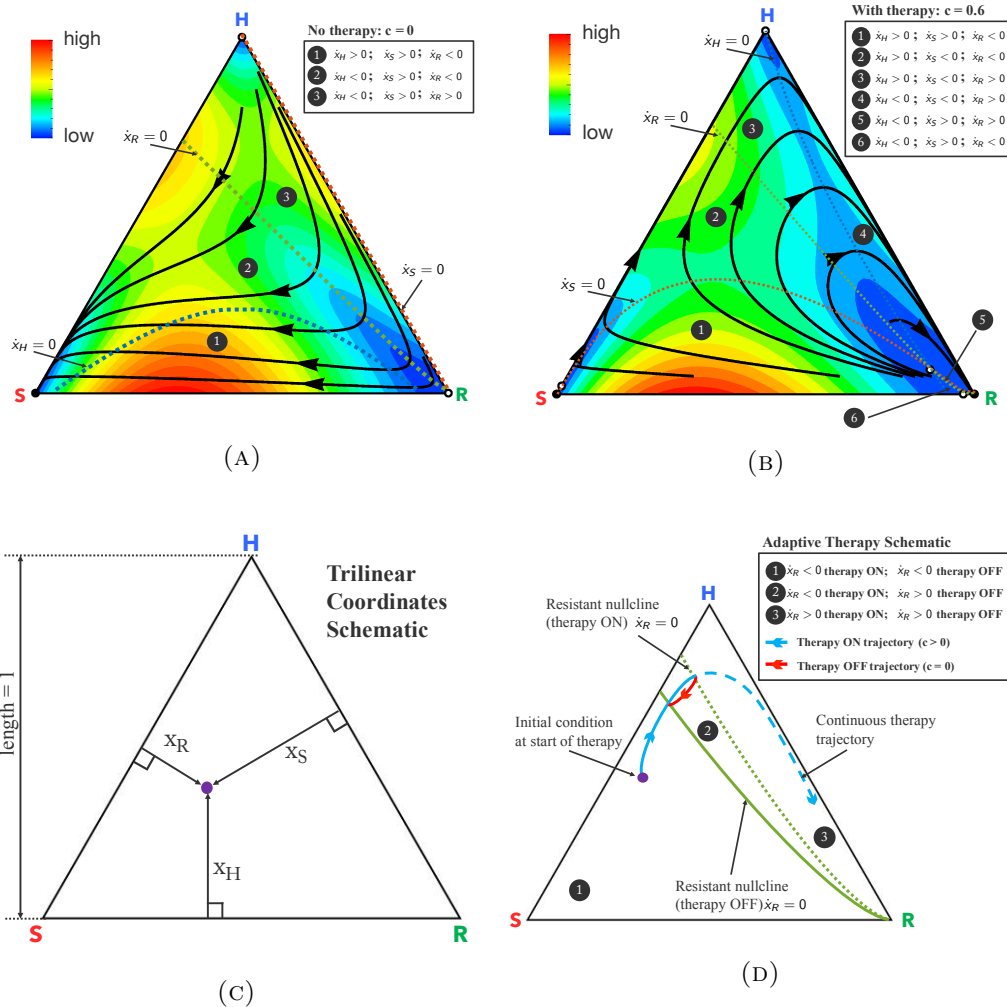


**FIGURE 5.7: Dynamic phase portraits before and during chemotherapy** — Top left: before chemotherapy, the healthy (H), sensitive (S), and resistant (R) populations compete on a dynamical fitness landscape, with several solution trajectories shown (black) and the instantaneous relative velocity indicated by background color gradient (red to blue). All internal trajectories lead to tumor growth and eventual saturation of the sensitive population (bottom left corner). Each population nullcline (line of zero growth:  $\dot{x}_i = 0$ ) is plotted: healthy (dashed blue), sensitive (dashed red), and resistant (dashed green). Top right: chemotherapy alters the selection pressure to the disadvantage of chemo-sensitive cancer population and advantage of the healthy population (shown for  $c = 0.6 \cdot \gamma_2 = 0.020$ ,  $\gamma_3 = 0.018$ ,  $w = 0.1$ ). Solution trajectories (black) show initial trajectory toward healthy saturation (triangle top) but eventual relapse toward resistant population (bottom right of triangle) upon passing the resistant nullcline. Bottom Left: a schematic of proposed adaptive therapy concept using the resistant nullclines to determine therapy “on” and “off” times in order to trap the tumor in the controllable region 2, and reach approximate cycle that repeats back on itself in red. The continuous therapy is also plotted in dashed blue, for comparison.

population. The control paradigm is as follows: a continuous dose of therapy is administered until the nullcline ( $\dot{x}_R = 0$ ) is reached (see figure 5.7b). This is the starting point of positive growth for the resistant population (further therapy would result in  $\dot{x}_R > 0$ ). At this point, a drug holiday (no therapy administered) is imposed until the second nullcline is reached (see figure 5.7a). The sensitive population is allowed to regrow until it is large enough to suppress the resistant population once again (and when  $\dot{x}_R = 0$ ). Therapy is administered to allow the tumor to cycle back and forth between the two nullclines. Targeting the resistant population for control allows an extension of relapse times by shaping the fitness landscape at the right time in order to return to an amenable, controllable tumor burden and tumor composition. A schematic of this control paradigm is shown in figure 5.7d.

The control paradigm is tested in figure 5.8 for identical initial conditions using a range of drug concentration dose values (low dose: blue; medium dose: red; high dose: yellow). The low and medium dose adaptive therapy strategies adequately outperform the continuous, constant dose (dashed lines). As seen in the fishplots on the right, the resistant population (green) is suppressed during the “off” times of drug holidays, leading to an extended time without relapse for low and medium dose concentration (therapy 1 and 2). However, a higher dose (during therapy “on”) leads to less tumor control and eventual relapse. The low- and medium-dose adaptive therapy strategies are successful for two reasons. First, the drug holidays allow an adequate sensitive population size to suppress the growth of the lower-fitness resistant population. Second, the resistant population is never allowed to reach a positive growth ( $\dot{x}_R > 0$ ) during therapy “on” time periods. This positive growth region for the resistant population is the “point of no return” where the tumor will no

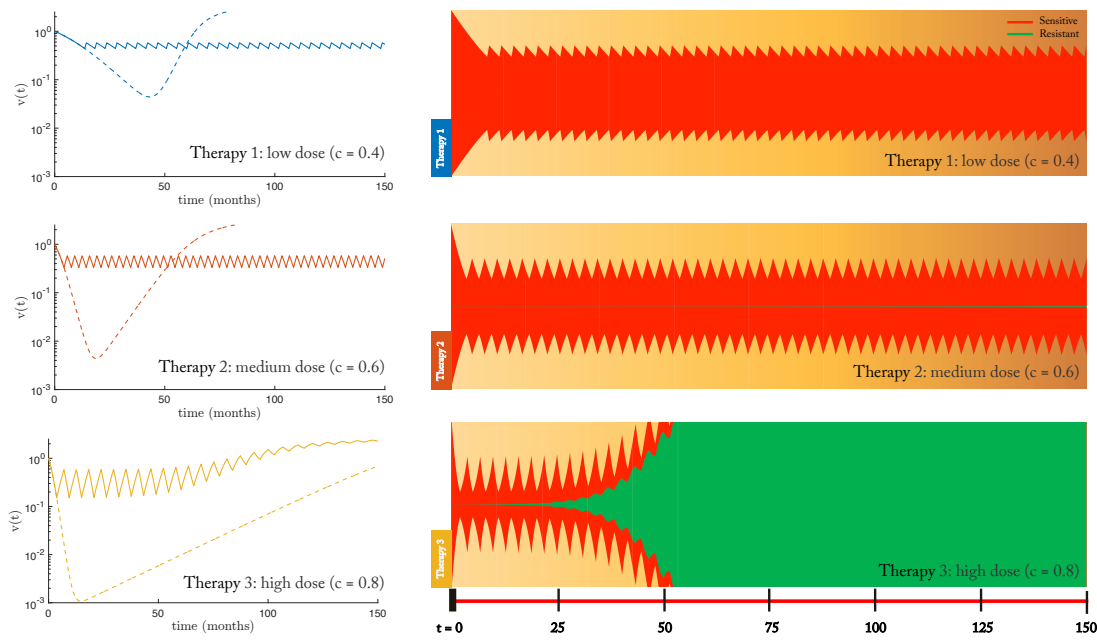


**FIGURE 5.8: Adaptive therapy strategy to control resistant population** — Left: Low dose (blue; top:  $c = 0.4$ ), medium dose (red; middle:  $c = 0.6$ ) and high dose (yellow; bottom:  $c = 0.8$ ) are shown for continuous therapy (dashed line) and adaptive therapy (solid line). Right: the respective fishplot is shown to the right of each therapy (low, medium, high) dose level. The adaptive therapy control paradigm administers therapy (ON) until the nullcline is reached ( $x_R = 0$ ; see figure 5.5, right). At this point, further therapy will result in the growth of the resistant population (i.e.  $x_R > 0$ ). Therapy is then turned OFF (a drug “holiday”) until the second nullcline is reached (see figure 5.5, left), allowing the sensitive population to regain a stable and adequate size useful to suppress the resistant population. This control paradigm works well for low and medium dose, but stable control is not achieved for high dose.

longer be controllable via the same drug.

## 5.5 Discussion

Previous models of competitive release (e.g. equation 5.1) have been shown to be good descriptions of changing tumor size during therapy for many types of cancer [152], yet include no evolutionary concepts. As these models cannot be used to test adaptive chemotherapy drug schedules that are designed to anticipate and correct for the evolutionary trajectory of

a tumor, a model was proposed here using a pairwise prisoner’s dilemma in the replicator equation. Key parameters of the model include the initial growth rates of the chemo-sensitive and chemo-resistant population ( $\gamma_2, \gamma_3$ ), the cost of resistance ( $\gamma_2 - \gamma_3$ ), and the initial fraction of resistance. The most important parameter was determined to be the cost of resistance, with a small change exhibiting a large difference in time to relapse. The key concept of the fitness landscape in the replicator equation is that the drug, designed to kill proliferating chemo-sensitive cells, can be modeled as a change in the fitness landscape via the selection pressure parameter,  $w$ . Resistant subclones, by definition, resist any change in fitness due to the drug. Traditionally, chemotherapy drugs are tested by maximizing the kill rate, or maximizing the progression free survival time. Time to relapse is shown to be a more meaningful parameter to judge continuous chemotherapy drugs, even though all simulated tumors eventually relapse if there is pre-existing resistance at the start of therapy. Finally, an adaptive therapy concept was introduced to indirectly control the resistant population by leaving a stable tumor burden designed to suppress the resistant population. The adaptive therapy concept was informed by the resistant nullclines in the dynamics phase plane for the therapy “on” and “off” state space. The concept was shown to have good success at extending relapse times for low- or medium-dose therapies.

Tumor adaptations only adapt to local and current selection forces and never anticipate the future. Here, oncologists and modelers may have an advantage if we can anticipate the evolutionary adaptations of the tumor and design therapies that exploit or mitigate the harmful effects of potential future adaptions. As the tumor is growing according to Darwinian principles, so must our treatment schedules be designed with these same Darwinian principles in mind. Treatment must be dynamic and models must be evolutionary

in scope. The goal here isn't to develop a new drug, but to optimize scheduling for existing drugs and better understand the dynamics of competitive release with the goal of control, and therefore, life extension. This life extension may give researchers the necessary time to improve existing drugs or develop new targeted drugs.

## Chapter 6

# High Performance Computing Techniques

The Center for High-Performance Computing (HPC) at the University of Southern California claims the 8th fastest supercomputer cluster in the United States, a resource made available to researchers at the university. The HPC is comprised of 2,225-node, 4-core, 6-core, and 12-core dual-processors manufactured by Dell, Oracle Sun, Hewlett-Packard and IBM connected on a 10-gigaabit Myrinet backbone. This computing cluster is ideal for the development of massive computational research jobs that require high-speed communications among parallel computational elements [168].

In order to fully utilize the resources on the HPC for this research project, algorithms were implemented using the standard message passing system Message Passing Interface (MPI) and the shared memory multiprocessing API OpenMP. The purpose of using these

high performance computing resources is to scale simulations to large cell numbers, increase the speed of single stochastic simulations, and to scale the number of stochastic simulations output by the previously described models.

## 6.1 Hybrid MPI + OpenMP Parallelization

In order to scale the number of cells in the single site, primary tumor ecology models, a hybrid message-passing and shared-memory (MPI + OpenMP) system was implemented. Figure 6.1 shows a schematic diagram of the process. During a single simulation,  $n_p$  nodes are allocated, and  $n_{td}$  threads are spawned on each of those nodes. The communication between nodes is handled by MPI, and the thread communication is handled by OpenMP.

In Algorithm 1, the single thread, single node process for the primary tumor ecology model is shown (a moran process with mutations and selection). The procedure calculates the probability vectors for birth and death ( $p_{birth}$ ,  $p_{death}$ ), chooses a single cell for birth and death each time step, and checks if the daughter cell incurred a mutation during the birth event during each time step, or cell division.

The birth, death, and mutation processes are then parallelized on  $n_p$  nodes (i.e. an MPI task) each with  $n_{td}$  threads, as seen Algorithm 2. The single thread algorithm runs simultaneously on each thread. The MPI\_Send command sends the  $p_{birth}$  and  $p_{death}$  vectors to each node. Next, each node forks into  $n_{td}$  threads. Each thread simulates  $nThreadLoops$

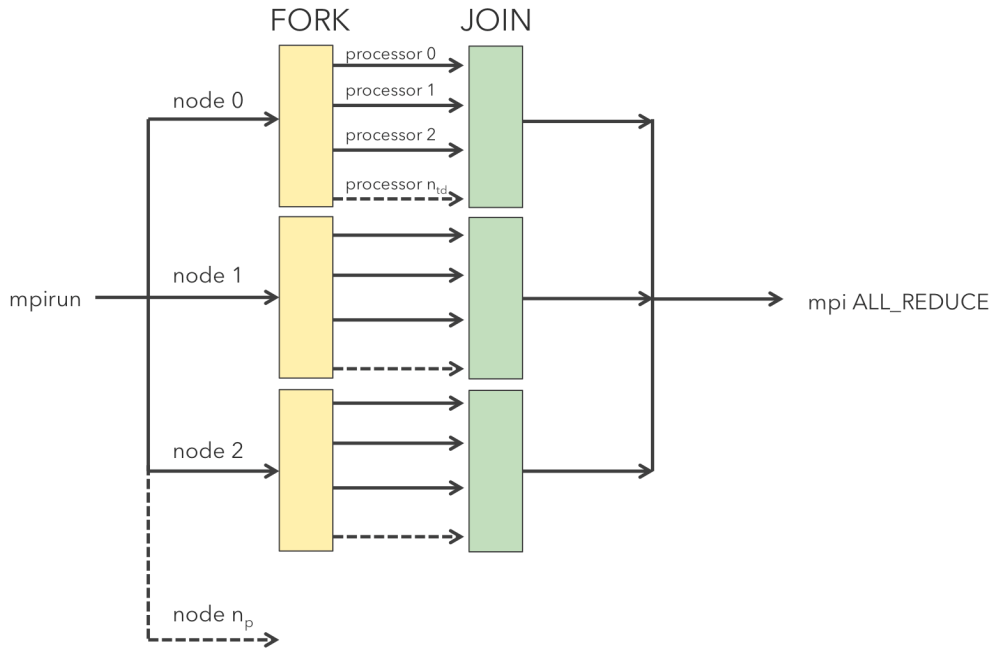


FIGURE 6.1: Schematic diagram of the Hybrid MPI + OpenMP Parallelization technique.

In order to scale primary tumor growth simulations to large numbers of cells, a double Fork/Join process was used. MPI was used to fork to  $n_p$  nodes and OpenMP was used to fork to  $n_{td}$  threads. A join process for all nodes and threads is used in order to keep the possible error in the  $p_{birth}$  and  $p_{death}$  vectors to a minimum.

birth, death and mutation processes without updating the  $p_{birth}$  and  $p_{death}$  vectors. Each thread keeps a local version of the change in state vector,  $\Delta x$ .

## 6.2 Error in Hybrid MPI + OpenMP Parallelization

During the fork/join process, error in the  $p_{birth}$  and  $p_{death}$  vectors accumulates. This occurs because each node (and each subsequent thread) operates independently during the duration of the fork process. The state of the system (i.e. the total number of cancer cells) is tracked independently for each of the forks (a local system state), and the global state is estimated by the local system state on each fork. Not until the fork comes to an end at the

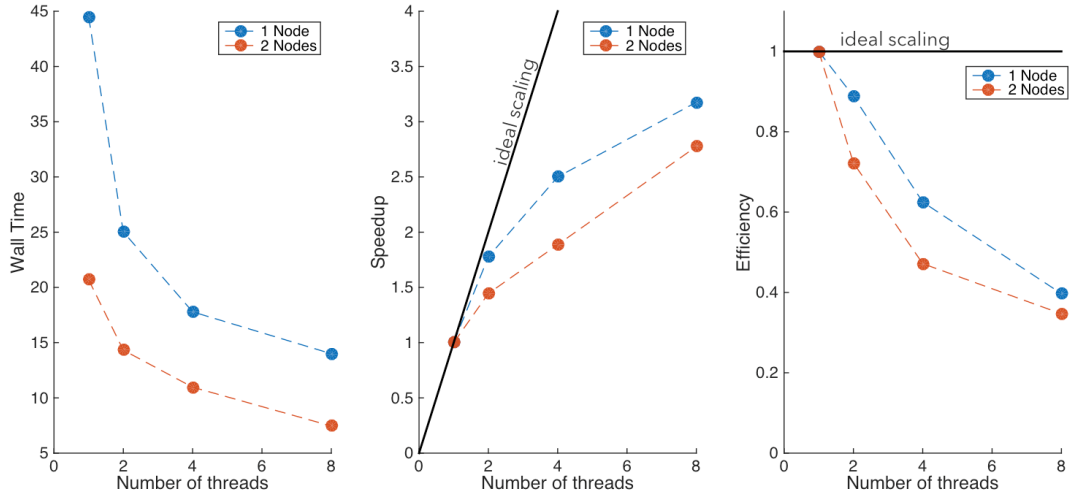


FIGURE 6.2: **Strong scalability of Hybrid Parallelization** — A sample primary tumor ecology model simulation using Algorithm 2 (Hybrid MPI + OpenMP) for  $N = 10^6$  cells, mutation rate  $m = 0.2$ , and selection pressure  $w = 0.5$ . The simulations were performed on Dual Quadcore nodes with AMD Opteron 2.3 GHz processors with 16GB Memory. The simulation was duplicated with a single node ( $n_p = 1$ , blue line) and a 2 node ( $n_p = 2$ , red line) setup with varying thread count ( $n_{td} = 1, 2, 4, 8$ ). Left: total wall time required to finish the simulation ( $2.5e7$  timesteps) for each value of  $n_p$  and  $n_{td}$ . Middle: speedup calculated from 6.1. Right: efficiency of scaling, calculated from 6.2.

---

**Algorithm 1** Moran Process using Single-Thread Computation

---

```

1: procedure MORAN
2:   calculate  $p_{birth}$  and  $p_{death}$                                  $\triangleright$  birth and death probability vectors
3:   while  $t < totalTime$  do
4:     update  $p_{birth}$  and  $p_{death}$ 
5:     choose cell type for birth
6:     check for mutation during birth process
7:     choose cell type for death
8:     update state vector,  $\vec{x}$ 
9:      $t = t + 1$ 
10:   end while
11: end procedure

```

---

MPI\_Allreduce step is the global state known to the each fork. Meanwhile, the local state is used in the calculation of the birth and death probability vectors. Between updates to the global state, the number of timesteps executed will be  $n_{total} = n_p \cdot n_{td} \cdot nThreadLoops$ . In general, the longer the fork, the higher error accumulated. The error is also increased

---

**Algorithm 2** Moran Process using Mutli-Thread Computation

---

```

1: procedure MORAN
2:   calculate  $p_{birth}$  and  $p_{death}$                                  $\triangleright$  birth and death probability vectors
3:   while  $t < totalTime$  do
4:     update  $p_{birth}$  and  $p_{death}$ 
5:     MPI SEND  $p_{birth}$  and  $p_{death}$  to nodes 0 -  $n_p$ 
6:     FORK into  $n_{td}$  threads on each node
7:     loop                                               $\triangleright$  each thread performs  $nThreadLoops$ 
8:       choose cell type for birth
9:       check for mutation during birth process
10:      choose cell type for death
11:      update local  $\Delta\vec{x}$ 
12:    end loop
13:    JOIN
14:    MPI ALL REDUCE each node's  $\Delta\vec{x}$  local state vector to update the global state
    vector  $\vec{x}$ 
15:     $t = t + (n_p \cdot n_{td} \cdot nThreadLoops)$ 
16:  end while
17: end procedure

```

---

for lower number of cells and higher number of threads or nodes. It is useful to understand

how the error in the probability of birth and death for cancer cells changes during the fork.

In Figure 6.3, this error is documented. The maximum error in the birth and death vectors

can be easily computed by considering the case that maximizes  $\Delta p_{birth}$  and  $\Delta p_{death}$  in the

$n_{total}$  timesteps.

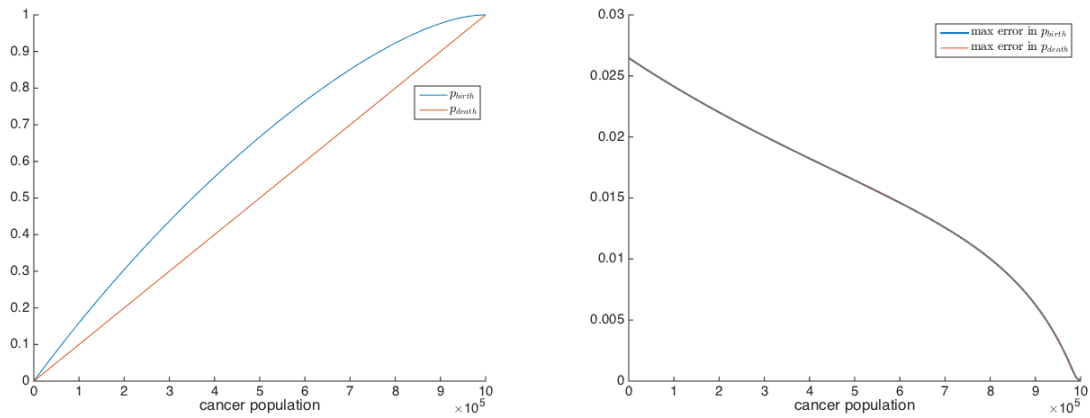


FIGURE 6.3: Error in the Hybrid MPI + OpenMP primary tumory growth simulation. Left: The probability of a cancer birth (blue) and cancer cell death (red) for  $w = 0.5$  and  $N = 10^6$  cells. A Fork/Join process for  $n_p = 2$ ,  $n_{td} = 8$  and  $nThreadLoops = 1000$  was employed. Right: the maximum  $\Delta p_{birth}$  and maximum  $\Delta p_{death}$  possible during the fork process.

### 6.3 Speedup and Efficiency

In order to measure the effectiveness of the hybrid parallelization of the primary tumor growth model, the speedup and efficiency, speedup and efficiency was plotted for fixed-problem sized scaling. The speedup for  $n_p$  MPI processes and  $n_{td}$  OpenMP threads is shown in equation 6.1 and efficiency is shown in equation 6.2. In Figure 6.2, the speedup and efficiency is plotted. As the number of nodes or processes increase, the speedup departs from ideal scaling, with a maximum of 3 times speedup for  $n_p = 2$  and  $n_{td} = 8$ .

$$S_p = \frac{T(n_p, n_{td} = 1)}{T(n_p, n_{td} = p)} \quad (6.1)$$

$$E_p = \frac{S_p}{p} \quad (6.2)$$

### 6.4 Performance Tunability

The performance of a Hybrid MPI + OpenMP algorithm can be tuned to find the best combination of threads and nodes. Each simulation is run with fixed-size problem ( $N = 10^6$  cells), keeping the total number of processes  $P = n_p \times n_{td}$  constant. The results are shown in Table 6.1.

The optimal combination is 1 node with 8 threads. It is important to note that most simulations with large number of cells ( $> 10^9$ ) will require more than a combination of 8 threads and nodes, but the underlying principle here is that a maximum number of threads should be used, over a maximum of nodes.

**TABLE 6.1: Performance Tuning**

Number of OpenMP threads, $n_{td}$	Number of MPI processes, $n_p$	Wall Time, $W_T$
1	8	1.4709
2	4	2.5882
4	2	4.5893
8	1	0.5955

## Chapter 7

# Future Work

Mathematical models of the type developed in this thesis will play an increasingly important role in identifying and implementing novel chemotherapeutic strategies and will join the arsenal of tools that clinicians will turn to as they continue to develop strategies to fight cancer. Future progress will increasingly require the interactions of an interdisciplinary array of scientists, including applied mathematicians, to develop mathematical models of tumorigenesis and therapy response as a complex process [169]. Active collaboration among experimentalists, clinicians, and modelers will help produce an integrative and comprehensive view of the disease. With this in mind, we outline briefly some extensions and new developments we plan to pursue related to this thesis.

## 7.1 Chemotherapy scheduling and metastasis

As the role of specific genetic events that enable the tolerance and propagation of genome instability is elucidated, more data will become available to predict evolutionary trajectory and subsequent metastatic initiation and evolution [29]. Mathematical modeling will help uncover the role of competition as well as the role of mutations in driving or supporting metastasis. Current evolutionary models (such as those developed in this thesis) can be extended to include cell trafficking through circulatory and lymphatic systems, integrating metastatic data [87, 170]. The successful development of targeted cancer drugs has been limited by drug resistant subclones, especially in a metastatic setting. Full cell-trafficking models can address questions about the trafficking of clones as well as the effect of drug treatment on circulating tumor cells.

## 7.2 Control theory methods to minimize stable tumor bur-

### den

The replicator equation models competitive release [41, 116] as an evolutionary trade off of developing resistance mechanisms at the cost of the growth rates of resistant populations. The model is an ideal one for testing chemotherapeutic strategies designed to exploit this fitness cost by allowing a stable burden of sensitive population that suppresses the growth of the resistant population. One such example of an adaptive therapy (see chapter 5) uses the nullclines to determine the time boundaries of bang-bang (on-off) control.

Further research can explore more complicated methods of control including varying the dose concentration as well as the length of drug holidays. Importantly, other groups have developed models of competitive release using spatial evolutionary models, which allows for drug penetration to be modelled [171]. Microenvironmental effects are shown to be important to the development of resistance, and can be considered in future models [172, 173].

The current model (chapter 5) assumes perfect information about the fraction of resistant population and the underlying phase portrait dynamics, an impractical assumption in clinical settings. Further research can integrate probabilistic models predicting the occurrence of resistance based on known or estimated mutation rates (see [56, 152, 174–176])

Others have looked at optimal combinations or sequences of three or more drugs [34, 138, 177], or the evolutionary relationship of multiple treatments (see [139]). The current model (chapter 5) can be extended to include multiple non-cross resistant drugs [137, 166].

### 7.3 Heterogeneity drives tumor growth

There are a wide array of classical models used to describe tumor growth [96]. The underlying biological mechanisms of such growth models, often remain unclear [4, 178]. Kendal has developed a description of the role of heterogeneity in driving tumor growth using methods borrowed from statistical mechanics [85], which has also been reviewed in the context of models developed for this thesis (see [32]). These methods can be extended to modern growth models to better understand the role of heterogeneity in more sophisticated model paradigms. These statistical methods could be used to explore differences between neutral

models of evolution [179], Darwinian models of evolution (linear and branched models) [150] and models of clonal interactions [29].

## 7.4 Integrating preclinical and clinical trial data

A changing paradigm shift has led to a change in the strategy of treating cancer [143] from “cure” to “control” paradigms. Evolutionary models have had success in predicting existence of an evolutionary double bind [26, 29, 139] in the order of administering multiple treatments. Other strategies target trunk mutation driver events that are present in every tumor cell, target parallel evolutionary events, forcing the tumor down a specific evolutionary path, resulting in acquired sensitivity (sequential therapy), and dynamic therapies that maintain a stable population of treatment-sensitive cells [150].

The challenge will be in integrating molecular, genomic, phylogenetic, and serum marker (e.g. PSA counts in prostate cancer) data to inform existing models and aid the development of new evolutionary and ecological models of tumor initiation, with a goal of predicting tumor adaptations and exploiting that prediction using fundamental evolutionary principles. Data describing the evolutionary effect of cancer treatments are becoming increasingly available, in the form of preclinical trials [164, 165] and is currently extended to an on-going clinical trial (NCT02415621).

# Bibliography

- [1] Douglas Hanahan and Robert A Weinberg. The hallmarks of cancer. *Cell*, 100(1):57–70, 2000.
- [2] Philip Gerlee. The model muddle: in search of tumor growth laws. *Cancer Research*, 73(8):2407–2411, 2013.
- [3] Michael Clinton Perry. *The Chemotherapy Source Book*. Lippincott Williams & Wilkins, 2008.
- [4] Anna Kane Laird. Dynamics of tumour growth. *British journal of cancer*, 18(3):490, 1964.
- [5] Benjamin Gompertz. On the nature of the function expressive of the law of human mortality, and on a new mode of determining the value of life contingencies. *Philosophical transactions of the Royal Society of London*, 115:513–583, 1825.
- [6] Emil Frei and George P Canellos. Dose: a critical factor in cancer chemotherapy. *The American Journal of Medicine*, 69(4):585–594, 1980.
- [7] L Norton and R Simon. Tumor size, sensitivity to therapy, and design of treatment schedules. *Cancer Treatment Reports*, 61(7):1307, 1977.

- [8] Howard E Skipper, Frank M Schabel Jr, and William S Wilcox. Experimental evaluation of potential anticancer agents. xxi. on the criteria and kinetics associated with curability of experimental leukemia. *Cancer Chemotherapy Reports. Part 1*, 35:1, 1964.
- [9] Howard E Skipper. Laboratory models: some historical perspective. *Cancer Treatment Reports*, 70(1):3–7, 1986.
- [10] Lauren MF Merlo, John W Pepper, Brian J Reid, and Carlo C Maley. Cancer as an evolutionary and ecological process. *Nature Reviews Cancer*, 6(12):924–935, 2006.
- [11] Camille Stephan-Otto Attolini and Franziska Michor. Evolutionary theory of cancer. *Annals of the New York Academy of Sciences*, 1168(1):23–51, 2009.
- [12] Steven A Frank. *Dynamics of Cancer: Incidence, Inheritance, and Evolution*. Princeton University Press, 2007.
- [13] Mel Greaves. *Cancer: The Evolutionary Legacy*. Oxford University Press, 2001.
- [14] Robert Axelrod, David E Axelrod, and Kenneth J Pienta. Evolution of cooperation among tumor cells. *Proceedings of the National Academy of Sciences*, 103(36):13474–13479, 2006.
- [15] Martin A Nowak. *Evolutionary Dynamics*. Harvard University Press, 2006.
- [16] IPM Tomlinson. Game-theory models of interactions between tumour cells. *European Journal of Cancer*, 33(9):1495–1500, 1997.

- [17] Sabine Hummert, Katrin Bohl, David Basanta, Andreas Deutsch, Sarah Werner, Günter Theißen, Anja Schroeter, and Stefan Schuster. Evolutionary game theory: cells as players. *Molecular BioSystems*, 10(12):3044–3065, 2014.
- [18] Thomas L Vincent. Carcinogenesis as an evolutionary game. *Advances in Complex Systems*, 9(04):369–382, 2006.
- [19] Franziska Michor, Yoh Iwasa, and Martin A Nowak. Dynamics of cancer progression. *Nature Reviews Cancer*, 4(3):197–205, 2004.
- [20] Martin A Nowak and Karl Sigmund. Evolutionary dynamics of biological games. *Science*, 303(5659):793–799, 2004.
- [21] John von Neumann. Sur la théorie des jeux. *Comptes Rendus de l'Académie des Sciences*, 186(25):1689–91, 1928.
- [22] John Maynard Smith. *Evolution and the Theory of Games*. Cambridge University Press, 1982.
- [23] William Poundstone. *Prisoner's Dilemma*. Anchor, 2011.
- [24] Peter C Nowell. The clonal evolution of tumor cell populations. *Science*, 194(4260):23–28, 1976.
- [25] Mel Greaves and Carlo C Maley. Clonal evolution in cancer. *Nature*, 481(7381):306–313, 2012.
- [26] David Basanta and Alexander RA Anderson. Exploiting ecological principles to better understand cancer progression and treatment. *Interface focus*, 3(4):20130020, 2013.

- [27] Robert A Gatenby, Robert J Gillies, and Joel S Brown. Of cancer and cave fish. *Nature Reviews Cancer*, 11(4):237–238, 2011.
- [28] Thomas S Deisboeck, Zhihui Wang, Paul Macklin, and Vittorio Cristini. Multiscale cancer modeling. *Annual review of biomedical engineering*, 13:127–155, 2011.
- [29] David Basanta and Alexander Anderson. Homeostasis back and forth: An eco-evolutionary perspective of cancer. *bioRxiv*, page 092023, 2016.
- [30] S Venkatesan and C Swanton. Tumor evolutionary principles: How intratumor heterogeneity influences cancer treatment and outcome. In *American Society of Clinical Oncology educational book. American Society of Clinical Oncology. Meeting*, volume 35, pages e141–9, 2016.
- [31] Robert J Gillies, Daniel Verduzco, and Robert A Gatenby. Evolutionary dynamics of carcinogenesis and why targeted therapy does not work. *Nature Reviews Cancer*, 12(7):487–493, 2012.
- [32] J West, Z Hasnain, P Macklin, J Mason, and PK Newton. An evolutionary model of tumor cell kinetics and the emergence of molecular heterogeneity and gompertzian growth. *SIAM Review*, 58(4):716–736, 2016.
- [33] Robert A Gatenby and Thomas L Vincent. Application of quantitative models from population biology and evolutionary game theory to tumor therapeutic strategies. *Molecular cancer therapeutics*, 2(9):919–927, 2003.
- [34] Ivana Bozic, Johannes G Reiter, Benjamin Allen, Tibor Antal, Krishnendu Chatterjee, Preya Shah, Yo Sup Moon, Amin Yaqubie, Nicole Kelly, Dung T Le, et al.

- Evolutionary dynamics of cancer in response to targeted combination therapy. *Elife*, 2:e00747, 2013.
- [35] Rick Durrett, Jasmine Foo, Kevin Leder, John Mayberry, and Franziska Michor. Intratumor heterogeneity in evolutionary models of tumor progression. *Genetics*, 188(2):461–477, 2011.
- [36] Rebecca A Burrell, Nicholas McGranahan, Jiri Bartek, and Charles Swanton. The causes and consequences of genetic heterogeneity in cancer evolution. *Nature*, 501(7467):338–345, 2013.
- [37] Thomas M Cover and Joy A Thomas. *Elements of Information Theory*. John Wiley & Sons, 2012.
- [38] Douglas Hanahan, Gabriele Bergers, and Emily Bergsland. Less is more, regularly: metronomic dosing of cytotoxic drugs can target tumor angiogenesis in mice. *The Journal of Clinical Investigation*, 105(8):1045–1047, 2000.
- [39] K Lien, S Georgsdottir, L Sivanathan, K Chan, and U Emmenegger. Low-dose metronomic chemotherapy: a systematic literature analysis. *European Journal of Cancer*, 49(16):3387–3395, 2013.
- [40] Jeffrey West and P.K. Newton. Chemotherapeutic dose scheduling based on tumor growth rates: The case for low dose metronomic high entropy therapies. *USC Preprint*, 2017.
- [41] Jeffrey West, Yongqian Ma, and Paul K Newton. Jeffrey west, yongqian ma, paul k. newton

harnessing the evolutionary cost of chemotherapeutic resistance by shaping the fitness landscape of a tumor. *USC Preprint*, 2017.

[42] Robert A Gatenby, Ariosto S Silva, Robert J Gillies, and B Roy Frieden. Adaptive therapy. *Cancer Research*, 69(11):4894–4903, 2009.

[43] Marc Crommelinck, Bernard Feltz, and Philippe Goujon. *Self-organization and emergence in life sciences*. Springer, 2006.

[44] AR Kansal, S Torquato, EA Chiocca, and TS Deisboeck. Emergence of a subpopulation in a computational model of tumor growth. *Journal of Theoretical Biology*, 207(3):431–441, 2000.

[45] Jeffrey West, Zaki Hasnain, Jeremy Mason, and Paul K Newton. The prisoner’s dilemma as a cancer model. *Convergent Science Physical Oncology*, 2(3):035002, 2016.

[46] Bernard Crespi and Kyle Summers. Evolutionary biology of cancer. *Trends in Ecology & Evolution*, 20(10):545–552, 2005.

[47] Steven A Frank. *Dynamics of cancer: incidence, inheritance, and evolution*. Princeton University Press, 2007.

[48] Charles Swanton. Intratumor heterogeneity: evolution through space and time. *Cancer Research*, 72(19):4875–4882, 2012.

[49] Robert Weinberg. *The biology of cancer*. Garland science, 2013.

[50] Iñigo Martincorena and Peter J Campbell. Somatic mutation in cancer and normal cells. *Science*, 349(6255):1483–1489, 2015.

- [51] Lucy R Yates and Peter J Campbell. Evolution of the cancer genome. *Nature Reviews Genetics*, 13(11):795–806, 2012.
- [52] A Farrell, E Hutchinsin, B Marte, and N McCarthy. Nature milestones: cancer. *Nat*, 440:S7–S23, 2006.
- [53] Robert Allan Weinberg. *One renegade cell: how cancer begins*. Basic Books, 1998.
- [54] John S Spratt and John A Spratt. What is breast cancer doing before we can detect it? *Journal of surgical oncology*, 30(3):156–160, 1985.
- [55] James H Goldie and Andrew J Coldman. *Drug resistance in cancer: mechanisms and models*. Cambridge University Press, 2009.
- [56] Yoh Iwasa, Martin A Nowak, and Franziska Michor. Evolution of resistance during clonal expansion. *Genetics*, 172(4):2557–2566, 2006.
- [57] John Von Neumann and Oskar Morgenstern. *Theory of games and economic behavior*. Princeton university press, 2007.
- [58] J Maynard Smith. Evolutionary game theory. In *Vito Volterra symposium on mathematical models in biology*, pages 73–81. Springer, 1980.
- [59] M Nowak. Evolutionary dynamics: Exploring the equations of life. *Cambridge: Harvard University Press*, 2006.
- [60] Martin A Nowak and Karl Sigmund. Evolutionary dynamics of biological games. *science*, 303(5659):793–799, 2004.

- [61] Stefan Schuster, Jan-Ulrich Kreft, Anja Schroeter, and Thomas Pfeiffer. Use of game-theoretical methods in biochemistry and biophysics. *Journal of biological physics*, 34(1-2):1–17, 2008.
- [62] John F Nash et al. Equilibrium points in n-person games. *Proceedings of the national academy of sciences*, 36(1):48–49, 1950.
- [63] John Nash. Non-cooperative games. *Annals of mathematics*, pages 286–295, 1951.
- [64] Josef Hofbauer and Karl Sigmund. *Evolutionary Games and Population Dynamics*. Cambridge University Press, 1998.
- [65] Robert M Axelrod. *The evolution of cooperation*. Basic books, 2006.
- [66] David Basanta and Andreas Deutsch. A game theoretical perspective on the somatic evolution of cancer. *Modeling and Simulation in Science, Engineering and Technology*, page 97, 2008.
- [67] Michael Doebeli and Christoph Hauert. Models of cooperation based on the prisoner’s dilemma and the snowdrift game. *Ecology letters*, 8(7):748–766, 2005.
- [68] Michael Doebeli, Christoph Hauert, and Timothy Killingback. The evolutionary origin of cooperators and defectors. *science*, 306(5697):859–862, 2004.
- [69] Robert A Gatenby and Thomas L Vincent. An evolutionary model of carcinogenesis. *Cancer Research*, 63(19):6212–6220, 2003.
- [70] Robert A Gatenby and Thomas L Vincent. Application of quantitative models from population biology and evolutionary game theory to tumor therapeutic strategies. *Molecular cancer therapeutics*, 2(9):919–927, 2003.

- [71] C Hauert. Evolution from cellular to social scales. *Evolutionary Dynamics*, pages 11–44, 2008.
- [72] Christoph Hauert and György Szabó. Game theory and physics. *American Journal of Physics*, 73(5):405–414, 2005.
- [73] Katrin Bohl, Sabine Hummert, Sarah Werner, David Basanta, Andreas Deutsch, Stefan Schuster, Günter Theißen, and Anja Schroeter. Evolutionary game theory: molecules as players. *Molecular BioSystems*, 10(12):3066–3074, 2014.
- [74] Irina Kareva. Prisoner’s dilemma in cancer metabolism. *PloS one*, 6(12):e28576, 2011.
- [75] Martin Nowak. Stochastic strategies in the prisoner’s dilemma. *Theoretical Population Biology*, 38(1):93–112, 1990.
- [76] Martin A Nowak and Robert M May. Evolutionary games and spatial chaos. *Nature*, 359(6398):826–829, 1992.
- [77] Arne Traulsen and Christoph Hauert. Stochastic evolutionary game dynamics. *Reviews of nonlinear dynamics and complexity*, 2:25–61, 2009.
- [78] Jørgen W Weibull. *Evolutionary game theory*. MIT press, 1997.
- [79] Richard Dawkins. *The selfish gene*. Oxford university press, 2016.
- [80] Zhen Wang, Satoshi Kokubo, Marko Jusup, and Jun Tanimoto. Universal scaling for the dilemma strength in evolutionary games. *Physics of life reviews*, 14:1–30, 2015.
- [81] Erez Lieberman, Christoph Hauert, and Martin A Nowak. Evolutionary dynamics on graphs. *Nature*, 433(7023):312–316, 2005.

- [82] Jeffrey West, Zaki Hasnain, Paul Macklin, and Paul K Newton. An evolutionary model of tumor cell kinetics and the emergence of molecular heterogeneity driving gompertzian growth. *SIAM Review*, 58(4):716–736, 2016.
- [83] Anna Kane Laird. Dynamics of tumour growth: comparison of growth rates and extrapolation of growth curve to one cell. *British Journal of Cancer*, 19(2):278, 1965.
- [84] Steven A Frank and Martin A Nowak. Problems of somatic mutation and cancer. *Bioessays*, 26(3):291–299, 2004.
- [85] WS Kendal. Gompertzian growth as a consequence of tumor heterogeneity. *Mathematical Biosciences*, 73(1):103–107, 1985.
- [86] Thomas M Cover and Joy A Thomas. *Elements of information theory*. John Wiley & Sons, 2012.
- [87] Paul K Newton, Jeremy Mason, Brian Hurt, Kelly Bethel, Lyudmila Bazhenova, Jorge Nieva, and Peter Kuhn. Entropy, complexity, and markov diagrams for random walk cancer models. *Scientific reports*, 4, 2014.
- [88] Larry Norton and Richard Simon. Growth curve of an experimental solid tumor following radiotherapy. *Journal of National Cancer Institute*, 58(6), 1977.
- [89] Peter Dear. *The intelligibility of nature: How science makes sense of the world*. University of Chicago Press, 2008.
- [90] EP Wigner. The unreasonable effectiveness of mathematics in the natural sciences. In *Philosophical Reflections and Syntheses*, pages 534–549. Springer, 1995.

- [91] CO Nordling. A new theory on the cancer-inducing mechanism. *British journal of cancer*, 7(1):68, 1953.
- [92] Alfred G Knudson. Mutation and cancer: statistical study of retinoblastoma. *Proceedings of the National Academy of Sciences*, 68(4):820–823, 1971.
- [93] Ian PM Tomlinson, MR Novelli, and WF Bodmer. The mutation rate and cancer. *Proceedings of the National Academy of Sciences*, 93(25):14800–14803, 1996.
- [94] Charles M Rubin. The genetic basis of human cancer. *Annals of Internal Medicine*, 129(9):759–759, 1998.
- [95] Sten Friberg and Stefan Mattson. On the growth rates of human malignant tumors: implications for medical decision making. *Journal of surgical oncology*, 65(4):284–297, 1997.
- [96] Sébastien Benzekry, Clare Lamont, Afshin Beheshti, Amanda Tracz, John ML Ebos, Lynn Hlatky, and Philip Hahnfeldt. Classical mathematical models for description and prediction of experimental tumor growth. *PLoS Comput Biol*, 10(8):e1003800, 2014.
- [97] Richard Durrett and Stephen Moseley. Evolution of resistance and progression to disease during clonal expansion of cancer. *Theoretical population biology*, 77(1):42–48, 2010.
- [98] Natalia L Komarova and Dominik Wodarz. Drug resistance in cancer: principles of emergence and prevention. *Proceedings of the National Academy of Sciences of the United States of America*, 102(27):9714–9719, 2005.

- [99] Natalia Komarova. Stochastic modeling of drug resistance in cancer. *Journal of theoretical biology*, 239(3):351–366, 2006.
- [100] James H Goldie and Andrew J Coldman. *Drug resistance in cancer: mechanisms and models*. Cambridge University Press, 2009.
- [101] Nicholas Navin, Alexander Krasnitz, Linda Rodgers, Kerry Cook, Jennifer Meth, Jude Kendall, Michael Riggs, Yvonne Eberling, Jennifer Troge, Vladimir Grubor, et al. Inferring tumor progression from genomic heterogeneity. *Genome research*, 20(1):68–80, 2010.
- [102] Andriy Marusyk and Kornelia Polyak. Tumor heterogeneity: causes and consequences. *Biochimica et Biophysica Acta (BBA)-Reviews on Cancer*, 1805(1):105–117, 2010.
- [103] Robert G Abbott, Stephanie Forrest, and Kenneth J Pienta. Simulating the hallmarks of cancer. *Artificial Life*, 12(4):617–634, 2006.
- [104] Gloria H Heppner. Tumor heterogeneity. *Cancer research*, 44(6):2259–2265, 1984.
- [105] Michail Shipitsin, Lauren L Campbell, Pedram Argani, Stanislawa Weremowicz, Noga Bloushtain-Qimron, Jun Yao, Tatiana Nikolskaya, Tatiana Serebryiskaya, Rameen Beroukhim, Min Hu, et al. Molecular definition of breast tumor heterogeneity. *Cancer cell*, 11(3):259–273, 2007.
- [106] Marco Gerlinger, Andrew J Rowan, Stuart Horswell, James Larkin, David Endesfelder, Eva Gronroos, Pierre Martinez, Nicholas Matthews, Aengus Stewart, Patrick

- Tarpey, et al. Intratumor heterogeneity and branched evolution revealed by multiregion sequencing. *N Engl j Med*, 2012(366):883–892, 2012.
- [107] Gloria H Heppner and Bonnie E Miller. Tumor heterogeneity: biological implications and therapeutic consequences. *Cancer and Metastasis Reviews*, 2(1):5–23, 1983.
- [108] John Adam and Nicola Bellomo. *A survey of models for tumor-immune system dynamics*. Springer Science & Business Media, 2012.
- [109] Geoffrey B West, James H Brown, and Brian J Enquist. A general model for ontogenetic growth. *Nature*, 413(6856):628–631, 2001.
- [110] Robyn P Araujo and DL Sean McElwain. A history of the study of solid tumour growth: the contribution of mathematical modelling. *Bulletin of mathematical biology*, 66(5):1039, 2004.
- [111] Randall T Schuh. *Biological systematics: principles and applications*. Cornell University Press, 2000.
- [112] Tiffany A Traina, Ute Dugan, Brian Higgins, Kenneth Kolinsky, Maria Theodoulou, Clifford A Hudis, and Larry Norton. Optimizing chemotherapy dose and schedule by norton-simon mathematical modeling. *Breast Disease*, 31(1):7–18, 2010.
- [113] LH Abbott and F Michor. Mathematical models of targeted cancer therapy. *British Journal of Cancer*, 95(9):1136–1141, 2006.
- [114] Paul Macklin and John Lowengrub. Nonlinear simulation of the effect of microenvironment on tumor growth. *Journal of theoretical biology*, 245(4):677–704, 2007.

- [115] Sheldon M Ross. *Introduction to Probability Models: Solutions Manual for Introduction to Probability Models. Solu*, 4. Acad. Press, 1989.
- [116] Arne Traulsen, Jens Christian Claussen, and Christoph Hauert. Coevolutionary dynamics: from finite to infinite populations. *Physical review letters*, 95(23):238701, 2005.
- [117] Katarzyna A Rejniak and Alexander RA Anderson. Hybrid models of tumor growth. *Wiley Interdisciplinary Reviews: Systems Biology and Medicine*, 3(1):115–125, 2011.
- [118] Vittorio Cristini, John Lowengrub, and Qing Nie. Nonlinear simulation of tumor growth. *Journal of mathematical biology*, 46(3):191–224, 2003.
- [119] Steven M Wise, John S Lowengrub, Hermann B Frieboes, and Vittorio Cristini. Three-dimensional multispecies nonlinear tumor growth—i: model and numerical method. *Journal of theoretical biology*, 253(3):524–543, 2008.
- [120] Hermann B Frieboes, Fang Jin, Yao-Li Chuang, Steven M Wise, John S Lowengrub, and Vittorio Cristini. Three-dimensional multispecies nonlinear tumor growth—ii: tumor invasion and angiogenesis. *Journal of theoretical biology*, 264(4):1254–1278, 2010.
- [121] Yangjin Kim, Magdalena A Stolarska, and Hans G Othmer. The role of the microenvironment in tumor growth and invasion. *Progress in biophysics and molecular biology*, 106(2):353–379, 2011.
- [122] CL Frenzen and JD Murray. A cell kinetics justification for gompertz'equation. *SIAM Journal on Applied Mathematics*, 46(4):614–629, 1986.

- [123] Frank Kozusko and Željko Bajzer. Combining gompertzian growth and cell population dynamics. *Mathematical Biosciences*, 185(2):153–167, 2003.
- [124] P Tracqui. Biophysical models of tumour growth. *Reports on Progress in Physics*, 72(5):056701, 2009.
- [125] Thomas Robert Malthus. *An essay on the principle of population: or, A view of its past and present effects on human happiness*. Reeves & Turner, 1888.
- [126] Robert S Kerbel and Barton A Kamen. The anti-angiogenic basis of metronomic chemotherapy. *Nature Reviews Cancer*, 4(6):423–436, 2004.
- [127] Timothy Browder, Catherine E Butterfield, Birgit M Kräling, Bin Shi, Blair Marshall, Michael S O'Reilly, and Judah Folkman. Antiangiogenic scheduling of chemotherapy improves efficacy against experimental drug-resistant cancer. *Cancer Research*, 60(7):1878–1886, 2000.
- [128] Giannoula Klement, Sylvain Baruchel, Janusz Rak, Shan Man, Katherine Clark, Daniel J Hicklin, Peter Bohlen, and Robert S Kerbel. Continuous low-dose therapy with vinblastine and vegf receptor-2 antibody induces sustained tumor regression without overt toxicity. *The Journal of Clinical Investigation*, 105(8):R15–R24, 2000.
- [129] J West, Z Hasnain, J Mason, and PK Newton. The prisoner's dilemma as a cancer model. *Converg. Sci. Phys. Oncol.*, 2(3), 2016.
- [130] Sébastien Benzekry, Eddy Pasquier, Dominique Barbolosi, Bruno Lacarelle, Fabrice Barlési, Nicolas André, and Joseph Ciccolini. Metronomic reloaded: Theoretical

- models bringing chemotherapy into the era of precision medicine. *Seminars in Cancer Biology*, 35:53–61, 2015.
- [131] Dominik Wodarz and Natalia L Komarova. *Dynamics of Cancer: Mathematical Foundations of Oncology*. World Scientific, 2014.
- [132] Gerhard Held, Joerg Schubert, Marcel Reiser, Michael Pfreundschuh, German High-Grade Non-Hodgkin-Lymphoma, and Study Group. Dose-intensified treatment of advanced-stage diffuse large b-cell lymphomas. *Seminars in Hematology*, 43(4):221–229, 2006.
- [133] Sotiris Prokopiou, Eduardo G Moros, Jan Poleszczuk, Jimmy Caudell, Javier F Torres-Roca, Kujtim Latifi, Jae K Lee, Robert Myerson, Louis B Harrison, and Heiko Enderling. A proliferation saturation index to predict radiation response and personalize radiotherapy fractionation. *Radiation Oncology*, 10(1):1, 2015.
- [134] Philip Gerlee and ARA Anderson. An evolutionary hybrid cellular automaton model of solid tumor growth. *J. Theor. Bio.*, 246(4):583–603, 2007.
- [135] Michael Doebeli and Christoph Hauert. Models of cooperation based on the prisoner’s dilemma and the snowdrift game. *Ecology Letters*, 8(7):748–766, 2005.
- [136] Michael Doebeli, Christoph Hauert, and Timothy Killingback. The evolutionary origin of cooperators and defectors. *Science*, 306(5697):859–862, 2004.
- [137] Robert A Beckman, Gunter S Schemmann, and Chen-Hsiang Yeang. Impact of genetic dynamics and single-cell heterogeneity on development of nonstandard personalized medicine strategies for cancer. *Proceedings of the National Academy of*

- Sciences*, 109(36):14586–14591, 2012.
- [138] Jasmine Foo and Franziska Michor. Evolution of resistance to anti-cancer therapy during general dosing schedules. *Journal of Theoretical Biology*, 263(2):179–188, 2010.
- [139] David Basanta, Robert A Gatenby, and Alexander RA Anderson. Exploiting evolution to treat drug resistance: combination therapy and the double bind. *Molecular Pharmaceutics*, 9(4):914–921, 2012.
- [140] David Liao, Luis Estévez-Salmerón, and Thea D Tlsty. Conceptualizing a tool to optimize therapy based on dynamic heterogeneity. *Physical Biology*, 9(6):065005–18, November 2012.
- [141] RB Martin. Optimal control drug scheduling of cancer chemotherapy. *Automatica*, 28(6):1113–1123, 1992.
- [142] Charalambos Loizides, Demetris Iacovides, Marios M Hadjiandreou, Gizem Rizki, Achilleas Achilleos, Katerina Strati, and Georgios D Mitsis. Model-based tumor growth dynamics and therapy response in a mouse model of de novo carcinogenesis. *PloS one*, 10(12):e0143840, 2015.
- [143] Robert A Gatenby. A change of strategy in the war on cancer. *Nature*, 459(7246):508–509, 2009.
- [144] Ian F Tannock et al. Docetaxel plus prednisone or mitoxantrone plus prednisone for advanced prostate cancer. *The New Eng. J. of Med.*, 351(15):1502–1512, 2004.

- [145] David R Spigel et al. A phase 2 study of higher dose weekly topotecan in relapsed small-cell lung cancer. *Clinical Lung Cancer*, 12(3):187–191, 2011.
- [146] Maxwell Lewis Neal, Andrew D Trister, Tyler Cloke, Rita Sodt, Sunyoung Ahn, Anne L Baldock, Carly A Bridge, Albert Lai, Timothy F Cloughesy, Maciej M Mrugala, et al. Discriminating survival outcomes in patients with glioblastoma using a simulation-based, patient-specific response metric. *PLoS One*, 8(1):e51951, 2013.
- [147] Joseph H Connell. The influence of interspecific competition and other factors on the distribution of the barnacle chthamalus stellatus. *Ecology*, 42(4):710–723, 1961.
- [148] Peter R Grant. Convergent and divergent character displacement. *Biological journal of the Linnean Society*, 4(1):39–68, 1972.
- [149] William L Brown and Edward O Wilson. Character displacement. *Systematic Zoology*, 5(2):49–64, 1956.
- [150] Charles Swanton. Tumor evolutionary principles: How intratumor heterogeneity influences cancer treatment and outcome. *American Society of Clinical Oncology*, 2016.
- [151] C Athena Aktipis, Virginia SY Kwan, Kathryn A Johnson, Steven L Neuberg, and Carlo C Maley. Overlooking evolution: a systematic analysis of cancer relapse and therapeutic resistance research. *PloS One*, 6(11):e26100, 2011.
- [152] Ivana Bozic and Martin A Nowak. Resisting resistance. *Annual Review of Cancer Biology*, 2017.

- [153] K-A Kreuzer, P Le Coutre, O Landt, I-K Na, M Schwarz, K Schultheis, A Hochhaus, and B Dörken. Preexistence and evolution of imatinib mesylate-resistant clones in chronic myelogenous leukemia detected by a pna-based pcr clamping technique. *Annals of Hematology*, 82(5):284–289, 2003.
- [154] Catherine Roche-Lestienne and Claude Preudhomme. Mutations in the abl kinase domain pre-exist the onset of imatinib treatment. In *Seminars in Hematology*, volume 40, pages 80–82. Elsevier, 2003.
- [155] Kristel Kemper, Oscar Krijgsman, Paulien Cornelissen-Steijger, Aida Shahrabi, Fleur Weeber, Ji-Ying Song, Thomas Kuilman, Daniel J Vis, Lodewyk F Wessels, Emile E Voest, et al. Intra-and inter-tumor heterogeneity in a vemurafenib-resistant melanoma patient and derived xenografts. *EMBO Molecular Medicine*, 7(9):1104–1118, 2015.
- [156] Alessandro Romanel, Delila Gasi Tandefelt, Vincenza Conteduca, Anuradha Jayaram, Nicola Casiraghi, Daniel Wetterskog, Samanta Salvi, Dino Amadori, Zafeiris Zafeiriou, Pasquale Rescigno, et al. Plasma ar and abiraterone-resistant prostate cancer. *Science Translational Medicine*, 7(312):312re10–312re10, 2015.
- [157] Luis A Diaz Jr, Richard T Williams, Jian Wu, Isaac Kinde, J Randolph Hecht, Jordan Berlin, Benjamin Allen, Ivana Bozic, Johannes G Reiter, Martin A Nowak, et al. The molecular evolution of acquired resistance to targeted egfr blockade in colorectal cancers. *Nature*, 486(7404):537–540, 2012.
- [158] Pierre Laurent-Puig, Deniz Pekin, Corinne Normand, Steve K Kotsopoulos, Philippe Nizard, Karla Perez-Toralla, Rachel Rowell, Jeff Olson, Preethi Srinivasan, Delphine

- Le Corre, et al. Clinical relevance of kras-mutated subclones detected with picodroplet digital pcr in advanced colorectal cancer treated with anti-egfr therapy. *Clinical Cancer Research*, 2014.
- [159] Roland F Schwarz, Charlotte KY Ng, Susanna L Cooke, Scott Newman, Jillian Temple, Anna M Piskorz, Davina Gale, Karen Sayal, Muhammed Murtaza, Peter J Baldwin, et al. Spatial and temporal heterogeneity in high-grade serous ovarian cancer: A phylogenetic analysis. *PLoS Med*, 12(2):e1001789, 2015.
- [160] A Sorana Morrissy, Livia Garzia, David JH Shih, Scott Zuyderduyn, Xi Huang, Patryk Skowron, Marc Remke, Florence MG Cavalli, Vijay Ramaswamy, Patricia E Lindsay, et al. Divergent clonal selection dominates medulloblastoma at recurrence. *Nature*, 529(7586):351–357, 2016.
- [161] Pedro M Enriquez-Navas, Jonathan W Wojtkowiak, and Robert A Gatenby. Application of evolutionary principles to cancer therapy. *Cancer research*, 75(22):4675–4680, 2015.
- [162] Ivana Bozic and Martin A Nowak. Timing and heterogeneity of mutations associated with drug resistance in metastatic cancers. *Proceedings of the National Academy of Sciences*, 111(45):15964–15968, 2014.
- [163] Li Ding, Timothy J Ley, David E Larson, Christopher A Miller, Daniel C Koboldt, John S Welch, Julie K Ritchey, Margaret A Young, Tamara Lamprecht, Michael D McLellan, et al. Clonal evolution in relapsed acute myeloid leukaemia revealed by whole-genome sequencing. *Nature*, 481(7382):506–510, 2012.

- [164] Pedro M Enriquez-Navas, Yoonseok Kam, Tuhin Das, Sabrina Hassan, Ariosto Silva, Parastou Foroutan, Epifanio Ruiz, Gary Martinez, Susan Minton, Robert J Gillies, et al. Exploiting evolutionary principles to prolong tumor control in preclinical models of breast cancer. *Science Translational Medicine*, 8(327):327ra24–327ra24, 2016.
- [165] Sarah Seton-Rogers. Chemotherapy: Preventing competitive release. *Nature Reviews Cancer*, 16(4):199–199, 2016.
- [166] Robert A Beckman and Chen-Hsiang Yeang. Nonstandard personalized medicine strategies for cancer may lead to improved patient outcomes. *Personalized Medicine*, 11(7):705–719, 2014.
- [167] Artem Kaznatcheev, Robert Vander Velde, Jacob G Scott, and David Basanta. Cancer treatment scheduling and dynamic heterogeneity in social dilemmas of tumour acidity and vasculature. *British Journal of Cancer*, 116(6):785–792, 2017.
- [168] University of Southern California. Hpc infrastructure — hpc — usc, 2015. URL <https://hpcc.usc.edu/about/hpcc-infrastructure/>. [Online; accessed 6-July-2015].
- [169] Alexander RA Anderson and Vito Quaranta. Integrative mathematical oncology. *Nature Reviews Cancer*, 8(3):227–234, 2008.
- [170] Paul K Newton, Jeremy Mason, Kelly Bethel, Lyudmila A Bazhenova, Jorge Nieva, and Peter Kuhn. A stochastic markov chain model to describe lung cancer growth and metastasis. *PloS one*, 7(4):e34637, 2012.

- [171] Jill A Gallaher, Pedro M Enriquez-Navas, Kimberly A Luddy, Robert A Gatenby, and Alexander RA Anderson. Adaptive therapy for heterogeneous cancer: Exploiting space and trade-offs in drug scheduling. *bioRxiv*, page 128959, 2017.
- [172] Olivier Trédan, Carlos M Galmarini, Krupa Patel, and Ian F Tannock. Drug resistance and the solid tumor microenvironment. *Journal of the National Cancer Institute*, 99(19):1441–1454, 2007.
- [173] Mark B Meads, Robert A Gatenby, and William S Dalton. Environment-mediated drug resistance: a major contributor to minimal residual disease. *Nature reviews cancer*, 9(9):665–674, 2009.
- [174] Cristian Tomasetti and Doron Levy. An elementary approach to modeling drug resistance in cancer. *Mathematical biosciences and engineering: MBE*, 7(4):905, 2010.
- [175] Franziska Michor, Timothy P Hughes, Yoh Iwasa, Susan Branford, Neil P Shah, Charles L Sawyers, and Martin A Nowak. Dynamics of chronic myeloid leukaemia. *Nature*, 435(7046):1267–1270, 2005.
- [176] Natalia L Komarova, Lin Wu, and Pierre Baldi. The fixed-size luria–delbrück model with a nonzero death rate. *Mathematical biosciences*, 210(1):253–290, 2007.
- [177] Jasmine Foo and Franziska Michor. Evolution of resistance to targeted anti-cancer therapies during continuous and pulsed administration strategies. *PLoS Computational Biology*, 5(11):e1000557, 2009.

- [178] Peter W Sullivan and Sydney E Salmon. Kinetics of tumor growth and regression in  
igg multiple myeloma. *Journal of Clinical Investigation*, 51(7):1697, 1972.
- [179] Andrea Sottoriva, Haeyoun Kang, Zhicheng Ma, Trevor A Graham, Matthew P Sa-  
lomon, Junsong Zhao, Paul Marjoram, Kimberly Siegmund, Michael F Press, Darryl  
Shibata, et al. A big bang model of human colorectal tumor growth. *Nature genetics*,  
47(3):209–216, 2015.